



Universiteit
Leiden
The Netherlands

Design and synthesis of paramagnetic probes for structural biology

Liu, W.

Citation

Liu, W. (2013, November 25). *Design and synthesis of paramagnetic probes for structural biology*. Retrieved from <https://hdl.handle.net/1887/22357>

Version: Not Applicable (or Unknown)

License: [Leiden University Non-exclusive license](#)

Downloaded from: <https://hdl.handle.net/1887/22357>

Note: To cite this publication please use the final published version (if applicable).

Cover Page



Universiteit Leiden



The handle <http://hdl.handle.net/1887/22357> holds various files of this Leiden University dissertation.

Author: Liu, Wei-Min

Title: Design and synthesis of paramagnetic probes for structural biology

Issue Date: 2013-11-25

Design and synthesis of paramagnetic probes for structural biology

Wei-Min Liu

Design and synthesis of paramagnetic probes for structural biology

Wei-Min Liu

Doctoral Thesis, Leiden University, 2013

ISBN number: 978-94-6203-470-9

© 2013, Wei-Min Liu

Printed by CPI-Wöhrmann Print Service – Zutphen

Design and synthesis of paramagnetic probes for structural biology

Proefschrift

ter verkrijging van
de graad van Doctor aan de Universiteit Leiden,
op gezag van Rector Magnificus Prof. mr. C. J. J. M. Stolker,
volgens besluit van het College voor Promoties
te verdedigen op maandag 25 November 2013
klokke 15.00 uur

door
Wei-Min, Liu
geboren te Kaohsiung, Taiwan in 1983

Promotiecommissie

Promotor: Prof. Dr. M. Ubbink
Co-promotor: Dr. M. Overhand
Overige leden : Prof. Dr. J. Brouwer
Prof. Dr. L. Bouwman
Dr. M. Merkx (Technische Universiteit Eindhoven)
Prof. Dr. M. Zweckstetter (Georg-August-Universitat
Gottingen, Duitsland)

Cover Image: Model of CLaNP-7 attached to Cyt *c* N56C/L58C.

Cover designed by Ching-Ya, Huang

The investigations described in this thesis were performed at the Protein Chemistry department of the Leiden Institute of Chemistry, Leiden University, Leiden, the Netherlands.

Financial support for the research was provided by the Netherlands Organisation for Scientific research (NWO), grant 700.58.441.

'Lanthanoids: These elements perplex us in our researches, baffle us in our speculations, and haunt us in our very dreams. They stretch like an unknown sea before us; mocking, mystifying and murmuring strange revelations and possibilities.'- *Sir William Crookes, Royal Society of Chemistry, 1887*

To My Family

Contents:

List of abbreviations	1
Chapter I Introduction and thesis outline	3
Chapter II A pH sensitive, colorful, lanthanoid-chelating paramagnetic NMR probe.....	31
Chapter III The development of new methods for the attachment of caged lanthanoids NMR probes.....	51
Chapter IV CLaNP-5 derivatives: An approach to obtain multiple paramagnetic restraints sets from a single mutation site	83
Chapter V The application of spin labels	101
Chapter VI General discussion, conclusions and prospects.....	117
Reference List	123
Nederlandse Samenvatting	135
English Summary	139
Appendices	141
List of Publications.....	149
Curriculum vitae	150

List of abbreviations

<i>aq</i>	aqueous
AzF	<i>p</i> -azido phenylalanine
Boc	<i>tert</i> -butyloxycarbonyl
calcd.	Calculated
CLaNP	caged lanthanoid NMR probe
CuAAC	copper-catalyzed 1,3-dipolar azide-alkyne cycloaddition
Cyt <i>c</i>	cytochrome <i>c</i>
Cys	cysteine
δ	chemical shift
d	doublet
Da	Dalton
dd	double doublet
DCM	dichloromethane
DHP	3,4-dihdropyran
DIPEA	diisopropylethyl amine
DMF	<i>N,N</i> -dimethylformamide
DMSO	dimethylsulfoxide
DOTA	1,4,7,10-tetraazacyclododecane-1,4,7,10-tetraacetate
DTPA	diethylene triamine pentaacetic acid
DTT	dithiothreitol
EDC	1-ethyl-3-(3-dimethyl-aminopropyl)-carbodiimide
equiv.	molar equivalent
h	hour(s)
HATU	1-[Bis(dimethylamino)methylene]-1H-1,2,3-triazolo[4,5-b]pyridinium 3-oxid hexafluorophosphate
His	histidine
HOBt	<i>N</i> -hydroxybenzotriazole
HPLC	high performance liquid chromatography
HRMS	high resolution mass spectrometry
Hz	Hertz
IR	infrared
<i>J</i>	coupling constant
K	Kelvin
LC/MS	liquid chromatography/mass spectrometry
M	molar
m	multiplet
<i>m</i> CPBA	meta-chloroperoxybenzoic acid
MeCN	acetonitrile
min	minute(s)
MsCl	methanesulfonylchloride
<i>m/z</i>	mass-to-charge ratio

NHS	<i>N</i> -hydroxysuccinimide
NMR	nuclear magnetic resonance
<i>p</i>	para
Paz	pseudoazurin
PCS	pseudocontact shift
ppm	parts per million
PPTs	pyridinium <i>p</i> -toluenesulfonate
PRE	paramagnetic relaxation enhancement
q	quartet
RT	room temperature
s	singlet
sat.	saturated
SDS-PA gel	sodium dodecyl sulphate-poly acrylamide gel electroforesis
Su	succinimidyl
t	triplet
TBTA	<i>tris</i> -(Benzyltriazolylmethyl)amine
THP	tetrahydropyranyl
HTFA	trifluoroacetic acid
TLC	thin layer chromatography

Chapter I

Introduction and thesis outline

Based on the research article:

Liu, W. -M.; Overhand, M.; Ubbink, M. 'The application of lanthanoid ions in NMR spectroscopy on proteins' (*Coord. Chem. Rev.***2013**, under revision)

Abstract

Lanthanoids are gaining popularity as paramagnetic centers for high resolution nuclear magnetic resonance (NMR) spectroscopy. They provide valuable angular and long-distance restraints for structure calculations of proteins and protein complexes. The introduction of lanthanoids into a protein sample is complicated by the many requirements for functional artificial paramagnetic probes. For many applications, the probe needs to be attached site-specifically and rigidly to the protein and the coordination of the lanthanoid by the tag must result in a unique anisotropy of the magnetic susceptibility. The variety of lanthanoid coordination systems that has been explored to design paramagnetic probes that meet these demands is reviewed. Also the applications of the tags are discussed, including protein and protein complex structure determination, assignment of protein NMR spectra and the study of protein dynamics. It is concluded that lanthanoid probes bear great potential for further applications in protein NMR spectroscopy, provided that various aspects can be improved further.

1. Introduction

The lanthanoid series comprises the fifteen elements with atomic numbers 57 to 71. The symbol Ln is used to refer to any lanthanoid. All but one of the lanthanoids are f-block elements, so-called due to the filling of the 4f electron shell. Lutetium, a d-block element, is also generally considered to be a lanthanoid due to its chemical similarities with the other fourteen. Lanthanoid ions have been broadly used as luminescent chemosensors for biological imaging and analysis,¹ catalysts for organic synthesis,² anion sensors in aqueous solution,³ contrast agents for magnetic resonance imaging,⁴ and as paramagnetic centers for high resolution nuclear magnetic resonance (NMR) spectroscopy⁵, which is the topic of this thesis.

In NMR spectroscopy, paramagnetic lanthanoids have been used as chemical shift mediators and line broadening agents to determine the conformations of biomolecules in solution since 1970s.^{6,7} They are superior sources of paramagnetic effects with several advantages. First, lanthanoids do not exist naturally in biological systems, yet can readily substitute Ca^{2+} and Mg^{2+} , due to their ionic radii being of similar sizes. Second, they have a single stable oxidation state of +3 in aqueous solutions. Third, all Ln^{3+} ions except La^{3+} and Lu^{3+} have multiple unpaired electrons in the 4f orbitals, which are shielded by the $5s^2 5p^6$ subshells.⁸ Due to this property, the unpaired electrons are largely inert in reactions and the lanthanoid series all have similar chemical behavior. Consequently, paramagnetic as well as diamagnetic (control) samples can be readily prepared using different lanthanoids. This is essential when analyzing paramagnetic restraints, because the paramagnetic effects are defined by the difference between the diamagnetic and paramagnetic signal resonance intensities or positions. Fourth, lanthanoids produce varying paramagnetic effects, depending on the number of unpaired electrons. Some of them are strongly paramagnetic (Dy^{3+} , Tb^{3+} , Tm^{3+}) and others only moderately (Er^{3+} , Ho^{3+} , Yb^{3+}).⁹ Finally, Tb^{3+} and Eu^{3+} localized close to an aromatic antenna, such as a tryptophan (Trp) residue, yield a long-lived luminescence that enables easy detection and quantification.^{10,11}

Other common sources of single or multiple unpaired electrons include nitroxide radicals and certain metal ions such as Cu^{2+} , Fe^{3+} and Mn^{2+} . In the last decade, however, the use of lanthanoids in paramagnetic NMR on biomolecules has rapidly gained popularity. Therefore, this chapter focuses on the paramagnetic effects of lanthanoid ions, the development of paramagnetic NMR probes and the

application of paramagnetism for the study of biomolecules. Two approaches to use the lanthanoids can be distinguished. One is the addition of soluble paramagnetic centers that interact purely in a steric way with the biomolecule. The effect caused by a soluble paramagnetic agent is concentration-dependent and can be used to map the solvent-accessible areas of biomolecule allowing the mapping of interfaces of biomolecules.¹² The second approach is site-specific attachment of probes to the biomolecule of interest. In this chapter, we will focus on the latter application.

2. Types of paramagnetic restraints

The paramagnetic nature of a single paramagnetic center can be characterized by the magnetic susceptibility tensor χ , which is described by three components χ_{xx} , χ_{yy} and χ_{zz} . The χ tensor describes the contributions of electron magnetic moments, which are orientation-dependent. The χ tensor can be decomposed into an isotropic component χ_{iso} and an anisotropic component, the $\Delta\chi$ -tensor. The $\Delta\chi$ -tensor is described by an axial ($\Delta\chi_{ax}$) and a rhombic ($\Delta\chi_{rh}$) component, according to the formulae:

$$\Delta\chi_{ax} = \chi_{zz} - \frac{\chi_{xx} + \chi_{yy}}{2} \text{ and } \Delta\chi_{rh} = \chi_{xx} - \chi_{yy} \quad (1)$$

The three paramagnetic effects that are utilized most often are paramagnetic relaxation enhancement (PRE), pseudocontact shift (PCS) and residual dipolar coupling (RDC).

The magnetic dipolar interaction between an unpaired electron and a nuclear spin enhances the nuclear transversal relaxation rate R_2 . Two mechanisms, named after Solomon and Curie, are responsible for increased nuclear relaxation rate and both are distance-dependent. Solomon relaxation is a dipole-dipole interaction between the electron and the nucleus, similar to the cross-relaxation observed for coupled nuclei. Relaxation is caused by the fluctuating dipolar interaction, which is a consequence of molecular tumbling in solution, as well as the rapid flipping of the electron spin due to its fast longitudinal relaxation. Hence, the relevant correlation time, τ_c , is determined by τ_s (the longitudinal electron relaxation time) and τ_r (the rotational correlation time of the vector connecting the paramagnetic center and the nucleus). For slowly tumbling molecules and long-lived electron spin states such as found for Gd^{3+} , the following (simplified) equation applies:¹³

$$R_2^{para} = \frac{1}{15} \left(\frac{\mu_0}{4\pi} \right)^2 \frac{\gamma_I^2 g_e^2 \mu_B^2 S(S+1)}{r_{IM}^6} \left(4\tau_c + \frac{3\tau_c}{1 + \omega_I^2 \tau_c^2} \right) \text{ and } \tau_c^{-1} = \tau_r^{-1} + \tau_s^{-1} \quad (2)$$

where g_e is the electron g-factor, μ_B is the Bohr magneton, S is the total electron spin quantum number, μ_0 is the permeability of vacuum and ω_I the Larmor frequency of the nucleus. The dependence on the squared nuclear gyromagnetic ratio (γ_I) indicates that ^1H is much more sensitive for PRE than ^{13}C and ^{15}N . The PRE decays very fast with the distance r_{IM} between the paramagnetic center and the nucleus, making it sensitive to lowly populated states of a protein or protein complex in solution in which the nucleus is closer to the lanthanoid than in the ground state.¹⁴

The Curie relaxation mechanism becomes prominent when the longitudinal electron relaxation is much faster than the molecular tumbling ($\tau_s \ll \tau_r$). It results from the interaction of the nuclear spin with the time-averaged (static) magnetic moment of the electron.¹⁵ This type relaxation has been used in paramagnetic haem proteins,¹⁶ but it has not yet been used much for relaxation caused by lanthanoids.

Changes in chemical shift caused by a paramagnetic center can be divided into two types; the contact shift (CS), which arises from delocalization of the unpaired electron onto the nucleus, and the pseudocontact shift (PCS), which is a consequence of the anisotropic dipolar (through-space) interaction. The unpaired electron delocalizes to nearby nuclei through the network of covalent bonds, yielding the CS. In general, for nuclei farther than three or four σ -bonds the CS can be neglected. The resonances of nuclei so close to the paramagnetic center are difficult to observe owing to the strong PRE and the chemical shift of nuclei in the coordination sphere of the lanthanoid is irrelevant when using an artificial paramagnetic probe to study a protein. Therefore, CS are rarely considered in paramagnetic NMR spectroscopy using lanthanoids.⁵ In contrast, the PCS (δ^{PCS}) provides valuable paramagnetic restraints, according to equation 3:

$$\delta^{PCS} = \frac{1}{12\pi r_{IM}^3} \left[\Delta\chi_{ax} (3\cos^2 \theta - 1) + \frac{3}{2} \Delta\chi_{rh} (\sin^2 \theta \cos 2\Omega) \right] \quad (3)$$

Where r_{IM} , θ and Ω are the spherical polar coordinates of the nucleus relative to the principal axes of the $\Delta\chi$ -tensor, and $\Delta\chi_{ax, rh}$ are the axial and rhombic components of the magnetic susceptibility tensor. The cubic dependence of the distance between metal and nucleus makes PCS an important source of long-distance restraints and significant PCSs can be measured up to 60 Å away from strongly paramagnetic lanthanoids. Furthermore, the PCS contains angular information of the nucleus

relative to the frame of the $\Delta\chi$ -tensor. Often, the orientation of this frame can be established relative to the molecular frame and thus information on the position of the nucleus can be translated to the molecular frame.

A paramagnetic center with a significant $\Delta\chi$ -tensor also generates a weak alignment in a magnetic field B_0 . The dipolar coupling between nuclei is no longer averaged to zero and residual dipolar couplings (RDCs) can be detected, analogous to creating partial alignment using external alignment media.¹⁷ The RDC (D^{res} , in Hz) between nucleus I and J can be described by equation 4:

$$D^{res} = -\frac{B_0^2}{15k_B T} \frac{\gamma_I \gamma_J h}{16\pi^3 r_{IJ}^3} \left[\Delta\chi_{ax} (3\cos^2 \theta - 1) + \frac{3}{2} \Delta\chi_{rh} \sin^2 \theta \cos 2\Omega \right] \quad (4)$$

where $\Delta\chi_{ax, rh}$ are the axial and rhombic components of the magnetic susceptibility tensor, T is the absolute temperature, h and k_B are the Planck and Boltzmann constants, respectively, r_{IJ} is the internuclear distance, and θ and Ω determine the orientation of the I-J vector relative to the $\Delta\chi$ -tensor. As seen from equation (4), the RDCs do not depend on the distance of the nuclei to the paramagnetic center and can be obtained for all residues throughout a protein as long as the protein is rigid relative to the paramagnetic center. Thus, RDCs contain valuable information on the structure. It is worth noting that the anisotropy of the magnetic susceptibility produces both the PCS and RDC, so both increase with the increasing values of $\Delta\chi_{ax}$ and $\Delta\chi_{rh}$. In general, the $\Delta\chi$ -tensor values obtained by fitting RDCs are smaller than those calculated from PCSs, because RDCs are more sensitive to the local motions in the protein.

3. Lanthanoid probes

3.1 Synthetic lanthanoid chelating probes

To obtain well-defined paramagnetic NMR restraints, site-specific labeling is important for incorporating paramagnetic metals into a protein. Labeling is usually achieved by one of three approaches, summarized in Figure 1. Synthetic probes coordinated to lanthanoids are site-specifically linked on a protein surface *via* uniquely reactive amino acid residues, such as cysteine or artificial amino acids (Figure 1A). Methanethiosulfonate or pyridylthio groups are thiol reactive agents, which can undergo disulfide exchange with cysteine to form disulfide bridges. Precursors functionalized with these groups are commercially available, hence they

are commonly employed (Figure 2). The usual coordination number for lanthanoids is 8 to 9, and therefore polyamino and polycarboxylate-types of ligands are commonly used as ligands. These compounds, such as ethylenediamine tetraacetic acid (EDTA), diethylenetriamine pentaacetic acid (DTPA), triaminohexaacetic acids (TAHA), and tetraazacyclododecane tetraacetic acid (DOTA), form thermodynamically stable complexes with lanthanoids.¹⁸ Synthetic probes based on such ligands are depicted in Figure 2. S-(2-pyridylthio)-cysteaminy-EDTA, **1**, is a commercially available probe, and can be easily made from EDTA anhydride. This pyridylthio group functionalized probe has been site-specifically attached to target proteins *via* disulfide linkages and generated valuable PCSs and RDCs by binding Co^{2+} and Yb^{3+} .^{19,20} As mentioned before, RDCs provide informative restraints to establish protein structures. Membrane proteins, however, are usually solubilized in detergents or lipids, which are not compatible with most external alignment media, making the use of RDCs to solve the NMR structures of membrane proteins impractical. As an alternative to external media, probe **1** coordinated to Tb^{3+} , Tm^{3+} or Yb^{3+} was linked to a membrane protein, yielding sizeable RDCs and multiple data sets could be obtained by using different lanthanoids or attachment sites.²¹ A drawback of probe **1** is that the EDTA-ligand coordinates the lanthanoid and forms chiral complexes due to the pseudoasymmetric nitrogen atom, marked with a star. When the chiral complexes are attached to achiral protein, it produces two diastereoisomers (Figure 3A) resulting in two sets of PCSs.²²⁻²⁴ To overcome this problem, chiral centers were introduced as shown in the EDTA-based probes **2** and **3**.^{25,26} Owing to the stereochemical purity, the [^1H , ^{15}N]-HSQC spectra of proteins tagged with **2** or **3** exhibit a single set of PCSs. Later on, a C_3 -symmetric nonadentate TAHA-ligand was used as ligand to produce a thermodynamically stable Ln-complex.²⁷ This highly symmetric probe **4** binds lanthanoids with femtomolar affinity²⁸ and displays a homogenously coordinated environment in the 278 K to 315 K temperature range. Probe **4** has been linked to a 90 kDa protein-DNA complex. The NMR spectra of this large complex were recorded at 317 K for 27 hours and no changes were observed even after two weeks.

DTPA, an octadentate ligand, tightly coordinates with lanthanoids and the $[\text{Gd}(\text{DTPA})]^{2-}$ complex was the first widely used MRI agent.²⁹ However, the lanthanoid complexes of DTPA exist as different diastereoisomers, as explained in Figure 3B.^{29,30} These isomers generate different coordination environments, resulting in

several $\Delta\chi$ -tensors and, thus, several PCS peaks were observed in the NMR spectra of the DTPA-based probe **5** tagged proteins.³¹ However, **5** has been coordinated to isotropic Gd^{3+} (that does not cause PCS) yielding valuable PREs that were used successfully for the study of a large protein-protein complex.³²

The macrocyclic DOTA is a highly symmetric lanthanoid ligand and when complexed with lanthanoids, exhibits extraordinary thermodynamic stability.^{33,34} Compared to DTPA, two-arm functionalized DOTA complexes are significantly more kinetically inert and produce fewer diastereoisomers (Figure 3).³⁵ Like DTPA, DOTA coordinated to Gd^{3+} has also been widely used in MRI.⁴ It is an excellent scaffold for designing synthetic paramagnetic probes. Probe **6** was the first example of a DOTA-based synthetic probe that can bind to two (engineered) cysteine residues of a protein target, while avoiding the elimination of symmetry.³⁶ Although probe **6** has C_2 -symmetry, two sets of PCSs peaks were observed in the HSQC spectra of $[\text{Yb-6}]^+$ tagged protein pseudoazurin.³⁶ This finding is explained by the fact that the four coordinating nitrogen atoms can generate two possible macrocyclic ring conformations ($\lambda\lambda\lambda\lambda$ and $\delta\delta\delta\delta$) along with the two preferred orientations of the carboxymethylene arms (Δ and Λ). As a result, the coordinating geometry adopts either a square antiprism (SA) or a twisted square antiprism (TSA). The isomers $\Delta\lambda\lambda\lambda\lambda$ and $\Lambda\delta\delta\delta\delta$ belong to the SA structures, whereas the pair of $\Lambda\lambda\lambda\lambda\lambda$ and $\Delta\delta\delta\delta\delta$ forms the TSA conformation. In solution state, the stereoisomers interconvert by ring inversion or arm rotation and this dynamic process is in a slow exchange on the NMR time scale (Figure 3C).^{30,37} In 2004, a mono-functionalized pyridine-*N*-oxide DOTA derivative coordinated to several lanthanoids was reported to exist mostly in an SA conformation in the crystal and solution states.³⁸ The pyridine-*N*-oxide coordinated to a lanthanoid ion generates a six-membered chelating ring, which destabilizes the TSA form considerably in solution state.³⁹ Using this finding as a basis, probe **7** was designed to have two pyridine-*N*-oxide functionalities for symmetry reasons and two methanethiosulfonates for attachment to two cysteine residues of a target protein.^{11,40} The synthesis of the symmetrically functionalized cyclen-based probe **7** is shown in Scheme 1. Herein, symmetrical di-*tert*-butyloxycarbonyl (Boc) protected cyclen was reacted with an excess of methyl bromoacetate. Subsequently, the two Boc protective groups were removed with trifluoroacetic acid and the opposing amines were functionalized with the desired coordinated ligand to give **7** (or **8**).⁴¹ To demonstrate that a two-point attached probe

is less mobile and gives larger paramagnetic effects than one with single-point attachment, the one-armed probe, **7a**, was also synthesized. The results showed that the two-point attachment dramatically enhances the PCSs and RDCs.⁴⁰ Since the pyridine-*N*-oxide is a good antenna for ligand-to-metal charge-transfer, its complexes with Eu^{3+} or Tb^{3+} can also be used as a luminescence probe to quantify protein samples. Furthermore, the position of the metal center can be easily predicted due to the two-point attachment. Probe **7b** gave the largest PCSs and RDCs observed so far. A drawback of this probe is its net charge, which is +3 after binding a lanthanoid ion. The additional charges might cause unexpected influence in protein-protein or protein-ligand recognition. Therefore, probe **8** was designed. Probe **8** contains two *p*-nitrophenol functionalities, rather than the pyridine-*N*-oxide groups, to reduce the net overall charge.⁴² The acidity of the phenolic protons is enhanced by the presence of the *p*-nitro groups, leading to deprotonation upon coordination of the Ln^{3+} .⁴³ Consequently, the net charge of the complex is +1. Similar to the pyridine-*N*-oxide, the *p*-nitrophenol group also forms a six-membered coordination system, yielding a single set of PCSs. In addition, a bright yellow color from the *p*-nitrophenol groups simplifies the sample handling, especially for colorless proteins. As part of the validation experiments of probe **8**, it was attached to yeast cytochrome *c*. The HSQC-spectra of $[\mathbf{8}\text{-Yb}]^+$ tagged cytochrome *c* unexpectedly gave two sets of peaks for most residues. The relative peak intensity and in certain cases the sign of the PCS, changed with the pH. For comparison, the structurally similar probe **7b** showed a single set of PCSs when it was attached to the same protein at the same position. A possible explanation of this finding is that the charge density of the coordinated oxygen of *p*-nitrophenol is lower, in comparison to the pyridine-*N*-oxide moiety. This results in a larger space for a ninth ligand, such as water, to coordinate the lanthanoid. Water coordination in itself does not result in double resonances, as this effect was not observed for probe **8** attached to other proteins. In this particular cytochrome *c* mutant, a histidine residue was in close proximity to the attachment site of the probe (Figure 4A). The imidazole ring could form a hydrogen bond with the ninth coordinated water and break the symmetry of the $[\text{Ln}\text{-}\mathbf{8}]^+$ complexes, creating diastereoisomers and causing double peaks. Protonation of the imidazole ring resulted in the pH dependence because the equilibrium between the two diastereoisomers was shifted (Figure 4B). The pH dependence was used to generate two sets of restraints with one $\text{Ln}\text{-}\mathbf{8}$ complex.

Although double-armed attachment successfully reduces the mobility of probes, the positions of the double cysteine residues have to be designed carefully. Moreover, the cysteine enriched protein might dimerize or precipitate during expression or purification. An alternative approach to obtain a single isomer is *via* the synthesis of chiral cyclen derivatives. For instance, DOTA-based probe **9** contains 8 chiral centers and was shown to form extremely rigid complexes with Ln^{3+} .⁴⁴ The ^1H NMR spectra indicated that there are no dynamic processes in this complex in the temperature range between 298 and 333 K. However, a second paramagnetic shift was observed for proteins tagged with **9**. The $\Delta\chi$ -tensor of the minor species was similar to that of the major species, but there was a 78° difference between these two tensors orientations. Moreover, the intensity of the minor peaks increased to about 50% when heating the protein sample to 323 K and the intensity ratio of these two sets of peaks was reversible when cooling to the 298 K. This phenomenon was explained by the slow rate of the cis-trans isomerization of the peptide bond, which is part of the single arm linker. Similarly, probe **10** provided a single enantiomeric conformation upon complexation to Ln^{3+} .⁴⁵ The benefit of introducing a chiral center or bulky group into paramagnetic probes is that they form stable, well-defined complexes. A drawback is that lanthanoids are difficult to incorporate into these kinds of molecules and harsh conditions are often necessary.

Tagging not only needs to be site-specific, the stability of the linkage is also important. Formation of disulfide bridges is the most convenient way for site-specific labeling, but these bonds are not very stable and can be broken easily by reductants. Alkylation with alkyl halides or Michael addition with α,β -unsaturated carbonyl to form thioethers are also well-known reactions in cysteine chemistry.⁴⁶ Recently, probe **12** was developed to address this stability issue.⁴⁷ A vinyl group was introduced into the *para*-position of a pyridine-core and produced thioether bond with cysteine by Michael addition. Additional heteroatoms were incorporated into the 2,6-positions of the pyridine-core to increase the Ln^{3+} binding affinity. The reaction products of **12** were stable in the presence of DTT or TCEP and the spectra were reported to be unchanged after several days at room temperature.

Another approach involves the site-specific labeling of a protein using an incorporated unnatural amino acid (UAA) residue.⁴⁸ The UAA, *p*-azido-L-phenylalanine (AzF), can specifically react with terminal alkynes, regiospecifically forming a triazole ring *via* a Cu(I) catalyzed cycloaddition reaction.⁴⁹ For this

purpose, probe **11** was decorated with a terminal alkyne and reacted with an AzF containing protein.⁵⁰ Compared to the usual disulfide linker, the triazole ring is more rigid and chemically inert. However, the reaction is non-trivial; the protein labeling experiment has to be conducted in the absence of oxygen and the copper catalyst can cause the protein sample to precipitate.

In comparison with the polyamino and polycarboxylate-type ligands, dipicolinic acid (DPA) based probes and cysteine derivatives are small (Figure 5). Owing to the shortage of donor atoms within the ligand, this class of probe works best with additional ligands from the protein, for example, by linking it to a cysteine residue (*i*) on an α -helix with a neighboring carboxylate amino acid, placed in the position *i* + 4 or *i* – 4.⁵¹ DPA is a rigid ligand and has no chiral centers. Consequently, the problem of forming diastereoisomers after coordinating to lanthanoids is avoided by using DPA-based probes **13**, **14** and **15**.⁵²⁻⁵⁴ Instead of non-chiral aromatic scaffolds, **16** and **17** are the derivatives of *L*-cysteine,^{55,56} and both can be easily synthesized. Moreover, the two-point attachment can also be achieved by using two **16** when two solvent exposed cysteine residues simultaneous present at an α -helix. For those single-point attached small ligands, the relatively low lanthanoid binding affinity compared with octadentate ligands, as evidenced by their exchange behavior and higher mobility relative to two-point attachment are disadvantages.

Non-covalent binding tags have been developed recently as well (Figure 6). Here, electrostatic forces play an important role in protein-probe recognition. These probes represent an alternative approach to study multiple cysteine residue containing proteins and other proteins for which site-specifically labeling is challenging. The DPA based non-covalent probe, $[\text{Ln}(\text{DPA})_3]^{3-}$, was first reported to bind specifically to an arginine-rich area of a protein and provided a single set of PCSs due to the fast chemical exchange between the bound and free $[\text{Ln}(\text{DPA})_3]^{3-}$.^{57,58} For proteins lacking positive charges, a non-covalent binding site can readily be generated by site-directed mutagenesis.⁵⁹ The use of DPA derivatives yields variable binding affinities and paramagnetic properties, broadening the use of non-covalent binding probes.⁶⁰ Two DOTA analogues, DOTAM and DOTP (Figure 6), serve as another example of non-covalent binding probes to study protein-protein interactions.⁶¹ The paramagnetic effect (in particular used for PREs) of non-covalent probes can easily be scaled by varying the concentration. The relatively low affinity of the non-covalent probes may limit the size of the observed effects and binding at

secondary sites needs to be excluded for unambiguous interpretation of the paramagnetic effects.

3.2 Lanthanoid binding metalloproteins and binding peptides

In metalloproteins, the trivalent lanthanoids have been widely used for replacing naturally occurring Ca^{2+} in proteins to generate paramagnetic constraints, because Ln^{3+} and Ca^{2+} ions have similar ionic radii and binding characteristics (Figure 1C).⁶² A very early application was the substitution of Yb^{3+} for Ca^{2+} bound to Carp parvalbumin, which provided valuable induced shifts in ^1H and ^{13}C NMR spectra.^{63,64} By loading different lanthanoids into monolanthanoid-substituted calcium binding proteins, such as calbindin $\text{D}_{9\text{k}}$, the three dimensional structure of the protein in solution state could be refined.^{65,66} For multiple Ca^{2+} binding proteins, a lanthanoid ion can be made to bind to a single site by tuning the affinity of the sites for Ln^{3+} .⁶⁷ The $\Delta\chi$ -tensors for the full series of lanthanoid ions could be reported for $\text{D}_{9\text{k}}$, since a protein provides a fairly constant coordination environment and a large number of NMR restraints for tensor calculation. The differences in orientations of the $\Delta\chi$ -tensors of all the lanthanoids are small, in line with the assumption that all Ln ions have a similar coordination chemistry.⁶⁸ In addition to Ca^{2+} binding proteins, in Mg^{2+} binding proteins, such as DNA polymerases, the metal can be replaced with Ln^{3+} for paramagnetic NMR spectroscopy.⁶⁹

Often, calcium binding proteins contain an EF hand motif, which is characterized by a helix-loop-helix structure of 12 or 14 amino acids.⁷⁰ This particular motif, which provides pure chirality and coordination rigidity, can be used as a paramagnetic tag by fusion with a target protein (Figure 1B). Usually, membrane proteins in lipid micelles are challenging samples for NMR due to the slow molecular tumbling. An EF hand motif chelating Yb^{3+} or Dy^{3+} was added to the N-terminus of the membrane protein Vpu, which provided RDCs for analyzing the three-dimensional structure in micelles.⁷¹ To increase the lanthanoid binding affinity, a Tb^{3+} specific lanthanoid binding peptide (LBP) was developed by combinatorial chemistry.^{72,73} A Trp, which acts as a photoantenna for Tb^{3+} , was inserted into the LBP, giving it not only paramagnetic, but also luminescent properties. This bi-functional LBP can be engineered genetically at the N or C terminus or into a loop region of a protein.^{10,74,75} In addition, LBP functionalized with a cysteine residue can also be site-specifically attached onto a protein surface to overcome the limitation of

protein fusion technology.⁷⁶ However, the mobility of LBP, either as a fusion with a protein or tagged on a specific position, reduces the paramagnetic effects.⁷⁷ To enhance the magnetic effects, a two-point attached LBP, *via* a disulfide bridge and an N-terminal fusion, was developed.⁷⁸ In comparison with the single-point attached LBP, the two-point attached LBP provided larger PCSs and RDCs.

4. Applications of paramagnetic lanthanoid tags to biological systems

4.1 NMR assignment

The assignment of the NMR spectrum is a prerequisite for detailed NMR studies of a biomolecule. For proteins, in general, heteronuclear multidimensional (3D/4D) spectra and concentrated isotope labeled samples are required. Assigning the resonances of nuclei of small proteins (<20 kDa) with those experiments can be considered routine.⁷⁹ However, obtaining the resonance assignments of larger proteins is challenging due to increased transverse relaxation of the nuclear spins and spectral overlap. Paramagnetic NMR spectroscopy provides a complementary or even alternative way for obtaining assignments. PCSs are particularly useful because of the long-range structural information they contain. Moreover, PCSs are readily observable and can be precisely measured, even at concentrations as low as 20 μM .⁸⁰ If only PCSs are used for assignment, prior knowledge of the protein structure or that of a homologue is required. Several software packages for the use of paramagnetic restraints in assignments have been developed, such as Echidna⁸¹, PLATYPUS⁸², Possum⁸³ and PARAssign⁸⁴.

4.2 Protein structure determination

NMR spectroscopy can be used for structure determination by itself or it can complement structure determination of biomolecules by X-ray diffraction of crystals, in cases where the solution structure differs or is more dynamic, as compared to the structure in the crystal. For example, calmodulin is a Ca^{2+} binding protein and its C- and N-terminal domains are connected by a flexible linker that rigidifies upon binding of calmodulin to peptides. Three lanthanoids were substituted for Ca^{2+} in the N-terminal domain and initial $\Delta\chi$ -tensors from PCSs restraints were calculated using the crystal structure of a calmodulin-peptide complex. Then, the structure of the complex in solution could be refined by simultaneous optimization of the $\Delta\chi$ -tensor

and the structure on the basis of PCSs and RDCs.⁸⁵ If a peptide is not bound to the protein, the linker is flexible and the domains are mobile. To describe the ensemble of conformers that the domains can occupy, the so-called maximum occurrences of domain orientations were calculated using paramagnetic restraints. Two independent sets of paramagnetic restraints were obtained. One of these was from the Ln^{3+} substitution for Ca^{2+} at the N-terminal domain and the other came from the C-terminal domain tagged with probe **7b**. The simultaneous use of the two independent sets of paramagnetic restraints significantly reduced the value of maximum occurrence compared with a single set of restraints, thus giving a better approximation of the true ensemble.⁸⁶

A paramagnetic probe containing Gd^{3+} can also be used as an intramolecular ruler providing nanometer scale distance measurements by using double electron-electron resonance (DEER) experiments, a particular type of EPR spectroscopy.⁸⁷ Such measurements only yield a single distance per Gd^{3+} pair, but the distances are quite accurate.⁸⁸ For example, ERp29 is a 51 kDa homodimer and its 3D structures were determined first for the rat protein by NMR spectroscopy and subsequently for the human ortholog by X-ray crystallography.^{89,90} The interfaces in both structures showed some differences, although the primary structures of the N-terminal domain are identical except for one residue. To characterize the interfaces of ERp29, probe **10** coordinated to Gd^{3+} was attached at two labeling sites at the same time.⁹¹ The bulkiness of probe **10** reduces the number of conformers and, thus, yields a narrower, better defined distribution of distances in the DEER measurements. Paramagnetic NMR effects were also obtained for this complex by using **10** coordinated to Tb^{3+} and Tm^{3+} . The paramagnetic NMR data and DEER results are in agreement with the dimer interface as observed in the crystal structure.

Extensive use was made of paramagnetic restraints from probe **10** and its stereoisomer to demonstrate that the dengue virus protease NS2B-NS3pro assumes a closed structure in the presence of an inhibitor.⁹² The NMR spectra of this protein were poor due to exchange broadening and peak overlap and PCSs were used both for assignment and validation of the structure, on the basis of the structure of an analogous protein from another virus. Moreover, a non-covalent paramagnetic probe⁵⁷ binding site was created on the NS2B-NS3pro surface by introducing two positively charged amino acid residues to assess the open state. The non-covalently

binding probe coordinated to Gd^{3+} generated PRE data that suggested that the open state, which is observed in the crystal state, is rarely present in solution.

4.3 Protein-Protein complexes

Interactions between proteins play a role in most biochemical pathways, so methods that can characterize such interactions at the atomic level can contribute considerably to the molecular understanding of cellular processes. When characterizing protein complexes in such detail, the individual protein structures are usually already known. Paramagnetic NMR restraints can be used to dock the proteins in the correct orientation. Until now, such docking studies assume that the protein backbones do not change their structure upon complex formation, an assumption that often holds for weak complexes, with dissociation constants in the μM range. This assumption is not essential; provided that sufficient restraints can be obtained, full structure determination is also possible, in principle.

Nitrite reductase is a homotrimeric copper protein of 110 kDa. It catalyzes the reduction of nitrite to gaseous nitric oxide. Pseudoazurin, a 14 kDa electron carrier protein, is the reductor of nitrite reductase in *Alcaligenes faecalis* S6. To determine how pseudoazurin binds the reductase, probe **5** loaded with Gd^{3+} was linked to nitrite reductase at three surface positions, one at a time, and the intermolecular PRE were measured using Transverse Relaxation Optimized Spectroscopy (TROSY)⁹³ experiments on ^2H , ^{15}N -labeled pseudoazurin. The simultaneous use of the three sets of PRE restraints and chemical shift perturbation (CSP) data generated a cluster of structures of the nitrite reductase-pseudoazurin complex, with an RMSD of 1.5 Å.³²

PCS-based restraints, which provide both distance and angular information, can also be used to determine the structures of protein complexes. The advantage of using PCSs is that chemical shifts are more easily and accurately quantified than relaxation enhancements, especially for poorly soluble proteins. PCSs and PREs were combined in the study of the 65 kDa complex of adrenodoxin reductase and its electron accepting partner adrenodoxin.⁸⁰ This complex was hard to study with NMR spectroscopy because the reductase tended to aggregate at high concentrations and, furthermore, the adrenodoxin contains a naturally paramagnetic cofactor, a Fe_2S_2 cluster, that broadens out the resonances of adrenodoxin nuclei that are part of the interface. A combination of intermolecular PCSs, PREs and CSPs was used to obtain the location and orientation of adrenodoxin with respect to its reductase (Figure 7A),

which was in agreement with the crystal structure of chemically cross-linked complex of adrenodoxin reductase and adrenodoxin.

The p62-PB1 complex tagged with a two-point anchored LBP is another example in which the protein-protein interaction was characterized by using PCS-based restraints.⁹⁴ With a single tag the degeneracy of the magnetic susceptibility tensor results in “ghost” solutions in structure calculation. To resolve this problem, the spacer length between the LBP and the protein surface was varied, resulting in different metal positions and different orientations of $\Delta\chi$ -tensor, and therefore several sets of paramagnetic restraints that could be used for docking.⁹⁵

In a recent study, a very large set of restraints (446) was obtained for the structure determination of the complex of cytochrome P450cam and putidaredoxin, attaching probe **8** to both proteins at three positions in total, generating PCSs, PREs and RDCs. The results showed excellent agreement for the position and orientation of putidaredoxin with respect to the cytochrome with the crystal structure of the complex that was reported in the same study and, independently, by a second group (Figure 7B).^{96,97} This NMR study shows that tagging with lanthanoid tags can yield sufficient restraints for accurate structure determination, without the need of other NMR data.

Paramagnetic tagging can also help to demonstrate the presence of dynamics in a protein complex. For example, probe **7b** was employed to characterize the encounter complex of yeast cytochrome *c* and bovine adrenodoxin.⁹⁸ In this study, **7b** loaded with Yb³⁺ was attached to the cytochrome *c* at an attachment site far from the interaction side with adrenodoxin. RDCs are distance-independent and depend only on the orientation of the H-N bond vector relative to the alignment tensor. Thus, if adrenodoxin were in a well-defined position within the complex with cytochrome *c*, the average size of the RDCs would be the same for both proteins, because the degree of alignment would be the same. However, the RDCs for adrenodoxin were very small, indicative of large intermolecular dynamics. On the basis of this averaging effect the degree of dynamics was estimated and shown to agree with previous published results based on other NMR data.⁹⁹

4.4 Protein-ligand interactions

In fragment-based drug discovery, small compounds that bind weakly to a protein target, are chemically combined or elaborated to increase binding affinity.

For rational design of the ligand, it is essential to know the orientation of the small compound and its location on the protein surface.¹⁰⁰ Usually, X-ray diffraction of protein-ligand co-crystals is used to obtain the structure of the protein-ligand complex. However, in many cases co-crystals cannot be obtained. Paramagnetic NMR spectroscopy offers an alternative approach to obtain the structural information. The two-point anchored LBP tagged Grb2 serves as an example.¹⁰¹ A combination of PREs and PCSs of the ligand NMR resonances was employed in screening for compound binding and structure determination of the protein-ligand complex. In this strategy, time-consuming side-chain assignment and NOE analysis is not required. The assignment of backbone protein signals is necessary, however, to define the $\Delta\chi$ -tensor of the LBP. This requirement is a drawback for large proteins and proteins that cannot be labeled with isotopes.

Recently, the protein FKBP12 was tagged with **7b** to determine the position and orientation of a ligand (Figure 8).¹⁰² PCSs were measured on the NMR resonances of the ligand, which was in large excess over the protein. Then, the PCSs were used to dock the ligand on the protein, applying two approaches. First, the location of the lanthanoids and the orientations of the $\Delta\chi$ -tensors were determined on the basis of PCSs measured on the FKBP12 backbone resonances, similar to the case of Grb2. The resulting ensemble of best solutions was compared with the structure of protein-ligand complex determined by ‘classic’ structure determination using intermolecular NOEs and showed an RMSD between the NOE-based structure and the mean of the ensemble of 2.8 Å (Figure 8B). Second, the position of the lanthanoid and the orientation of the $\Delta\chi$ -tensor were predicted purely on the basis of the structure of the free protein. Previous work had shown that prediction was possible by using a simple set of rules, because the two-armed attachment makes the probe rigid and the location well-defined.¹¹ The resulting ligand position had an RMSD from the NOE-based structure of 5 Å (Figure 8C), indicating that even without any NMR information from the protein, the ligand binding site can be obtained at low resolution.

For carbohydrate binding to proteins, a significant number of protein-ligand NOEs are difficult to obtain due to the generally weak binding and the highly solvated interfaces, and therefore other NMR restraints are required for analyzing such a protein-ligand complex. A combination of RDCs and PCSs was applied to determine the binding orientation of lactose to a fusion of the protein galectin-3 with

a C-terminal LBP, yielding a structure similar to the one of the crystallized complex.¹⁰³

As an alternative to tagging the protein, the ligand can be functionalized with a lanthanoid to identify the protein-ligand interaction surface. In comparison with tagging the protein, the design of a functionalized ligand is more challenging, because the changed size and charge may well affect the binding. To avoid the side effects, the linker between the lanthanoid binding group and the substrate should be long enough. However, the longer the linker, the smaller and more averaged the paramagnetic effects will be. Nevertheless, a Gd³⁺-binding bile acid analog has been made and the PRE restraints were successfully used to determine the binding hot spots of the liver bile acid binding protein.¹⁰⁴

4.5 Protein dynamics

Conformational flexibility is usually required for protein function. The dynamics that are most relevant for protein function, such as enzyme catalysis, are in the time-scales from microseconds to milliseconds.^{105,106} The interconverting states of proteins have different chemical shifts, and the shifts for the minor states can be obtained from relaxation dispersion experiments.¹⁰⁷ However, it remains difficult to translate the differences in chemical shifts between major and minor states into differences in structures. In an external alignment medium, also RDCs of the minor state can be measured from relaxation dispersion experiments and these provide more valuable structural information.^{108,109} In principle, PCSs can also be very valuable for structure determination of lowly populated states. The PCS gradient produced by a paramagnetic center can be a reference frame for studying protein dynamics. When part of a protein moves relative to the paramagnetic center, the nuclei ‘feel’ a fluctuating PCS that can be measured by relaxation dispersion experiments, in the same way as regular chemical shift differences.¹¹⁰ The PCS is more readily converted into useful structural restraints. To obtain accurate structural restraints in this way, the rigidity of the introduced paramagnetic center is essential. Therefore, probe **7b** appeared to be a good candidate for relaxation dispersion experiments, because it is linked to the protein *via* two arms and was reported to produce minimal averaging of PCSs and RDCs. To test **7b** for this application, it was coordinated to Tm³⁺, Yb³⁺ and Lu³⁺ and attached to the protein pseudoazurin at two locations, in a loop region and in a small α -helix. A short β -strand in cytochrome *c*

was also tagged.¹¹¹ By using ¹H CPMG relaxation dispersion experiments, dispersion effects were indeed obtained. However, these effects were most likely caused by the mobility of the tag, rather than of the protein. A comparison of the locations of the attachment sites showed that the loop region was affected more strongly by conformational exchange than the α -helix. So, even though the PCS derived from standard experiments gave an excellent fit between calculated and observed data, relaxation dispersion, apparently, detected a minor state in which the probe had moved relative to the protein. Nevertheless, this study indicates that paramagnetic relaxation dispersion analysis is very promising for the analysis of protein dynamics, provided a probe can be found that is rigid and does not exhibit mobility on the micro-millisecond timescale.

5. Proteins used in this study

5.1 Pseudoazurin

Pseudoazurin (Paz) isolated from *Alcaligenes faecalis* S6 is a small copper binding protein and is a member of the cupredoxin family of electron transfer proteins.^{112,113} Paz contains 123 amino acids and has a molecular weight of 13.5 kDa. The crystal structure of Paz (Figure 9) shows that the secondary structure consists of 8 β -strands and 2 α -helices. The copper center is coordinated by two His and one Cys and one Met ligands in a distorted tetrahedral configuration.¹¹⁴ The structure of the oxidized and reduced forms shows no differences in the main chain fold.¹¹⁵

5.2 T4 lysozyme

Lysozyme from bacteriophage T4 (T4Lys) is an endoacetylmuramidase. The molecular weight of the enzyme is around 18.5 kDa and it contains 164 amino-acid residues. The three-dimensional structure of T4Lys (Figure 10) can be described as 4 β -strands and 10 α -helices. The structure and folding process of T4Lys have been studied extensively.^{116,117} The advantages of using T4Lys are that it is easy to express and purify, the yield is high and it is very stable. Consequently, T4Lys is a good model protein for NMR spectroscopy.

5.3 Cytochrome *c*

Cytochrome *c* (Cyt *c*) is a small haem protein and is a component of the electron transport chain in mitochondria. The molecular weight of Cyt *c* is about 12

kDa, comprising 100 to 108 amino acid residues, depending on the source, and it harbors a *c*-type haem group. Such haem groups are covalently attached to the protein *via* two thioether bonds and in Cyt *c* the haem ion has six ligands; four are from the porphyrin and the other two from histidine and methionine (Figure 11B). During the electron-transfer processes, the haem ion interconverts between two oxidation states, Fe²⁺ and Fe³⁺. The shape of Cyt *c* is spherical and it consists of 5 α -helices and a short β -strand (Figure 11A). Several high resolution X-ray and NMR structures of both ferrous^{118,119} and ferric^{120,121,122} Cyt *c* have been reported.

5.4 Cytochrome P450cam

Cytochrome P450s are an important haem-containing monooxygenase family with more than 10,000 members.¹²³ They are involved in a number of vital processes, including carcinogenesis and drug metabolism as well as the biosynthesis of steroids or lipids and the degradation of xenobiotics. Among the P450 superfamily, the best characterized P450 is P450cam (Figure 12), which is isolated from the soil bacterium *Pseudomonas putida*. Conformational changes play an important role in substrate recognition for P450cam. When (+)-camphor binds to the protein, the protein is changed from an open to a closed state and the haem coordinating water molecule is released.¹²⁴ Therefore, the (+)-camphor is regioselectively and stereoselectively hydroxylized to 5-exo-hydroxycamphor by P450cam. It is worth noting that this family of enzymes all presents a common protein fold and P450cam it is one of the few water soluble members.^{125,126} Consequently, it is a good model protein to investigate the functionality of this family proteins.

6. Aim and outline of this thesis

The aim of this work was to develop new paramagnetic probes containing nitroxide radicals or lanthanoids, for the study of biomolecules. **Chapter 2** describes a new paramagnetic probe, CLaNP-7, for which the net charge of lanthanoids complexes was reduced to +1 by introducing *p*-nitrophenol. The $\Delta\chi$ -tensor of CLaNP-7 is pH-dependent when a histidine residue is located close to the attachment site. It is proposed that the pH dependence is due to the fact that the histidine forms a hydrogen bond with a water that acts as the ninth ligand of the Ln.

In order to enhance the stability of the tag linkers, two approaches, thioether and bioorthogonal reactions, were investigated in **Chapter 3**. The results showed

that a new thio-reactive CLaNP-9 was successfully attached to protein and the reaction product was stable in the reductive conditions.

The research described in **Chapter 4** entails the synthesis of CLaNP-5 derivatives with substitutions on the pyridine-*N*-oxide ring to obtain multiple NMR restraints *via* a single attachment site. Although the methoxyl derivative presented slightly different magnetic tensor compared to CLaNP-5, the side-chains of neighboring amino interacted with the methoxyl groups resulting two sets of paramagnetic effects. This finding, together with that in Chapter 2 demonstrates that amino acid side-chains can readily interact with the probe and influence its behavior.

Nitroxide radical probes are described in **Chapter 5**. Several rigid radical probes and inhibitor-based radical probes were synthesized. The co-crystal structures of protein with inhibitor-based probes were also presented.

In **Chapter 6**, the works in this thesis are summarized and discussed and future prospects based on these results are provided.

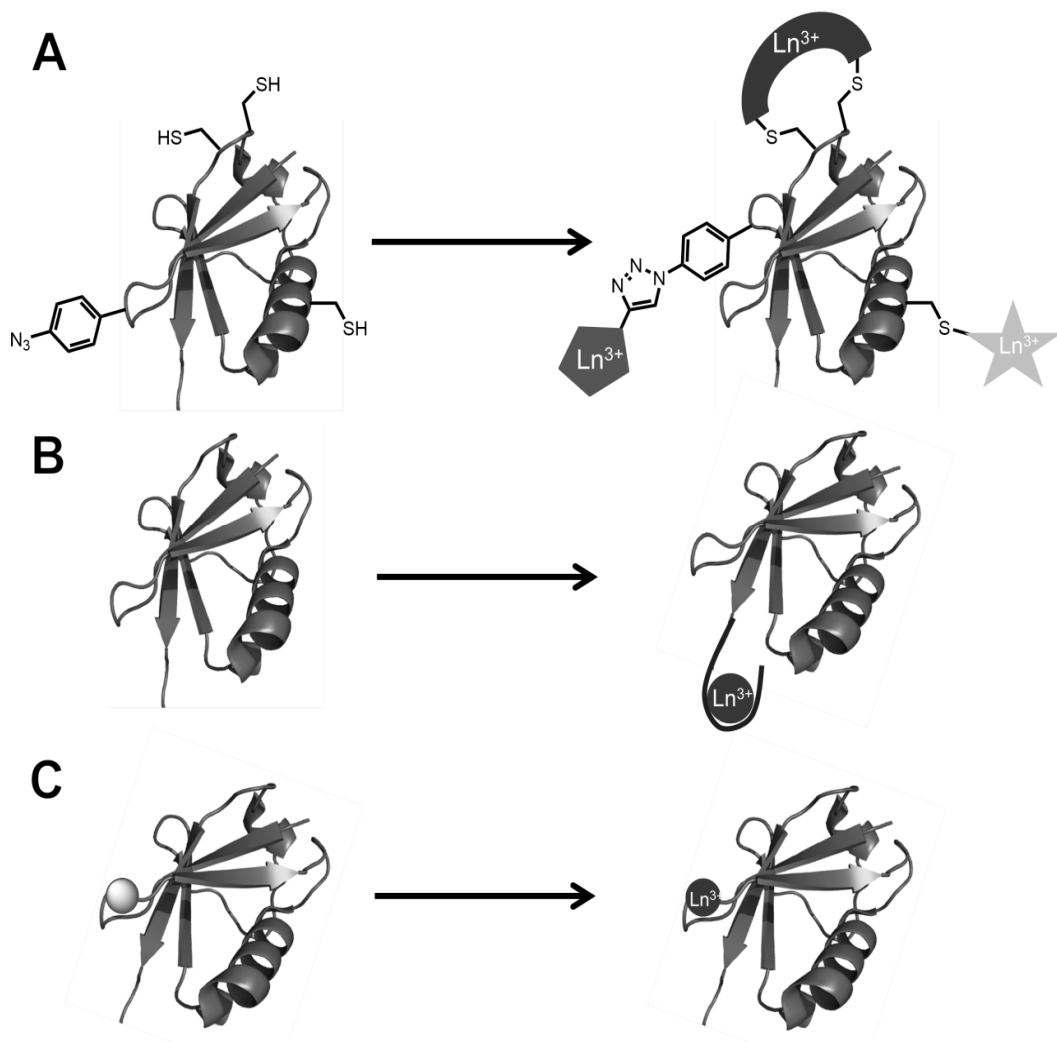


Figure 1. Different approaches for introducing a paramagnetic center on target proteins. (A) Synthetic tags are linked to a cysteine or an artificial amino acid. (B) A lanthanoid binding peptide is engineered genetically into a protein. (C) The metal ion of a metalloprotein is replaced by a lanthanoid.

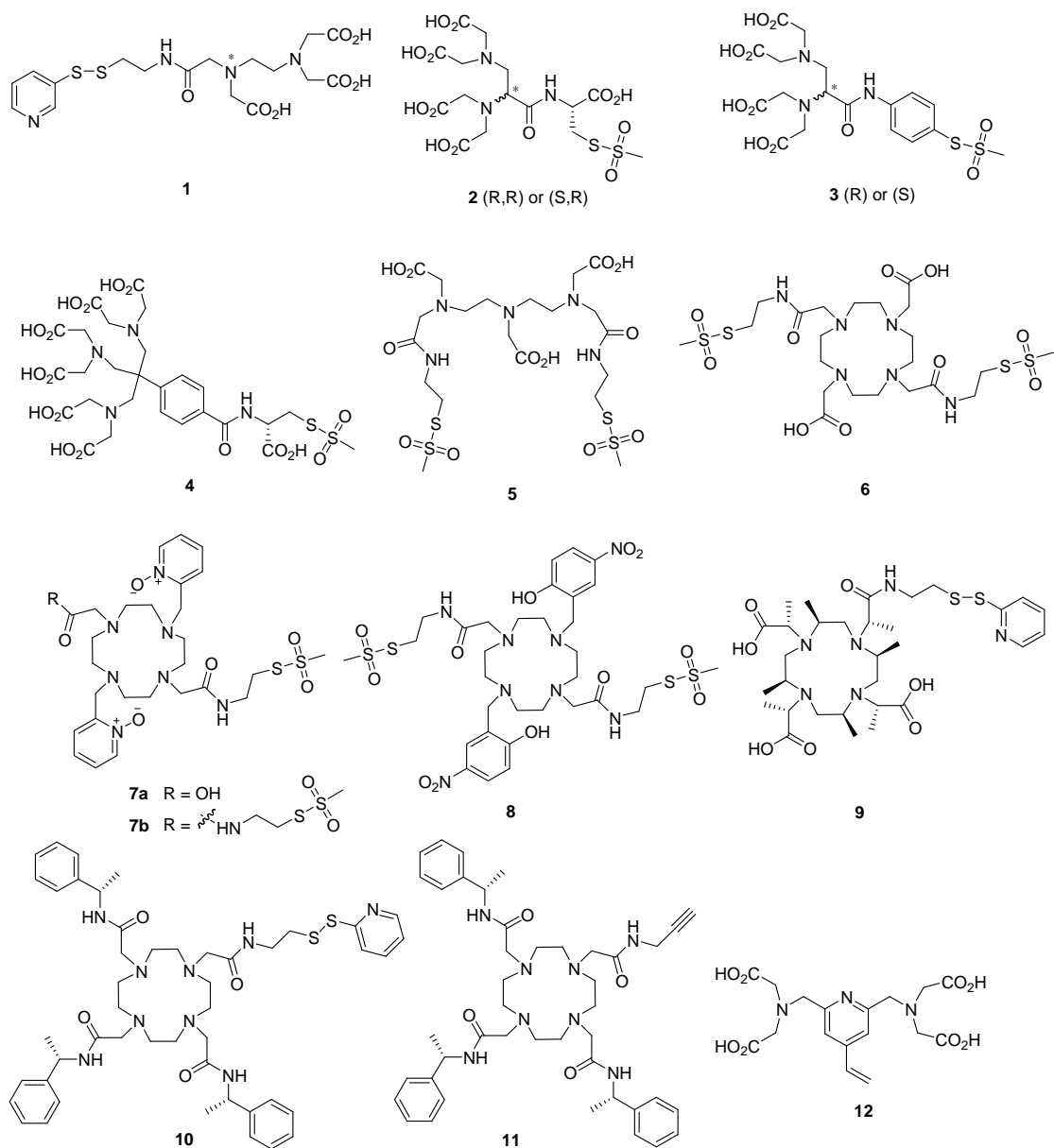
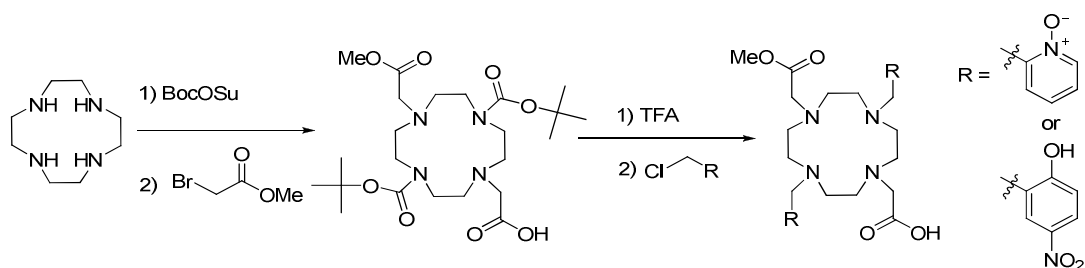


Figure 2. Structures of lanthanoid chelating probes. (1-3) EDTA-based probes: (S-(2-pyridylthio)-cysteaminy)-EDTA, **1**)¹⁹, (EDTA-CA-MTS, **2**)²², (ent-6, **3**)²⁶; (4) TAHA based probe: (Cys-Ph-TAHA, **4**)²⁷; (5) DTPA-based probe: (CLaNP1, **5**)³¹; (6-11) DOTA-based probes: (CLaNP3, **6**)³⁶, (CLaNP5, **7**)¹¹, (CLaNP7, **8**)⁴², (DOTAM8, **9**)⁴⁴, (C1, **10**)⁴⁵, (C4, **11**)⁵⁰; (12) pyridine-core probe: (4VPyMTA, **12**)⁴⁷.



Scheme 1. The synthesis of two-armed paramagnetic NMR probes **7** and **8**.

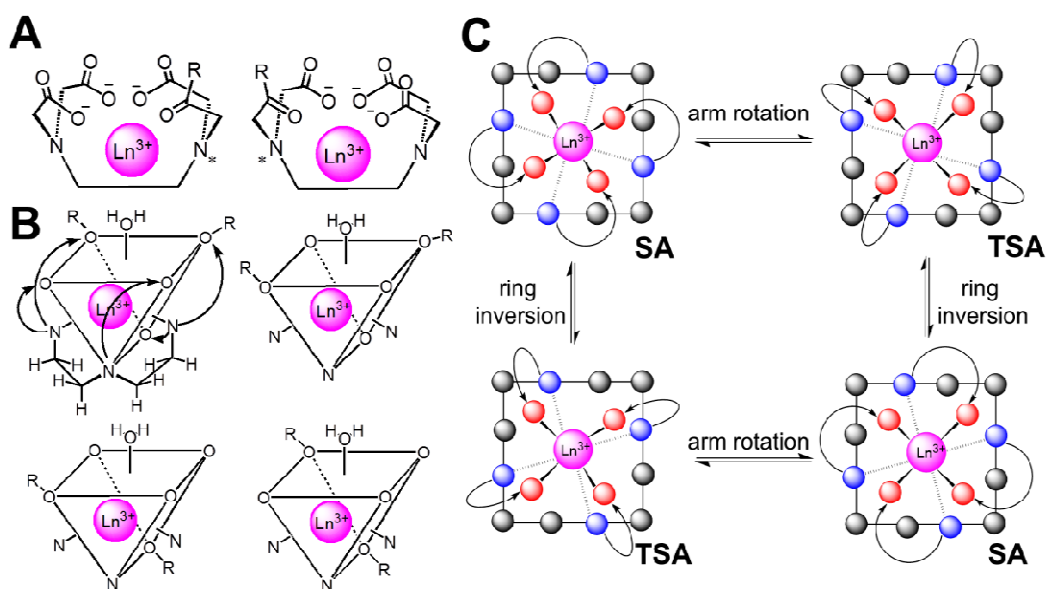


Figure 3. Isomerism of complexes with EDTA (A), DTPA (B) and DOTA (C) like ligands. (A) the pseudoasymmetric nitrogen is marked with a star and the linkers between probe and protein are shown in R.²⁴ (B) The nine coordination systems are shown in a tricapped trigonal prismatic model. The acetate arms are shown in round arrows and the linker between probe and protein in R.³⁰ (C) The DOTA ring is shown as a solid line and ligand arms as round arrows. The carbon atoms are shown in black, nitrogens in blue, oxygens in red and the lanthanoid ions in magenta. The figure is adapted from [24] and [30].

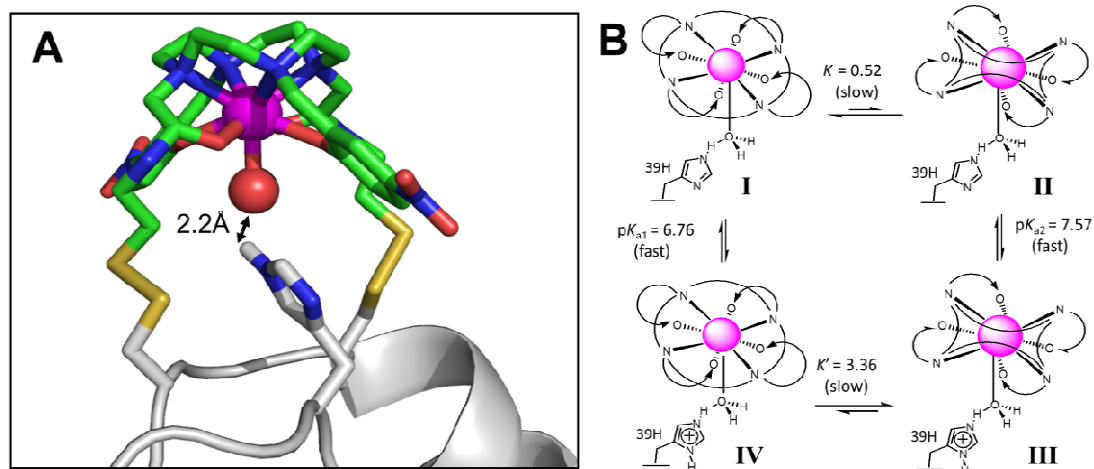


Figure 4. Model of probe **8** attached to cytochrome *c* and the proposed mechanism of pH dependence.⁴² (A) The position of lanthanoid (magenta) was derived from fitting the PCS data. The proposed ninth coordinated ligand, H₂O/OH, is shown in red. The protein main chain is displayed in gray. The cysteine and histidine side-chains are shown in CPK colors. The carbon atoms from probe **8** are shown in green and the nitrogen, oxygen and sulfur atoms in CPK colors. (B) The pH dependence of probe **8** was described by the shown model. The flip between two SA forms ($\Delta\lambda\lambda\lambda\lambda$ and $\Lambda\delta\delta\delta\delta$) are schematically represented by a change in the cyclen ring (lines connecting the N atoms) and the ligand arms (round arrows). Reprinted with permission from [42]. Copyright (2013) American Chemical Society.

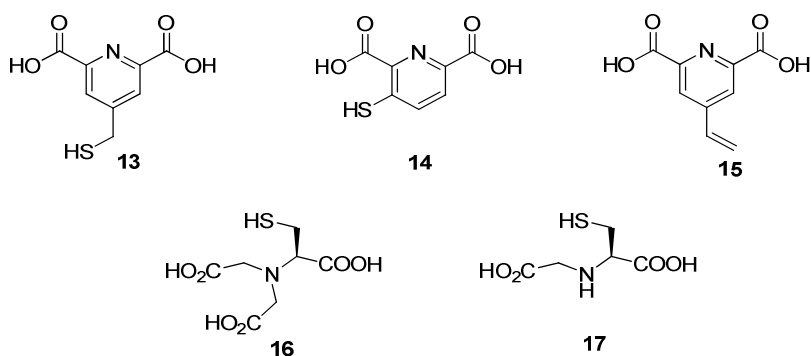


Figure 5. Structures of small lanthanoids chelating probes. DPA-based probes: (4MMDPA, **13**)⁵³, (3MDPA, **14**)⁵², (4-vinylpyridine-2,6-dicarboxylic acid, **15**)⁵⁴; cysteine derivatives: (NTA-SH, **16**)⁵⁶, (IDA-SH, **17**)⁵⁵.

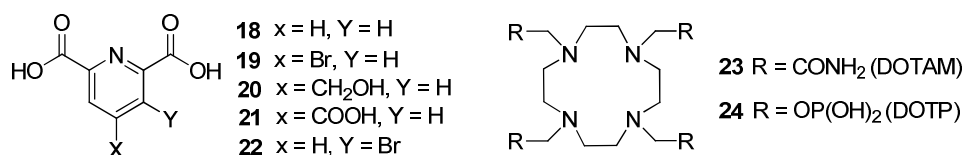


Figure 6. Structures of non-covalent binding probes. DPA-based probes (**18–22**)⁶⁰ and DOTA analogs (**23** and **24**)⁶¹.

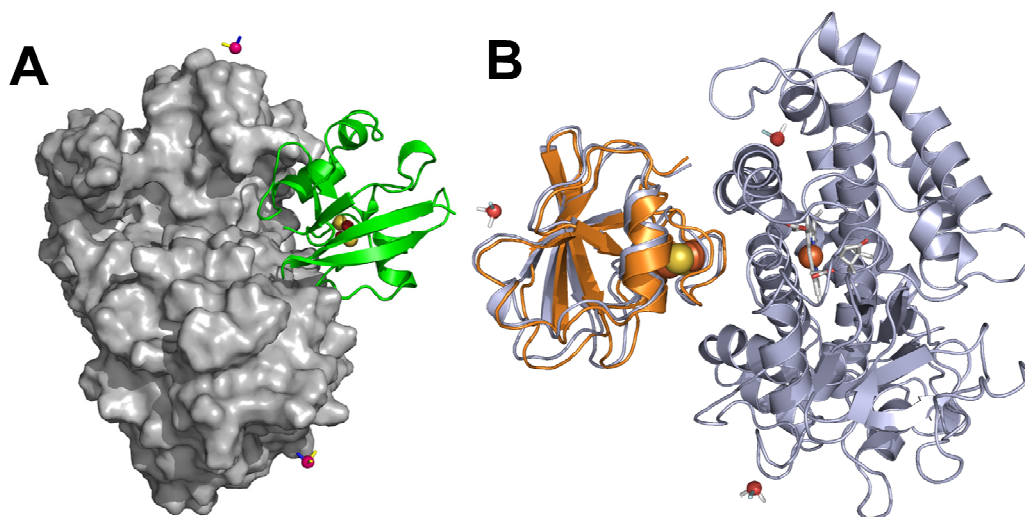


Figure 7. Solution models of the protein complexes. (A) The 65 kDa complex of adrenodoxin and adrenodoxin reductase was based on PCSs and PREs data.⁸⁰ Adrenodoxin is shown in green and the reductase is presented in gray surface representation. (B) The crystal structure (orange) and the solution structure, which based on PCSs, PREs and RDCs, closest to the mean (gray) of the oxidized putidaredoxin–cytochrome P450cam complex are shown in a ribbon representation with the P450cam structures aligned.⁹⁷ The iron-sulfur clusters of putidaredoxin and adrenodoxin are shown in CPK colors, the haem of cytochrome P450cam in stick and the haem iron in brown sphere. The position of lanthanoids chelated **7b** (A) and **8** (B), respectively, was attached to proteins, which are shown as red spheres. The axis frame represents the $\Delta\chi$ -tensor of lanthanoids in blue for the z-axes and in yellow for the x and y-axes. Reprinted with permission from [5] and [97]. Copyright (2013) Elsevier.

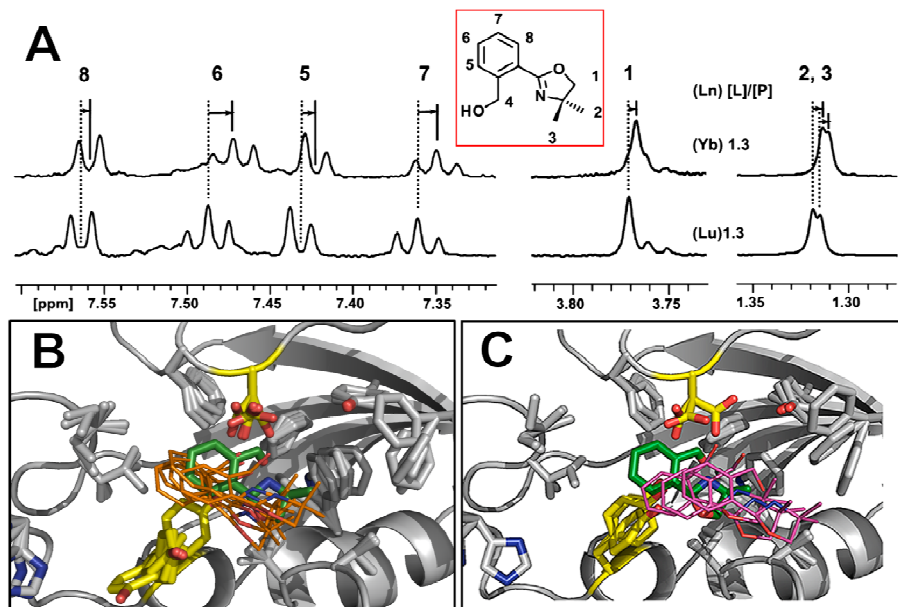


Figure 8. Localization of a ligand on the surface of a protein using ligand PCSs.¹⁰² (A) Overlay of 1D ^1H NMR spectra of ligand in the presence of Yb^{3+} -**7b** and Lu^{3+} -**7b** linked protein. The ligand PCS is defined by the difference between the resonance position for the Yb^{3+} (solid line) and the Lu^{3+} (dashed line) and the proton assignments of ligand are indicated by corresponding numbers on the structure. Due to the low affinity of the ligand for the protein, the spectra represent the PCSs for the ligand that is bound only 2% of the time and is in fast exchange between the free and bound states. (B, C) The lowest energy clusters of ligand positions, calculated using experimentally (B, orange) and predicted (C, magenta) determined $\Delta\chi$ -tensors. All of the calculated structures are superimposed on the NOE based structure (green). Reprinted with permission from [102]. Copyright (2013) American Chemical Society.

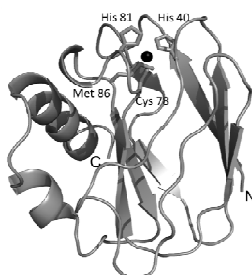


Figure 9. Structure of Paz (PDB code 8PAZ)¹²⁷. The protein is shown in grey, the copper in black and the ligands of the Cu in sticks labeled with residues numbers. This figures as well as 10 - 12 were made with the program PyMOL. [copyright 2010 Schrodinger, LLC]

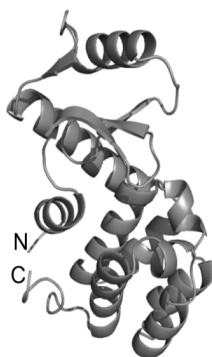


Figure 10. Ribbon structure of T4 Lys (PDB code 2LZM)¹²⁸.

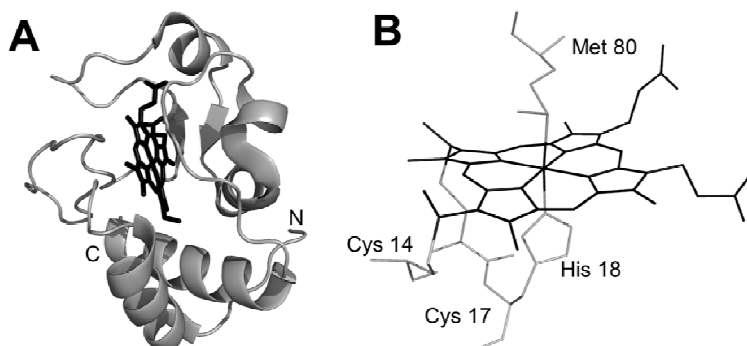


Figure 11. Structure of yeast Cyt *c* (PDB code 1YCC)¹¹⁸. (A) The ribbon represents the structure of Cyt *c* (grey) and the haem is shown in sticks (black). (B) The view of haem binding site. The porphyrin ring and two axial ligands, His 18 and Met 80, are coordinated to the haem ion, and the haem is covalently bound to the two cysteine residues, Cys 14 and Cys 17.

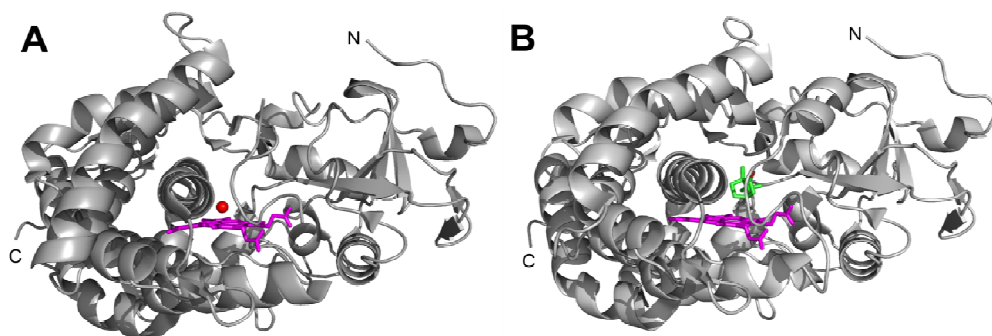


Figure 12. Structures of open state (A, PDB entry 3L62)¹²⁴ and closed state (B, PDB entry 3L63)¹²⁴ of P450cam. The P450cam is shown in gray ribbon, the haem in magenta, the coordinated water in red, and the camphor in green.

Chapter II

A pH sensitive, colorful, lanthanoid-chelating paramagnetic NMR probe

Based on the research article:

Liu, W. -M.; Keizers, P. H. J.; Hass, M. A. S.; Blok, A.; Timmer, M.; Sarris, A. J. C.; Overhand, M.; Ubbink, M. "A pH-sensitive, Colorful, Lanthanide-chelating Paramagnetic NMR Probe" *J. Am. Chem. Soc.* **2012**, *134*, 17306-17313.

Abstract

Paramagnetic lanthanoid ions are broadly used in NMR spectroscopy. The effects of unpaired electrons on NMR spectral parameters provide a powerful tool for the characterization of macromolecular structures and dynamics. Here, a new lanthanoid chelating NMR probe, Caged Lanthanoid NMR Probe-7 (CLaNP-7), is presented. It can be attached to protein surfaces *via* two disulfide bridges, yielding a probe that is rigid relative to the protein backbone. CLaNP-7 extends the application range of available probes. It has a yellow color, which is helpful for sample preparation. Its effects are comparable to those of CLaNP-5, but its charge is two units lower (+1) than that of CLaNP-5 (+3), reducing the change in surface potential after probe attachment. It also has a different magnetic susceptibility tensor, so by using both tags, two sets of structural restraints can be obtained per engineered cysteine pair. Moreover, it was found that the orientation of the magnetic susceptibility tensor is pH dependent ($pK_a \sim 7$) when a histidine residue is located in the neighborhood of the probe attachment site. The results show that the His imidazole group interacts with the CLaNP-7 tag. It is proposed that the histidine residue forms a hydrogen bond to a water/hydroxyl molecule that occupies the ninth coordination position on the lanthanoid, thus breaking the two-fold symmetry of the CLaNP tag in a pH-dependent way.

Introduction

In recent years, paramagnetic probes have been used broadly in nuclear magnetic resonance (NMR) spectroscopy. The effects of unpaired electrons on NMR spectral parameters, such as pseudocontact shifts (PCSs), residual dipolar couplings (RDCs) and nuclear relaxation enhancements (PREs), have been recognized as powerful tools for the characterization of macromolecular structures and their dynamics and interactions.^{5,9,95,129-133} Among the paramagnetic effects, PCSs yield valuable long-range distance and orientation information and RDCs are distance-independent, providing information on the whole protein, making them powerful restraints to refine protein structures and determine protein orientations in complexes.¹³⁴

To yield unambiguous restraints, the paramagnetic center must be site-specifically and rigidly attached to the protein. For Ca^{2+} or Mg^{2+} containing metalloproteins, lanthanoid ions can substitute the natural metal,^{66,135,136} but most proteins are devoid of these metal binding sites. Therefore, several methods have been developed to introduce artificial paramagnetic metals into protein. For instance, metal binding peptide tags were designed that can be engineered genetically at the N or C terminus or into a loop region of a protein.^{71,74,75,101,137} Other strategies use synthetic organic thio-functional tags, which can be introduced *via* cysteine mutations.^{5,44,56}

1,4,7,10-tetraazacyclododecane-1,4,7,10-tetraacetic acid (DOTA) is a typical ligand for lanthanoid ions. The coordination of DOTA to lanthanoid ions results in two stable diastereomers, a square antiprism (SA) and a twisted square antiprism (TSA).¹³⁸⁻¹⁴¹ Each diastereomer relates to one of two possible configurations of the macrocycle rings ($\lambda\lambda\lambda\lambda$ and $\delta\delta\delta\delta$) and one of two orientations of the chelate arms (Δ and Λ). The enantiomers $\Delta\lambda\lambda\lambda\lambda$ and $\Lambda\delta\delta\delta\delta$ belong to the SA structures, whereas the pair of $\Lambda\lambda\lambda\lambda\lambda$ and $\Delta\delta\delta\delta\delta$ forms the TSA conformation. In previous studies, we have developed paramagnetic lanthanoid probes based on cyclen.^{11,36,40} The probes are attached to target proteins *via* two disulfide bridges, which strongly reduces the mobility.⁴⁰ In the most recent version, two chelating pyridine-*N*-oxide arms force the probe to exist into one diastereomer, the SA form, in the solution state.^{11,39} This results in singular NMR resonances and one magnetic susceptibility tensor. This probe, named Caged Lanthanoid NMR Probe-5 (CLaNP-5, Figure 1), showed the largest PCSs and RDCs described so far.¹¹ A drawback is the total charge of the

probe, which is 3+ after chelation with a lanthanoid ion. When CLaNP-5 is linked to a protein surface, the extra charge changes the electrostatic potential, which may affect molecular interactions with ligands and proteins. In this chapter, a new tag is described (CLaNP-7, Figure 1) that has a reduced net charge while maintaining conformational rigidity. Ln-CLaNP-7 complexes have different magnetic susceptibilities than those of CLaNP-5 and its endogenous color allows for easy detection of tagged protein. Furthermore, we show that CLaNP-7 can interact with a nearby histidine residue, causing a pH dependence of the magnetic susceptibility tensor (χ -tensor). It was shown that two sets of distance restraints can be obtained, simply by changing the pH. A model for the pH dependent interaction is proposed.

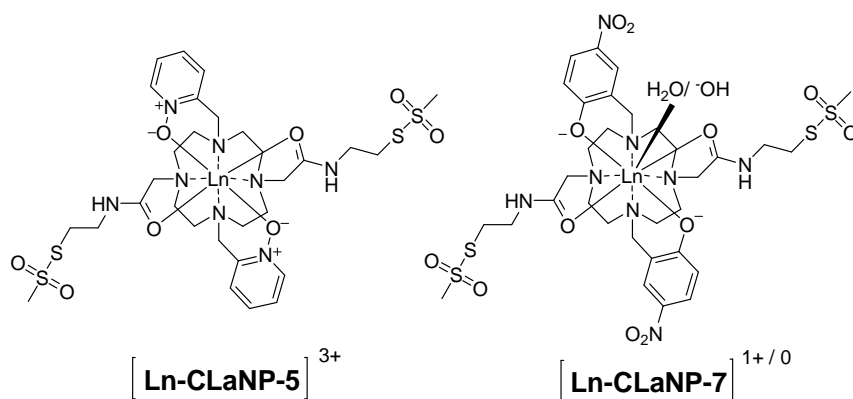


Figure 1. Structures of Ln-CLaNP-5¹¹ and Ln-CLaNP-7.

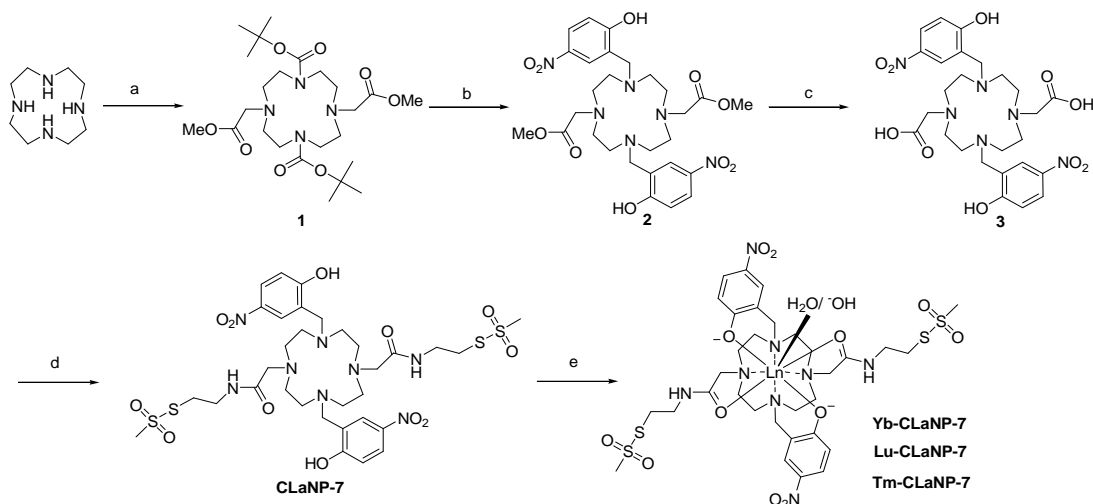
Results

Synthesis of Caged Lanthanoid NMR Probe-7 (CLaNP-7)

In 2004, Prof. A. D. Sherry's group published a study on a MRI contrast agent based on the cyclen scaffold and carrying a *p*-nitrophenol ligating group.⁴³ The crystal structure of the MRI contrast agent indicated that the phenol is deprotonated and a water molecule sits above the plane of the oxygen atoms. In order to design a rigid cyclen based probe with a reduction of net positive charge, the pyridine-*N*-oxide arms used for CLaNP-5 were replaced with *p*-nitrophenol arms (Figure 1). The *p*-nitro groups enhance the acidity of the phenolic protons and upon binding the lanthanoid, the phenol groups will be deprotonated. As the lanthanoid has a charge of +3, the net charge of the entire complex will be +1, unless a hydroxyl ion rather than a water molecule can coordinate, in which case the overall charge is zero (see

below). The two *p*-nitrophenol groups provide *C*₂-symmetry and it was anticipated that the two six-membered ring chelating systems (Figure 1) provide sufficient rigidity and thus lead to one preferred tetraazacyclododecane ring conformation.³⁹ The yellow color associated with *p*-nitrophenolate groups is convenient for the purification of tagged proteins.

The synthesis of CLaNP-7 is shown in Scheme 1. Commercially available cyclen was converted into **1** in 83% yield over two steps, in which two opposing amines were temporarily protected with *tert*-butoxycarbonyl (Boc) groups and the other two amines subsequently functionalized by reaction with methyl bromoacetate.⁴¹ Compound **1** was deprotected by trifluoroacetic acid (TFA) and reacted with 2-hydroxy-5-nitrobenzyl bromide at 80 °C to obtain **2**.^{43,142} Removal of the methyl ester group in the presence of base in 1,4-dioxane as solvent yielded **3**.¹⁴³ Condensation of **3** with excess 2-(aminoethyl)-methanethiosulfonate in presence of 1-ethyl-3-(3-dimethylaminopropyl)carbodiimide (EDC) and *N*-hydroxysuccinimide (NHS) yielded CLaNP-7 in 40% yield. The Yb-CLaNP-7, Tm-CLaNP-7 and Lu-CLaNP-7 complexes were obtained by chelating with the corresponding lanthanoid acetate salts in *N,N*-dimethylformamide (DMF). After chelation, the wavelength of the maximum absorbance shifted from 310 nm to 390 nm and the tag obtained a more intense yellow color (Figure 2A).



Scheme 1. Synthesis of CLaNP-7. (a) i) BocOSu, CHCl₃, RT 36 h; ii) methyl bromoacetate, K₂CO₃, RT, 12 h; (b) i) TFA, DCM, RT, 4 h; ii) 2-hydroxy-5-nitrobenzyl bromide, K₂CO₃, ACN, 80 °C, 12 h; (c) NaOH, 1,4-dioxane, RT, 4 h (d) aminoethyl-MTS, NHS, EDC, DMF, RT, 16 h; (e) Ln(OAc)₃, DMF, RT, 4 h, quant.

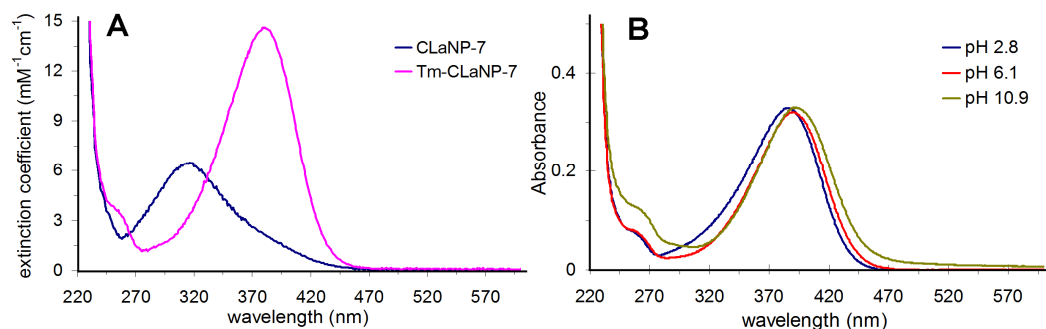


Figure 2. Electronic absorption spectra of CLaNP-7. (A) The absorbance spectra expressed as extinction coefficients are plotted for CLaNP-7 and Tm-CLaNP-7. (B) Lu-CLaNP-7 at different pH values.

Probe attachment and $\Delta\chi$ -tensors calculation:

The Zn²⁺-form of ¹⁵N-enriched E51C/E54C pseudoazurin (Paz) was reduced with dithiothreitol (DTT), washed, and directly incubated with Ln-CLaNP-7 for 16 h at 4 °C. The tagged protein was purified using a Superdex 75 column (GE Healthcare). The mass of the resulting ¹⁵N-Paz Yb-CLaNP-7 (14503 ± 2 Da) agreed with the expected mass of 14503 Da, assuming 98% ¹⁵N enrichment. In the [¹⁵N-¹H]-HSQC spectra, there were no significant differences between untagged and Lu-CLaNP-7 tagged spectra, except for a few residues close to the attachment site, enabling the resonance assignments to be made by comparison with previous spectra.³¹ Large shifts of resonances were observed when the protein was tagged with either Yb-CLaNP-7 or Tm-CLaNP-7 (Figure 3). The ¹⁵N rich Paz were kindly provided by Ms. Anneloes Blok and Dr. Monika Timmer (Leiden University, Inst. Chemistry).

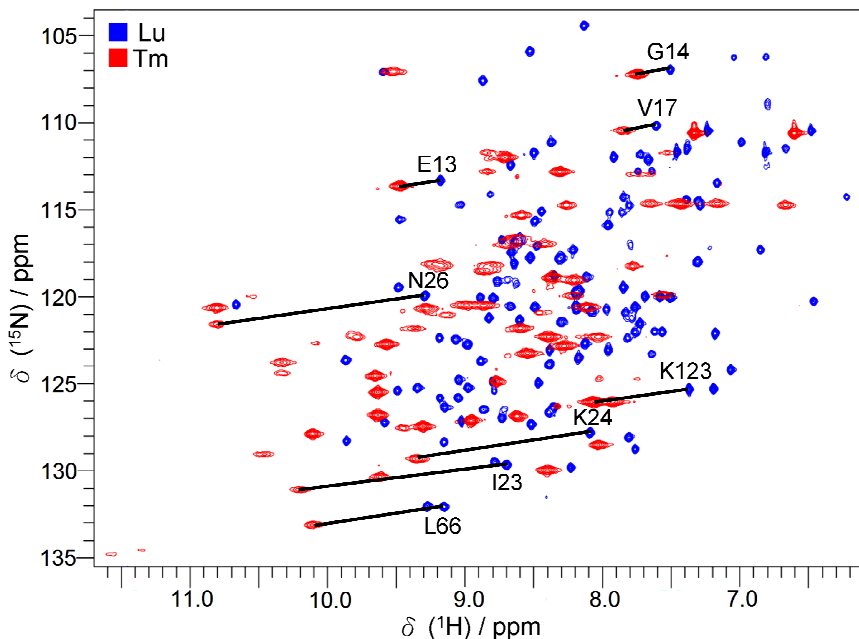


Figure 3. Overlay of $[\text{}^{15}\text{N}, \text{}^1\text{H}]$ -HSQC spectra of Paz E51C/E54C attached to Lu-CLaNP-7 (blue) and Tm-CLaNP-7 (red). Several PCSs are indicated with solid lines.

The difference in resonance frequency between the paramagnetic and the diamagnetic samples was defined as the PCS. The presence of large, single PCSs indicates the tag to be attached rigidly and to exist in one dominant conformation, which is expected to be the SA isomer due to the six-member chelating system (but see Discussion section).³⁹

For estimation of the anisotropic component of the magnetic susceptibility tensor ($\Delta\chi$ -tensors), an initial metal position was fixed according to a previously reported protocol.¹¹ An initial set of PCSs was used to determine the $\Delta\chi$ -tensor, with which more PCSs were predicted. In an iterative way, the $\Delta\chi$ -tensor and metal position were refined and additional resonances were assigned. The $\Delta\chi$ -tensor values for Tm- and Yb-CLaNP-7, along with those of CLaNP-5 are reported in Table 1 and the back-calculated PCSs are plotted versus the observed PCSs in Figures 4A and Appendix 1, respectively. The values of $\Delta\chi_{\text{ax}}$ and $\Delta\chi_{\text{rh}}$ of CLaNP-7 are similar to those of CLaNP-5 for Tm^{3+} , but not for Yb^{3+} . The $\Delta\chi$ -tensor of Yb-CLaNP-7 is much more rhombic. A possible explanation could be the presence of a ninth ligand, a water molecule or hydroxyl ion. This possibility is discussed in more detail in the next section. Tm-CLaNP-7 causes significant alignment of Paz at 600 MHz (14.1 T),

allowing RDCs up to 20 Hz to be observed. The observed RDCs were used to optimize the HN positions of Paz and the $\Delta\chi$ -tensor derived from PCS was used to back-calculate the RDCs on the basis of this structure, yielding a good agreement (Figure 4B). The large RDCs indicate a low mobility of CLaNP-7 relative to the protein backbone.

Table 1. PCSs-based $\Delta\chi$ -tensors of CLaNP-5¹¹ and CLaNP-7^a

Protein	Probe	Ln	$\Delta\chi_{ax}^c$	$\Delta\chi_{rh}^c$	Restrains	Q ^b
Paz E51C/E54C	CLaNP-5	Tm	55.5 \pm 0.8	10 \pm 1	89	0.03
		Yb	9.4 \pm 0.2	1.9 \pm 0.4	93	0.04
	CLaNP-7	Tm	41.4 \pm 0.6	9.6 \pm 0.8	94	0.04
		Yb	4.2 \pm 0.1	5.6 \pm 0.4	93	0.06
Cyt <i>c</i> N56/L58C	CLaNP-7 (pH = 6)	Yb	6.3 \pm 0.4	8.0 \pm 0.3	70	0.03
	CLaNP-7 (pH = 8)	Yb	5.5 \pm 0.9	9.6 \pm 0.3	60	0.06
Cyt <i>c</i> N56C/L58C/H39A	CLaNP-7 (pH = 6.3)	Yb	5.5 \pm 0.2	6.5 \pm 0.1	70	0.04
	CLaNP-7 (pH = 7.8)	Yb	5.5 \pm 0.1	6.1 \pm 0.1	62	0.04

^a The unit of axial and rhombic components ($\Delta\chi_{ax}$ and $\Delta\chi_{rh}$) is 10⁻³² m³.

^b The definition of Q is given in experimental section (eq 2).

^c The error is calculated by a jackknife procedure randomly removing 20% of the data and repeating the $\Delta\chi$ -tensor fit 100 times.

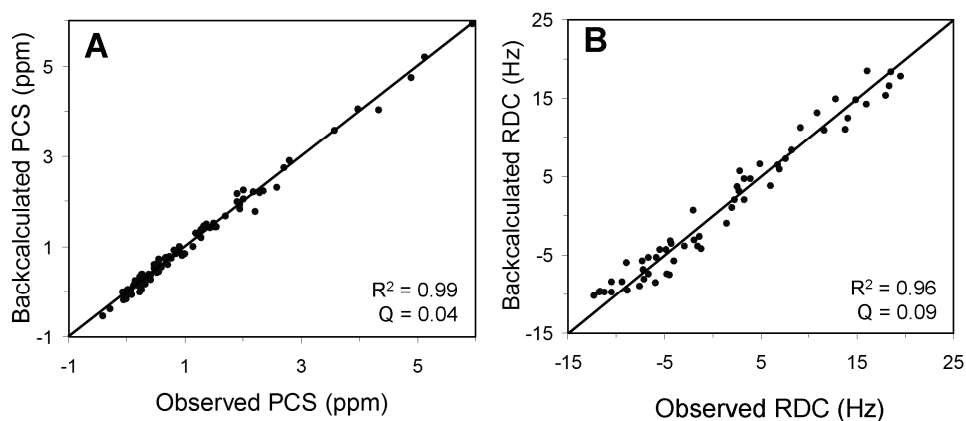


Figure 4. Experimentally observed amide proton PCSs and RDCs of Paz E51C/E54C Tm-CLaNP-7 plotted against the back-calculated PCSs (A, $Q = 0.04$) and RDCs (B, $Q = 0.09$), both based on the PCS derived $\Delta\chi$ -tensor. The NMR spectra were recorded at 14.1 T (600 MHz). The solid line represents a perfect match.

The pH dependence of CLaNP-7

In order to test CLaNP-7 on a second protein, yeast cytochrome *c* (Cyt *c*) N56C/L58C was tagged with CLaNP-7 coordinated to Yb³⁺ and Lu³⁺. In the diamagnetic spectrum (Lu-CLaNP-7) only single peaks were observed. However, at pH 7, the Cyt *c* tagged with Yb-CLaNP-7 showed two sets of peaks for most residues. The relative intensity and sometimes the sign as well changed with pH (Figures 5 and Appendix 2). From the PCSs obtained at pH 6 and pH 8, the $\Delta\chi$ -tensors were determined. A comparison of the PCSs shows that they differ significantly (Appendix 3). The sizes of the axial and rhombic components are similar at both pH values and somewhat larger than for Paz E51C/E54C (Table 1 and Appendix 4). The major difference between pH 6 and 8 is the orientation of the tensors (Figure 6A). The structurally highly similar tag Ln-CLaNP-5 shows a single set of resonances when attached to the same double Cys mutant of Cyt *c* (Appendix 5).⁹⁸ Also for CLaNP-7 attached to Paz E51C/E54C no pH dependence of the PCS was observed, so the observed effect is specific for CLaNP-7 attached to Cyt *c* N56C/L58C. The ¹⁵N rich Cyt *c* were kindly provided by Ms. Anneloes Blok and Dr. Monika Timmer (Leiden University, Inst. Chemistry).

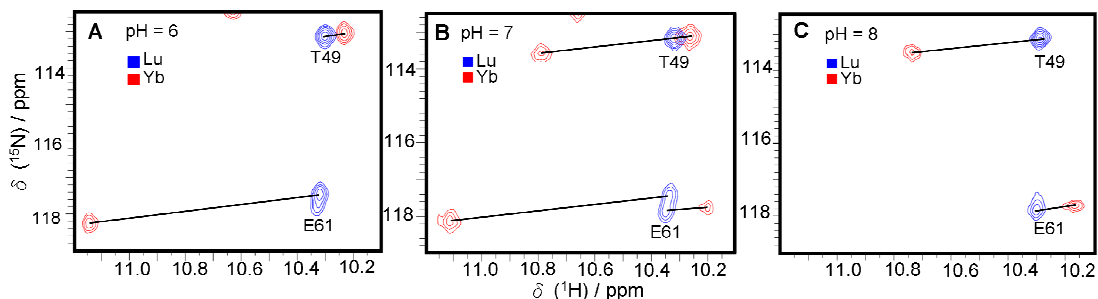


Figure 5. pH dependence of CLaNP-7. Detail of [¹⁵N, ¹H]-HSQC spectra of Cyt *c* N56C/L58C attached to Lu-CLaNP-7 (blue) and Yb-CLaNP-7 (red) at pH = 6.0 (A), pH = 7.0 (B) and pH = 8.0 (C).

Protonation of the phenol moiety of CLaNP-7 as an explanation for the pH dependence was ruled out by the electronic absorption spectrum. Protonation of the phenol shifts the absorbance maximum from 390 nm to 310 nm.¹⁴⁴ From Figure 2A, it is clear that in free CLaNP-7 purified by HPLC the phenol rings are protonated, but upon coordination to Tm³⁺ they are deprotonated at pH values between 3 and 11 (Figure 2B). In general, there is a water coordinated to the DOTA-like lanthanoid

ions complex in solution state.¹⁴⁵ The factors that affect water coordination are mainly the charge density of the lanthanoid ion and the steric strain at the water binding site.¹⁴⁶⁻¹⁴⁸ The substitution of the pyridine-*N*-oxide rings in CLaNP-5 with *p*-nitrophenol rings in CLaNP-7 lowers the charge of the coordinated oxygen of the ligand, which results in a larger space for a ninth coordination.^{39,43} Thus, it is likely that a water molecule or hydroxyl ion can be coordinated to the lanthanoid.

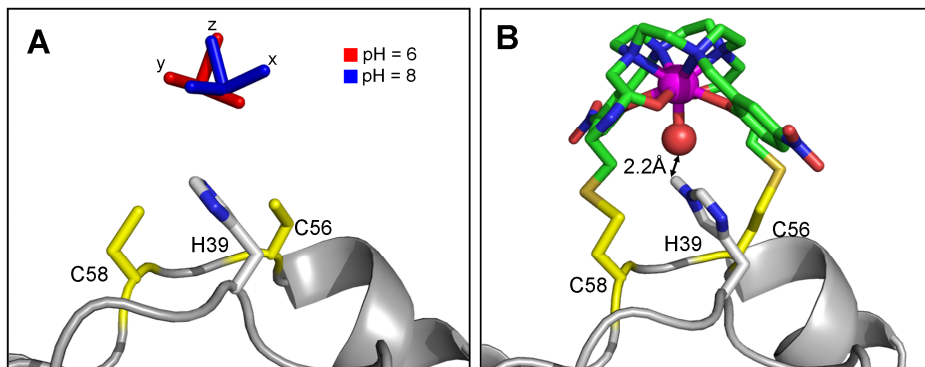


Figure 6. PCS-based positions of the tensor relative to the Cyt *c* structure with PDB entry code 1YCC.¹¹⁸ The Cys residues at positions 56 and 58 were modeled. (A) The principal axes of the $\Delta\chi$ -tensor of Yb-CLaNP-7 are shown as red (pH 6) and blue sticks (pH 8); (B) Model of CLaNP-7 attached to Cyt *c* N56C/L58C. The position of the Yb³⁺ (magenta) is derived from a fit to the PCS data. The red sphere shows the H₂O/OH at the ninth coordination position. The protein main chain is shown in grey. The Cys (N56C/L58C) and the His 39 side-chains are shown in CPK colors. The carbon atoms from CLaNP-7 are shown in green, nitrogen atoms in blue, oxygen atoms in red and sulfur atoms in yellow. The distance between the H^{ε2} of His 39 and the ligating oxygen atom is 2.2 Å.

In Cyt *c* N56C/L58C the Cys residues are located in a short β -strand and there is a histidine residue, His 39, in the neighboring strand, close to the tag attachment site. Fitting of the PCSs placed the lanthanoid close to His 39 and its imidazole ring can be rotated to be at hydrogen bond distance of a water molecule at the ninth coordination position (Figure 6B). Therefore, we propose that the observed pH dependence of the $\Delta\chi$ -tensor is caused by the imidazole of His 39.

In order to test this hypothesis, the His residue in Cyt *c* N56C/L58C was mutated to alanine and this variant was labeled with Ln-CLaNP-7. The pH dependence of the $\Delta\chi$ -tensor is no longer observed in the absence of the imidazole ring. The [¹⁵N, ¹H]-HSQC spectra shows single peaks at several pH values

(Appendix 6A) and the PCS and the $\Delta\chi$ -tensors are the same at low and high pH (Table 1 and Appendix 7). The peaks only exhibit small shifts due to the normal pH dependence of the protein and those shifts are identical in paramagnetic and diamagnetic samples (Appendix 6B). These observations support the proposal that His 39 influences the $\Delta\chi$ -tensor in a pH dependent manner. The ^{15}N rich Cyt *c* H39A/N56C/L58C were kindly provided by Ms. Anneloes Blok and Dr. Monika Timmer (Leiden University, Inst. Chemistry).

We wondered whether it was possible to introduce the pH dependence of the tensor by positioning the probe close to a His residue on a protein surface. For this purpose we returned to Paz, which is a β -sheet protein. His 6 is located on a long β -strand. In the neighboring strand two Cys residues were engineered, mutant I34C/V36C. The ^{15}N rich Paz I34C/V36C were kindly provided by Ms. Anneloes Blok and Dr. Monika Timmer (Leiden University, Inst. Chemistry). Using the published protocol for modeling of the CLaNP lanthanoid position,¹¹ it was predicted that the imidazole ring of His 6 would be sufficiently close to form a H-bond to a possible $\text{H}_2\text{O}/\text{OH}$ at the ninth coordination position (Appendix 8). The HSQC spectra clearly show two peaks for most resonances in this Paz variant labeled with Yb-CLaNP-7 and the intensity of these peaks indeed varies with pH, analogous to what was observed for Cyt *c* N56C/L58C (Figure 7). Note that Paz E51C/E54C labeled with CLaNP-7 did not show pH dependence. These results indicate that the pH dependence of the $\Delta\chi$ -tensor can be introduced when the probe is positioned on a β -sheet, next to a histidine residue. The pH dependence of CLaNP-7 may be used to obtain two independent sets of PCSs or RDCs from a single probe.

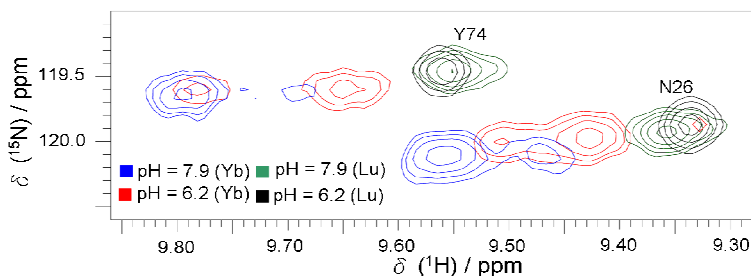


Figure 7. Detail of ^{15}N , ^1H -HSQC spectra of Ln-CLaNP-7 tagged ^{15}N -labeled Paz I34C/V36C. The spectra were recorded at pH 6.22 (black, Lu; red, Yb) and pH 7.9 (green, Lu; blue, Yb).

Discussion

Proposed mechanism for CLaNP-7 pH dependence

Based on the $\Delta\chi$ -tensor, the position of the Yb-CLaNP-7 linked to Cyt *c* N56C/L58C is the same within error at pH 6 and 8. However, the orientations of the tensors are different (Figure 6A). The two sets of peaks in the HSQC spectra of Yb³⁺ labeled protein indicate that these orientations are a consequence of two orientations/conformations of the probe that are in slow exchange on the NMR chemical shift timescale. In contrast to what is expected for a simple pH titration in which the two sets of peaks would correspond to a protonated and deprotonated form, here both sets of peaks remain (weakly) visible, even at the highest and lowest pH values applied. Furthermore, not only do the relative intensities of the pairs of peaks change with pH, the PCSs of both states also exhibit some pH dependence (Appendix 9).

In order to explain these observations, a four-state model is invoked (Figure 8). The model hypothesizes that the two-fold symmetry of the probe is broken by the interaction between the imidazole of the nearby histidine and the proposed H₂O/OH coordinated to the Yb³⁺. Consequently, the two SA enantiomers ($\Delta\lambda\lambda\lambda\lambda$ and $\Lambda\delta\delta\delta\delta$) no longer yield identical PCS and now cause double peaks, because cyclen ring flips are normally slow.^{149,150} Protonation/deprotonation of the imidazole shifts the equilibrium between these two states. It also causes the pH dependence of the PCSs of both states (Appendix 9). The intensity ratio (I_b/I_a) of the pairs of peaks can be described on the basis of this model by eq. 1:

$$\frac{I_b}{I_a} = K \frac{[1 + 10^{(pH - pK_{a2})}]}{[1 + 10^{(pH - pK_{a1})}]} \quad \text{eq.1}$$

Where I_a and I_b are the peaks intensity of the two sets of peaks and I_b is most intense at high pH, K is the equilibrium constant, and pK_{a1} and pK_{a2} are the proton association constants. Fitting the observed intensity ratio of the peaks for Cyt *c* N56C/L58C to eq. 1 yields the curve given in Figure 8B. The equilibrium changes from $K = 0.52$ to $K' = 3.36$, where $K' = K(K_{a1}/K_{a2})$, so state III becomes the dominant conformation when going from high to low pH. For Paz I34C/V36C the effect is also clearly present, although the shift in the equilibrium is smaller (Figure 8B). The equilibrium rates were kindly calculated by Dr. Mathias A. H. Hass (Leiden University, Inst. Chemistry).

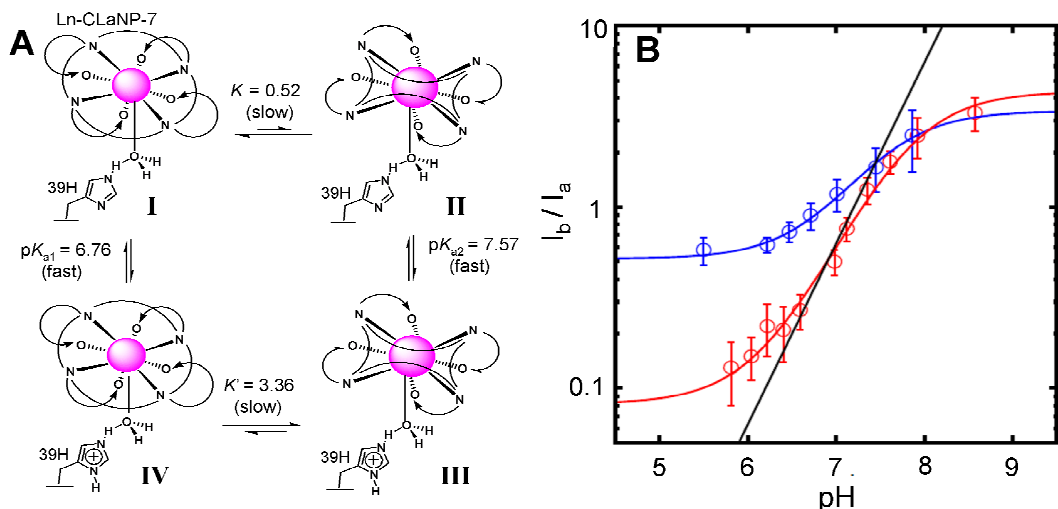


Figure 8. Proposed model to describe pH dependence of CLaNP-7. (A) The flip between two SA forms ($\Delta\lambda\lambda\lambda\lambda$ and $\Lambda\delta\delta\delta\delta$) are schematically represented by a change in the cyclen ring (lines connecting the N atoms) and the ligand arms (round arrows). The values were obtained from a fit to the I_b/I_a ratios of Cyt *c* N56C/L58C at multiple pH values (eq. 1). (B) Intensity ratios as a function of pH. The averaged intensity ratios for pairs of resonances in Cyt *c* N56C/L58C (red) and Paz I34C/V36C (blue) are plotted as a function of pH. The solid lines represent fits to the model described in the text (eq. 1). The intensity ratios are averaged from 13 residues for Cyt *c* and 10 residues for Paz and the error bars are the standard deviation. The black line represents a standard deprotonation curve.

Comparison with CLaNP-5

Tm-CLaNP-5 and Tm-CLaNP-7 were attached to Paz E51C/E54C and both cause large PCSs and RDCs, but these shifts and couplings differ in size and sometimes sign as well (Appendix 10). The position of the metal, as well as the size and orientation of the $\Delta\chi$ -tensor were obtained by fitting to the PCS data. The PCS histograms have an overall similar appearance for both tags because PCS is dominated by the distance between the nucleus and the metal. However, detailed inspection shows clear differences that reflect the somewhat smaller size and changed orientation of the CLaNP-7 $\Delta\chi$ -tensor. Also the positions of the Ln-ions are different by 3.4 Å (Figure 9C). The RDC histograms show many more differences (Appendix 10B), because RDC is solely dependent on the H-N bond vector orientation in the $\Delta\chi$ -tensor frame. The RDCs range from -15 Hz to +20 Hz for Tm-CLaNP-7 and from -20 Hz to +30 Hz for Tm-CLaNP-5 at 14.1 T (600 MHz). The

observed PCSs and RDCs of CLaNP-7 were plotted versus the observed PCSs and RDCs of CLaNP-5 (Figure 9) and show poor agreements between CLaNP-5 and CLaNP-7. It is concluded that the two probes cause sufficiently different effects to yield complementary structural restraints from a single attachment site.

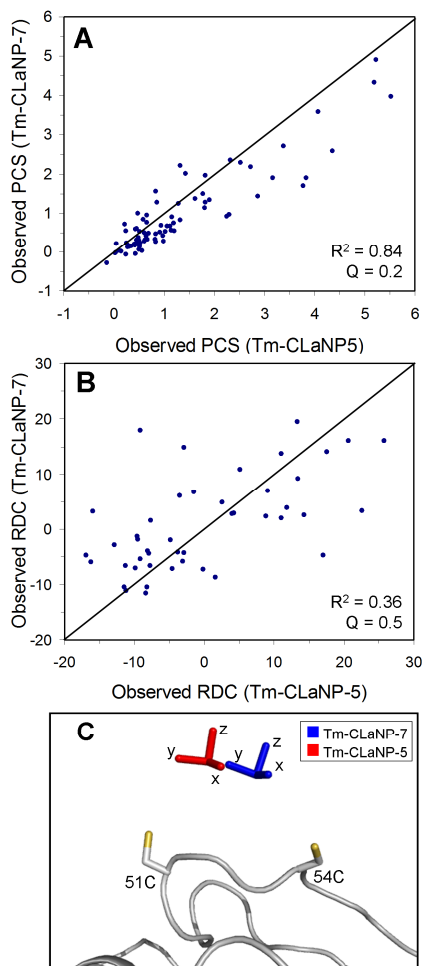


Figure 9. Comparison of CLaNP-5 and CLaNP-7. Experimentally observed PCSs and RDCs from Tm-CLaNP-7 plotted against the experimentally observed PCSs (A, $Q = 0.2$) and RDCs (B, $Q = 0.5$) from Tm-CLaNP-5 for Paz E51C/E54C. The solid line represents a perfect correlation. (C) Experimentally determined position and orientation of the Tm³⁺ $\Delta\chi$ -tensor relative to the Paz (PDB: 1PY0)³¹ structure for CLaNP-5 (red sticks) and for CLaNP-7 (blue sticks). The Cys side-chains are shown in CPK colors.

Conclusion

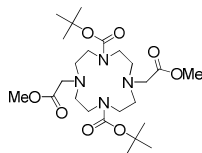
CLaNP-7 is a new two-armed lanthanoid chelating protein probe that provides large PCSs and RDCs. CLaNP-7 and CLaNP-5 have different magnetic susceptibility tensors, providing a convenient way to obtain different paramagnetic effects from the same target protein with a single set of engineered Cys residues. In addition, the lower net charge of CLaNP-7 will be beneficial in protein-protein interaction studies. CLaNP-7 has a bright yellow color simplifying the sample handling, and importantly, it is the first example of a pH sensitive paramagnetic probe offering a unique opportunity to tune paramagnetic effects.

Experimental Section

General

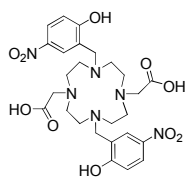
$\text{Ln}(\text{OAc})_3$, cyclen, 2-(aminoethyl)methanethiosulfonate hydrobromide, 2-hydroxy-5-nitrobenzyl bromide and all other chemicals were used as purchased without further purification. TLC-analysis was conducted on DC-alufolien (Merck, Kieselgel60, F254) with detection by UV-absorption (254 nm). Flash chromatography was performed on Screening Devices silica gel 60 (0.04-0.063 mm). A Biocad Vision HPLC (PerSeptive Biosystems, inc.) and an Akta Basic FPLC (GE Healthcare Inc.) were used for purifications. Analytical, semipreparative, and preparative reversed phase C18 columns were obtained from Phenomenex (Torrance, CA). Superdex 75, CM sepharose and HiTrap SP columns were obtained from GE Healthcare. NMR spectra were recorded on a Bruker AV-400 (400/100 MHz) and Bruker Avance-III 600 (600/150 MHz) spectrometer. A LCQ LCMS system and a Finnigan LTQ Orbitrap system were used for HRMS and protein conjugation analysis. FTIR was performed on a Perkin-Elmer (Shelton, CT) Paragon 1000 FTIR spectrometer. Melting points were obtained using a SMP3 scientific melting apparatus (Stuart, Bibby Sterlin Ltd.)

1,7-diBoc-1,4,7,10-tetraazacyclododecane-4,10-dimethyl acetate (1)



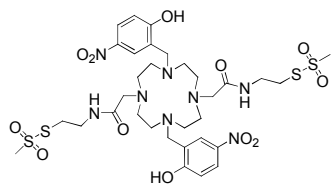
BocOSu (2.49 g, 11.6 mmol) was dissolved in dry CHCl_3 (20 mL) and was added under argon to a cyclen (1 g, 5.8 mmol) solution in CHCl_3 (40 mL). The reaction mixture was stirred at room temperature for 36 h. To the reaction mixture 3 M NaOH (30 mL) was added and

stirring was continued for 30 min. Brine (30 mL) was added and the solution was extracted with dichloromethane (3 x 20 mL). The organic fractions were combined, dried over MgSO_4 and concentrated *in vacuo*. The remaining colorless oil was dissolved in acetonitrile (30 mL). K_2CO_3 (1.94 g, 14.5 mmol) and methyl 2-bromoacetate (2.22 g, 14.5 mmol) were added into the solution and stirred for 12 h at room temperature. The reaction mixture was concentrated, dissolved in ethyl acetate and washed with brine. The organic layer was dried (MgSO_4), filtered and concentrated. The resulting residue was purified by column chromatography to yield compound **1** as a white amorphous solid (2.48 g, 83% yield). m. p. = 82–83 °C. R_f = 0.3 (5% MeOH in DCM). ^1H NMR (400 MHz CDCl_3): δ = 1.27 (s, 18H), 2.69 (br, 8H), 3.21 (br, 8H), 3.28 (s, 4H), 3.51 (s, 6H). ^{13}C NMR (100 MHz CDCl_3): δ = 28.14, 46.21, 50.98, 54.36, 54.54, 79.05, 155.51, 171.39. FTIR: 2975.8, 1739.6, 1683.9, 1364.7, 1157.3 cm^{-1} . HR-MS m/z : 517.3225 $[\text{M}+\text{H}]^+$, calcd $[\text{C}_{24}\text{H}_{45}\text{N}_4\text{O}_8]$: 517.3232.



1,7-dimethylene-(*p*-nitrophenol)-1,4,7,10-tetraazacyclo-dodecane-4,10-diacetic acid (3**)**

Compound **1** (400 mg, 0.75 mmol) was dissolved in a mixture of dichloromethane and trifluoroacetic acid (4 mL, 1:3 v/v) and stirred for 4 h at room temperature. The reaction mixture was concentrated under reduced pressure and coevaporated with toluene to remove the trifluoroacetic acid. The crude mixture was dissolved in acetonitrile (10 mL). 2-hydroxy-5-nitrobenzyl bromide (435 mg, 1.88 mmol) and K_2CO_3 (260 mg, 1.88 mmol) were added into the solution, which was stirred for 12 h at 80 °C. The reaction mixture was filtered and the solid was washed with acetonitrile (30 mL). The filtrate was concentrated *in vacuo* to give a yellow oil. The crude compound was dissolved in a solution mixture which contained 1,4-dioxane (final concentration was 15 mM) and 3 M NaOH (final concentration was 0.4 M). The solution was stirred at room temperature for 4 h, then concentrated under reduced pressure and purified by HPLC (0.1% TFA and a 10–50% acetonitrile gradient on C18 preparative column). ^1H NMR (400 MHz CD_3OD): δ = 3.19 (s, 8H), 3.33 (s, 4H), 3.44 (s, 8H), 4.64 (s, 4H), 7.12 (d, 2H), 8.30 (d, 2H), 8.54 (s, 2H). ^{13}C NMR (100 MHz CD_3OD): δ = 174.71, 164.29, 142.31, 130.87, 129.33, 117.59, 117.39, 54.15, 51.57, 49.87. FTIR: 3084.3, 1728.1, 1667.9, 1593.1, 1496.0, 1338.9, 1286.1, 1185.8, 1133.0, 1084.8 cm^{-1} . HR-MS m/z : 591.2409 $[\text{M}+\text{H}]^+$, calcd $[\text{C}_{26}\text{H}_{35}\text{N}_6\text{O}_{10}]$: 591.2409.



CLaNP-7

Compound **3** (296 mg, 0.5 mmol) was dissolved in *N,N*-dimethylformamide (10 mL) and treated with 2-(aminoethyl)methanethiosulfonate hydrobromide (283.4 mg, 1.2 mmol), *N*-hydroxysuccinide (345.3 mg, 3 mmol) and *N*-(3-dimethylaminopropyl)-*N'*-ethylcarbodiimide (574.5 mg, 3 mmol). The reaction mixture was stirred 16 h at room temperature. The reaction mixture was concentrated under reduced pressure and purified by HPLC (0.1% TFA and a 20–45% acetonitrile gradient on C18 preparative column) yielding **CLaNP-7** (40%) as a yellow oil. ^1H NMR (600 MHz, d^6 -DMSO, 323 K): δ = 3.09 (s, 8H), 3.21 (s, 4H), 3.27 (s, 8H), 3.31 (t, 4H), 3.47–3.53 (br, m, 10H), 7.12 (d, 2H), 8.21 (q, 2H), 8.47 (s, 2H), 8.51 (s, 2H). ^{13}C NMR (150 MHz, d^6 -DMSO, 323 K): δ = 34.87, 38.21, 48.68, 49.80, 50.17, 51.52, 53.92, 116.40, 127.11, 129.22, 139.12, 164.06, 169.98. FTIR: 3465.8, 1649.8, 1138.9, 1198.9, 1134.5, 1100.8 cm^{-1} . HR-MS m/z : 865.2358 $[\text{M}+\text{H}]^+$, calcd $[\text{C}_{32}\text{H}_{49}\text{N}_8\text{O}_{12}\text{S}_4]$: 865.2347.

Lu-CLaNP-7

$\text{Lu}(\text{OAc})_3$ (2.37 mg, 5.38 μmol) and CLaNP-7 (4.19 mg, 4.84 μmol) were separately dissolved in *N,N*-dimethylformamide (50 μL). Then, the CLaNP-7 solution was added into $\text{Lu}(\text{OAc})_3$ solution and stirred for 4 h at room temperature. Without further purification, Lu-CLaNP-7 was used to label protein samples. The other lanthanoid ions Yb^{3+} , and Tm^{3+} were chelated to CLaNP-7 following the same procedure. HR-MS m/z : 1036.1513 $[\text{M}]^+$, calcd $[\text{C}_{32}\text{H}_{46}\text{N}_8\text{O}_{12}\text{S}_4\text{Lu}]$: 1037.1520.

Protein production and purification

The production and purification of the ^{15}N enriched *Alcaligenes faecalis* pseudoazurin (Paz) double cysteine mutant E51C/E54C was performed as described before,³¹ with small modifications. Instead of *Escherichia coli* BL21 (DE3), *E. coli* BL21 (PlysS) was used to produce Paz E51C/E54C and Tris-HCl buffer (20 mM Tris-HCl, pH 7.0) was used for ion exchange chromatography on the CM column. Double cysteine mutations I34C/V36C were prepared by the QuikChange method using the expression plasmid of wt Paz as a template.¹⁵¹ The oligonucleotides 5'-GGCGACACGGTCACCTTTTGTCCG TGCGACAAAGGACATAATG-3' and its

complement were used as the forward and reverse primers, respectively. The expression and purification of the ^{15}N enriched variant was performed using the same conditions as described above. The final yield obtained for Paz I34C/V36C was 2.4 mg/L of culture. ^{15}N enriched yeast Cyt *c* N56C/L58C was produced and purified by the published method.⁹⁸ To create mutant Cyt *c* H39A/N56C/L58C, the forward and backward primers 5'-CTTGCATGGTATCTTTGGCAGAGCCTCTG GTCAAGCTGAAGGGTATTTCG-3' and its complement were used on the template encoding Cyt *c* N56C/L58C. Expression and purification was identical to that of N56C/L58C. The final yield was 2.8 mg/L of culture.

Paramagnetic Probe Attachment

To attach Ln-CLaNP7 to Paz and Cyt *c*, protein sample (1 mL, 150-300 μM) was treated with DTT (final concentration 5 mM) at 0 °C for 1 h to remove possible dimers. The reaction mixture was loaded on a PD-10 column (GE Healthcare) pre-equilibrated with labeling buffer (20 mM sodium phosphate, 150 mM NaCl and pH 7.0) to remove DTT. To avoid any reoxidation by air, the buffer was degassed and the PD-10 column kept under an argon atmosphere. To the eluted protein five equivalents Ln-CLaNP-7 were added. The solution was stirred 16 h at 4 °C. The probe attached Paz sample was concentrated to 500 μL and purified over a Superdex 75 gel filtration column. In the case of Cyt *c*, the protein was purified on a HiTrap-SP column. The yield of labeling, estimated from the intensity of diamagnetic peaks in the [^{15}N , ^1H]-HSQC spectra of samples with paramagnetic tags, was more than 90%.

NMR spectroscopy

The NMR samples of Paz Ln-CLaNP-7 (100-200 μM) were prepared in 20 mM sodium phosphate, 150 mM NaCl buffer and 6% (v/v) D_2O . All Cyt *c* samples (100-200 μM) contained 20 mM sodium phosphate buffer, 6% (v/v) D_2O and one eq. of ascorbic acid under an argon atmosphere to keep the Cyt *c* in the reduced state. The pH of these samples was set with small aliquots of 0.1 M HCl or 0.1 M NaOH and was checked before each titration point. All [^{15}N , ^1H]-HSQC and IPAP spectra¹⁵² were recorded at 298 K on a Bruker Avance III 600 MHz spectrometer. Data were processed with NMRPipe¹⁵³ and analyzed with CCPNMR Analysis version 2.1.¹⁵⁴ Assignments of the resonances were based on previous work.^{99,155 31}

PCS and RDC analysis

PCS were defined as the chemical shift difference for a resonance in the paramagnetic and diamagnetic sample. Positioning of the metal and optimization of the $\Delta\chi$ -tensor were performed as described for CLaNP-5,¹¹ by using XPLOR-NIH version 2.9.9¹⁵⁶ and Pararestraints.¹⁵⁷ The manuscript for XPLOR-NIH and the calculation of $\Delta\chi$ -tensor were kindly performed by Dr. Peter H. J. Keizers (Leiden University, Inst. Chemistry). The structures of Paz and Cyt *c* were taken from PDB entries 1PY0 and 1YCC and hydrogens were added.^{31,118} The variation in the Ln positions were calculated by randomly removing 20% PCS data and repeating the $\Delta\chi$ -tensor fit 100 times. For RDC analysis, the HN positions were optimized on the basis of the experimental RDCs. The optimized structure was used for back-calculation of the RDCs on the basis of the PCS-derived $\Delta\chi$ -tensor. The Q factor provides a normalized measure for the agreement between a set of observed and calculated experiment data. The Q factor was defined as eq. 2.¹⁵⁸

$$Q = \sqrt{\sum_i (O_i^{obs} - O_i^{calc})^2 / \sum_i (O_i^{obs} + O_i^{calc})^2} \quad \text{eq. 2}$$

where O_i^{obs} and O_i^{calc} are the observed and calculated PCSs or RDCs.

Chapter III

The development of new methods for the attachment of caged lanthanoids NMR probes

Manuscript in preparation

Liu, W. -M.; Skinner, S. P.; Timmer, M.; Blok, A.; Filippov, D.; Overhand, M.; Ubbink, M. 'Thioether linkage: A new inert lanthanide-chelating paramagnetic NMR probe'

Abstract

To generate significant paramagnetic effects, site-specific labeling is important. Among all of the possible modification methods, forming disulfide bridges is the most widely used because cysteine residues can be selectively modified in proteins. However, the weak disulfide bridge is easily cleaved by reductants, which restricts its application. Consequently, the development of new methods is important. To increase the stability of the probe-protein linkage, the possibilities of thioether bond formation and click chemistry were investigated. In this chapter, several paramagnetic NMR probes, **CLaNP-6**, **8-12** and **DIBO**, have been designed and synthesized. The experimental results showed that **CLaNP-6** and **CLaNP-8** were highly unstable in aqueous environment, **CLaNP-9** was difficult to purify, and the lanthanoid ions could not be coordinated to **CLaNP-10**. Nevertheless, **CLaNP-9** was still successfully used for tagging two proteins and provided significant PCSs and thus represents a new, more stable double-armed tag. Also, unnatural amino acid tagging was investigated using the artificial amino acid *p*-azido phenylalanine (AzF). AzF was incorporated into a protein and the complementary paramagnetic probes were made. However, the quality of AzF incorporated protein was questionable and the level of tagging was very low.

Introduction

Paramagnetic effects provided by lanthanoid ions, such as pseudocontact shifts (PCSs), residual dipolar couplings (RDCs) and nuclear relaxation enhancements (PREs), have been recognized as powerful tools for the study of biomolecules. To generate a specific paramagnetic effect, the paramagnetic center must be site-specifically and rigidly attached to biomolecules (Chapter 1). In metalloproteins, lanthanoids can be substituted for Ca^{2+} or Mg^{2+} ions in the metal binding sites.¹²⁹ However, many proteins do not possess such metal binding sites and in order to overcome this, site-specifically labeling methods for paramagnetic tags have been developed. In recent years, two approaches of site-specific lanthanoid incorporation have been investigated. One of these is the use of genetically engineered lanthanoid binding peptides (LBP) fused to the protein of interest.¹⁵⁹ A drawback of this method is that the engineered LBP region can only be tagged to the N- or C- terminus or into a specific loop region. The other approach is using synthetic Ln-binding probes to introduce the paramagnetic lanthanoids⁵ (Chapter 1). So far, most of the synthetic probes are attached to target proteins *via* one or two disulfide bonds. The advantages of this method are that the cysteine residues can be selectively modified in proteins and that they react specifically with thiol-reactive group, avoiding any undesired side-products.¹⁶⁰ However, these bonds are not stable and can be cleaved easily by reductants. As a result, the study of proteins in the presence of a reducing agent such as DTT or TCEP cannot be accomplished by using a paramagnetic tag connected *via* a disulfide bridge.

To increase the stability of the modification, two approaches, thioether bond formation and bioorthogonal chemistry, are employed. Thioether linkers, broadly used for protein modification,⁴⁶ are stable in the presence of reducing agents. Several paramagnetic NMR tags were designed for this purpose (Chart 1, **CLaNP-6** and **8-10**). These probes contain functionalities that can react by forming thioether linkages upon reaction with a cysteine residue. The functionalities include an α -ketobromide, a benzylic bromide and a primary bromide. In this chapter, the pitfalls in the synthetic routes towards the reactive **CLaNP-6**, **8-10** are described in detail. Nevertheless, **CLaNP-9** was successfully attached to two proteins and significant PCSs were observed. The HSQC spectra of the **CLaNP-9** tagged protein were identical in the presence and absence of DTT or TCEP.

Also, bioorthogonal chemistry is a widely used technique for specific labeling in cellular systems.⁴⁸ Among numerous bioorthogonal reactions that have been developed, the introduction of azide groups and their subsequent transformation is the most utilized. Moreover, the azide group can be genetically engineered into proteins at specific sites by using the unnatural amino acid residue *p*-azido phenylalanine (AzF).¹⁶¹ The azide group of AzF can undergo 1,3-dipolar cycloaddition with a terminal alkyne by using Cu(I) as a catalyst. The reaction product is rigid and only one stereoisomer is generally observed (Chart 2A).⁴⁹ The azide group of AzF can also react with cyclooctyne (Chart 2B). In this case, the catalyst Cu(I) is not needed but the cyclolization product has two isomers. Still, a reaction in the absence of the catalyst is advantageous because Cu(I) can denature the protein samples. Thus, AzF represents a potential alternative for Cys in site-specific labeling of proteins with lanthanoid containing probes. We introduced AzF into a test protein, T4 Lysozyme (T4Lys), and synthesized several alkyne containing probes to develop a new approach for the site-specifically tagging of paramagnetic NMR probes. However, the results of labeling were not satisfactory because no paramagnetic effects could be observed.

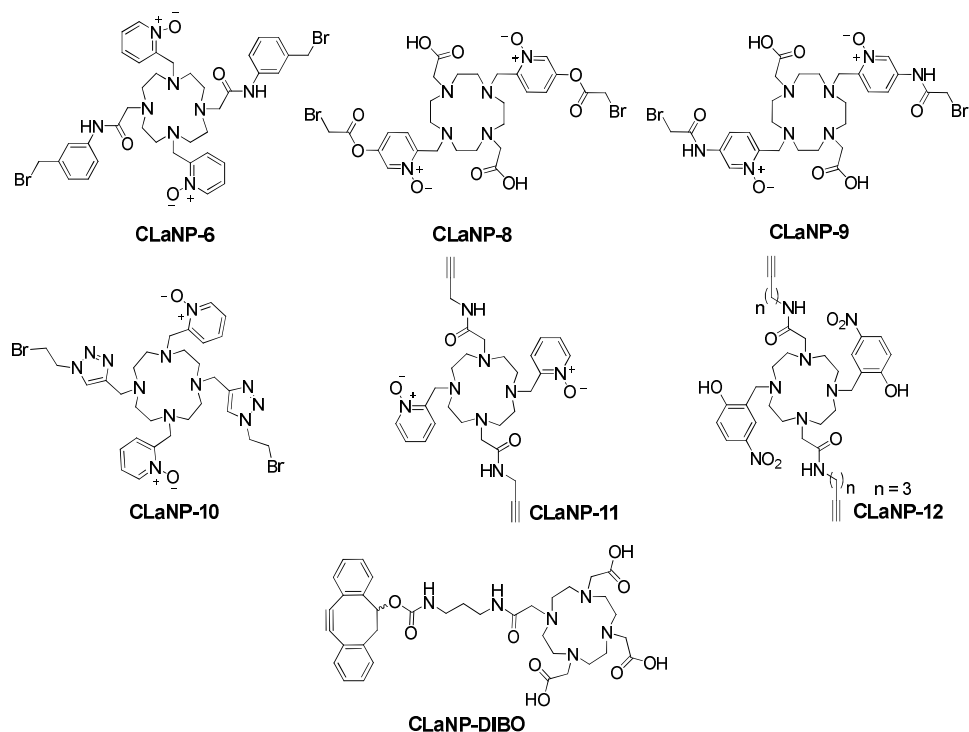


Chart 1. Structures of new CLaNPs, **CLaNP-6, 8-12** and **DIBO**.

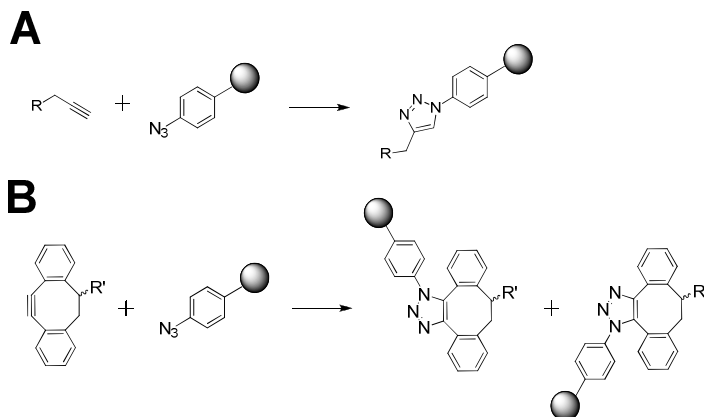


Chart 2. The reaction products of 1,3-dipolar cycloaddition (A) and [3+2] cycloaddition (B).

Results and discussion

Thioether linkage: A new inert lanthanoid-chelating paramagnetic NMR probe

Synthesis of CLaNP-functionalities

Alkyl halides, α -halocarbonyls and electron poor double bonds are typical thiol-reactive functional groups.⁴⁶ In order to design an appropriate paramagnetic tag, the labeling ability of acrylic acid, 3-bromo-1-propanol, 3-nitrobenzyl bromide, 4-iodobenzyl bromide, bromoacetic acid, and iodoacetic acid were investigated (Figure 1A). Double cysteine mutants testing proteins (Src SH3 T116C/E117C and T4 Lysozyme N55C/V57C) were first activated by DTT for an hour, and then the reductant was removed by a short gel filtration column. The activated protein was incubated with 10 equiv. of the reactive species at 4 °C or RT and product formation was monitored by LC/MS (Figure 1). The results showed that under these conditions benzylic bromide is the most reactive group among all of the test species. After 3 h, SH3 T116C/E117C was tagged with 3-nitrobenzyl bromide and 4-iodobenzyl bromide at 4 °C (Figure 1B and 1C). When the reaction temperature was raised to RT and the reaction time was increased, T4Lys N55C/V57C was also tagged with 2-bromoacetic acid and 2-iodoacetic acid (Figure 1C and 1D). Although α -ketoiodide is more reactive than α -ketobromide, it may also react with methionine and basic residues when cysteine is absent, resulting in non-specific labeling.^{162,163} Consequently, benzylic bromide (**CLaNP-6**), α -ketobromide (**CLaNP-8** and **9**) as well as a primary bromide (**CLaNP-10**) were chosen as the target functional groups. Protein expression and purification were kindly performed by Dr. Somireddy V. B.

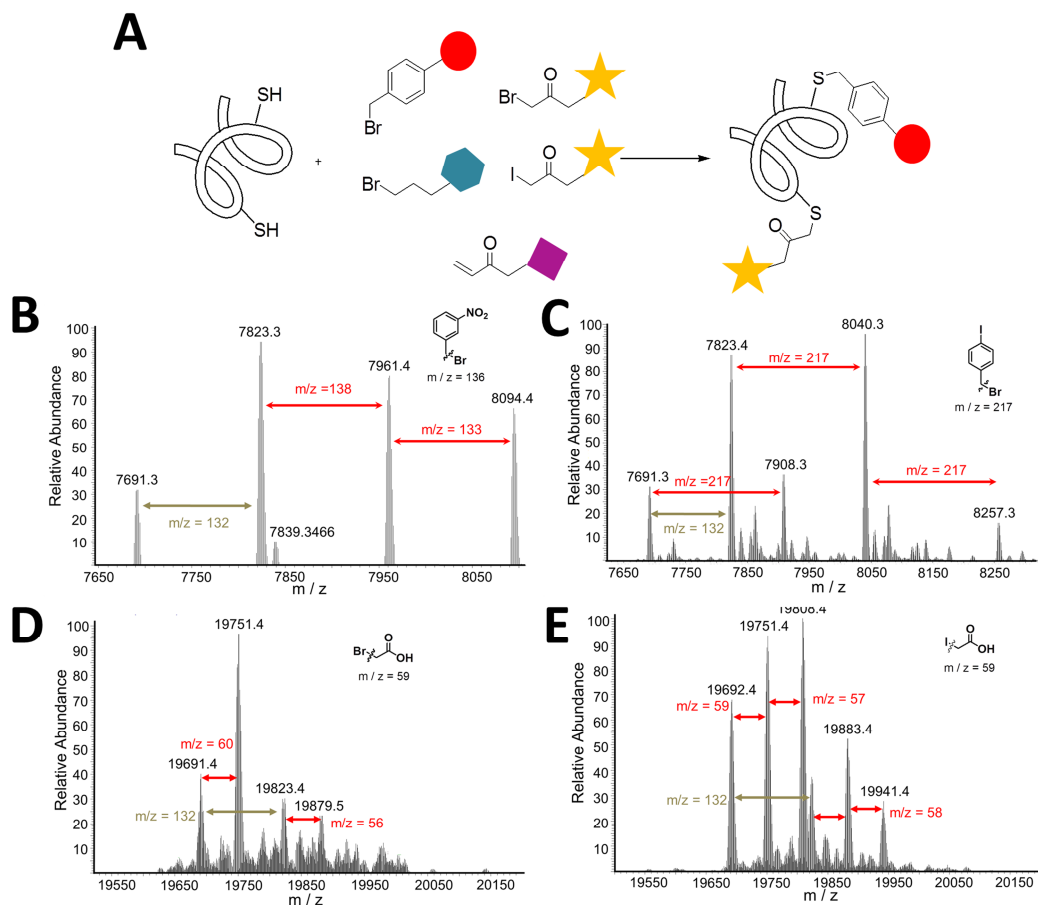
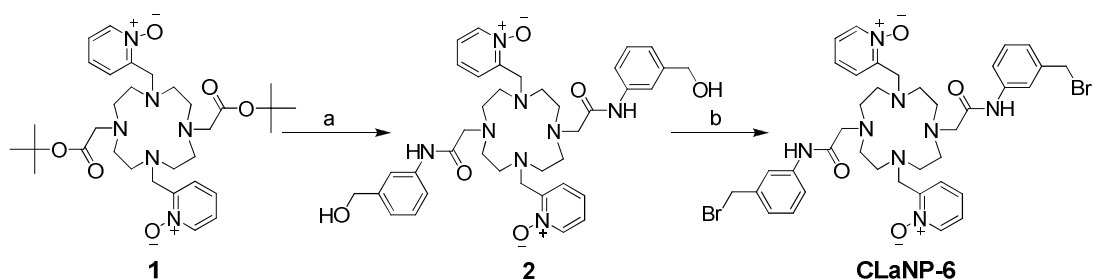


Figure 1. Protein labeling test. (A) In protein labeling experiment, several typical thiol-reactive functional groups were used. The labeling results were checked by LC/MS. For SH3 T116C/E117C, the results showed that the protein could be tagged by 1-(bromomethyl)-3-nitrobenzene (B) and 1-(bromomethyl)-4-iodobenzene (C) at 4 °C with continuous stirring for 3 h. When the temperature was increased to RT and the reaction time was elongated to 16 h. 2-bromoacetic acid (D) and 2-iodoacetic acid (E) were also attached to another test protein T4Lys N55C/V57C. The mass difference is indicated by a red arrow and the difference between untagged T4Lys with and without the methionine is shown with a dark green arrow.

The synthesis of **CLaNP-6** is depicted in Scheme 1. Removing the protective group of functionalized cyclen **1**¹¹ and coupling with 3-aminobenzyl alcohol resulted in benzylic alcohol **2** in high yield. The hydroxyl of **2** was converted to the bromide by using PPh₃Br₂ in dry MeCN and product formation was monitored by LC/MS. When the reaction was complete, water was added to quench the reaction. During the reaction **CLaNP-6** was formed, as evidenced by LC/MS, but the compound decomposed after the quenching with water (Figure 2).



Scheme 1. Synthesis of **CLaNP-6**. (a) i) TFA, CH₂Cl₂, RT, 4 h; ii) HATU, 3-aminobenzyl alcohol, TEA, DMF, RT, 16 h; (b) dry MeCN, PPh₃Br₂, 0 °C.

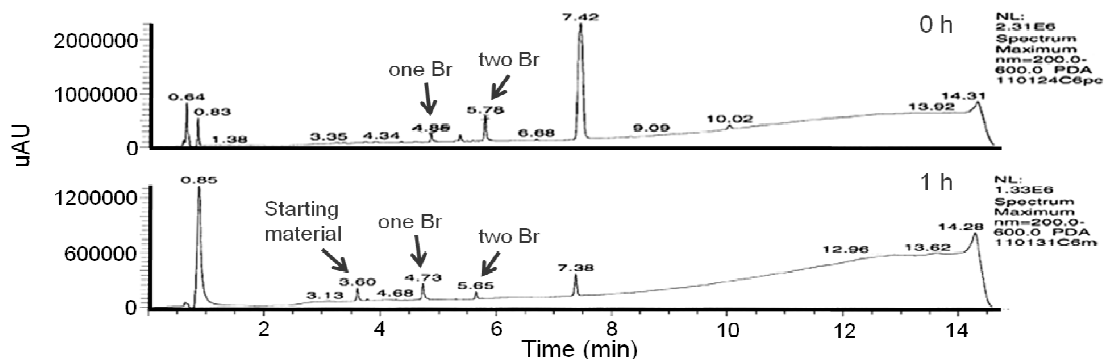
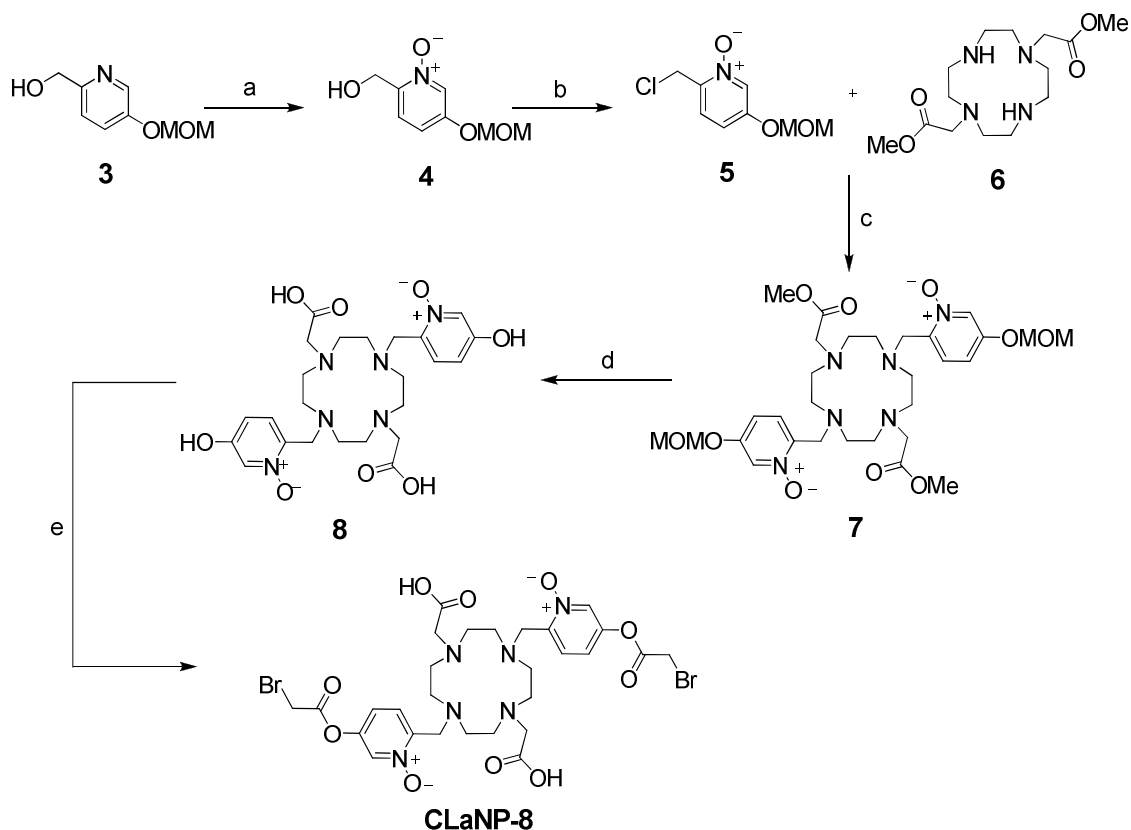


Figure 2. HPLC analysis of the **CLaNP-6**. (A) After quenching by water, a mixture of compounds (**CLaNP-6** with one or two Br) was detected. (B) The same HPLC sample was measured again after 1 h. The results show that **CLaNP-6** was hydrolyzed to the starting material **2**.

The synthetic route of **CLaNP-8** is shown in Scheme 2. The starting material **3**¹⁶⁴ was oxidized with *m*CPBA to produce pyridine-*N*-oxide **4** with a high yield. Substitution of the hydroxyl of **4** using MsCl and LiCl in dry CH₂Cl₂ yielded compound **5**. Functionalized cyclen **6**⁴² was treated with **5** and K₂CO₃ at 50 °C for 16

h to give compound **7**. Compound **8** was obtained by full deprotection of **7**. Reaction of **8** using bromoacetyl bromide gave the desired **CLaNP-8**. However, also this compound was not to be stable under aqueous conditions (Figure 3).



Scheme 2. Synthesis of **CLaNP-8**. (a) *m*CPBA, CHCl_3 , RT, 16 h; (b) *i* MsCl, dry CH_2Cl_2 , TEA, 2 h, 0°C *ii*) 10 equiv. LiCl, RT, 16 h; (c) K_2CO_3 , MeCN, 50°C , 16 h; (d) *i* NaOH, 1,4-dioxane, RT, 4 h; *ii*) TFA, CH_2Cl_2 , RT, 4 h; (e) dry MeCN, K_2CO_3 , RT, bromoacetyl bromide.

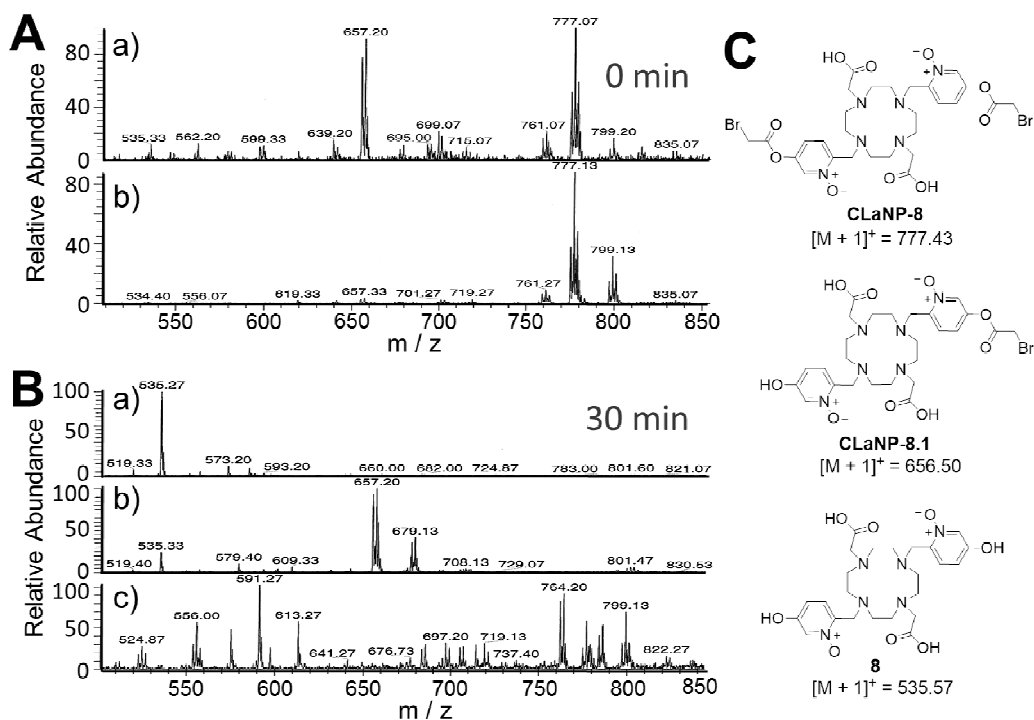
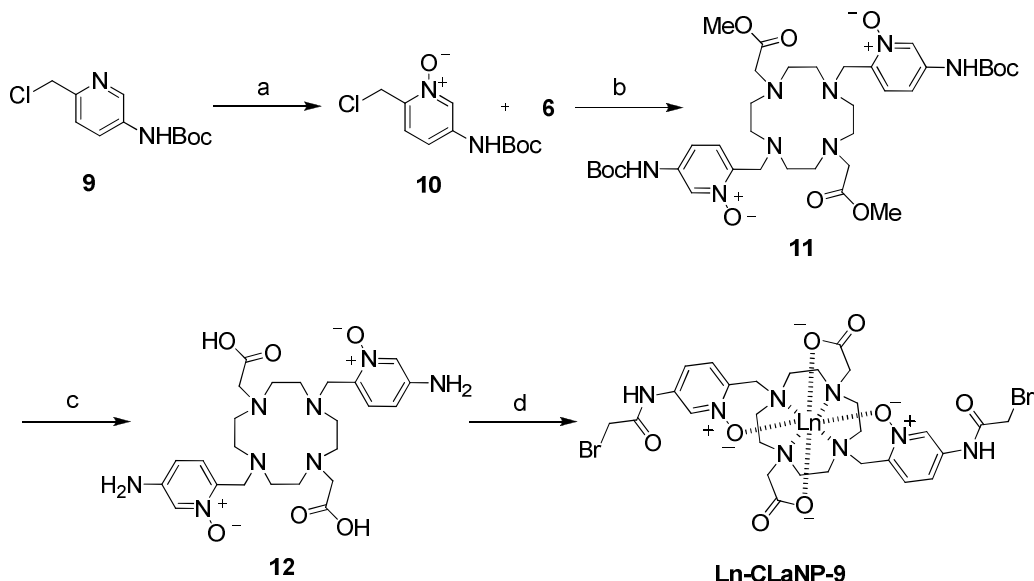


Figure 3. The reaction progress of **CLaNP-8** was monitored by LC/MS. (A) The reaction was quenched by water and the sample was immediately analyzed by mass spectrometry. The result showed that **CLaNP-8.1** (a) and **CLaNP-8** (b) were present. (B) After 30 min, the same sample was analyzed again and the results showed that **CLaNP-8** was hydrolyzed to compound **8** (a) and **CLaNP-8.1** (b) by water. Also, the final product was difficult to observe (c). The expected weights of **CLaNP-8**, **CLaNP-8.1** and **8** are presented in (C).

According to the results of LC/MS, the hydrolysis occurred at the active ester bond. Therefore, the ester was replaced with an amide to increase the stability of desired product, **CLaNP-9**, and the synthesis is shown in Scheme 3. The compound **9**^{165,166} was synthesized *via* following a previously published procedure and then oxidized with *m*CPBA, yielding **10**. Functionalized cyclen **6**⁴² was treated with **10** in MeCN at 50 °C and was converted into **11**. Removal of the protective groups in **11** followed by HPLC-purification yielded compound **12**. Subsequently, **12** was dissolved in dry MeCN, treated with bromoacetyl bromide and purified by HPLC to give **CLaNP-9** in very low yield (3 %), which was caused by the reactive carboxylic acid and *N*-oxide. Moreover, the final product was hydrolyzed after freeze drying.

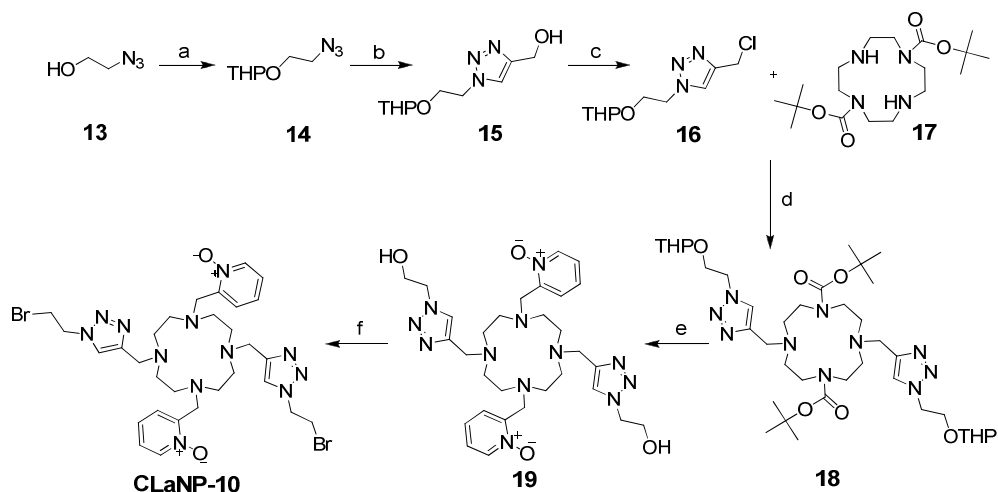
Hence, compound **12** was coordinated to $\text{Ln}(\text{OAc})_3$ to “block” the reactivity of the acids and *N*-oxides, and was subsequently treated with bromoacetyl bromide. Indeed, the reaction became cleaner and complete conversion to **Ln-CLaNP-9** was observed. The solution mixture was purified over a short PrevailTM C18 column (Alltech[®] Extract-CleanTM) to remove the impurities and the product was directly used for protein labeling (see probe attachment section).



Scheme 3. Synthesis of **CLaNP-9**. (a) *m*CPBA, CHCl_3 , RT, 4 h; (b) K_2CO_3 , MeCN, 50 °C, 2 days; (c) i) TFA, CH_2Cl_2 , RT, 4 h; ii) NaOH, 1,4-dioxane, RT, 4 h; (d) i) $\text{Ln}(\text{OAc})_3$, DMF, RT; ii) NaHCO_3 , dry MeCN, bromoacetyl bromide, RT, 30 min.

Compared to benzylic bromides and α -ketobromides, primary bromides are stable and can easily be purified. However, these compounds did not react with Cys residues during the labeling test. Nevertheless, the synthesis of **CLaNP-10** was undertaken and is shown in Scheme 4. The hydroxyl group of known compound **13**¹⁶⁷ was protected using a THP group and clicked with propargyl alcohol, yielding **15**. The alcohol of **15** was activated with MsCl and converted to chloride **16**, after which **16** was treated with protected cyclen **17**.⁴² The reaction was heated under reflux for 16 h and compound **18** was obtained. The protecting groups of **18** were removed by TFA and the crude compound was reacted with 2-(chloromethyl) pyridine-*N*-oxide to give **19**. Compound **19** was converted into **CLaNP-10** by using PPh_3Br_2 and purified by HPLC. However, **CLaNP-10** did not readily chelate

lanthanoid ions, which might be caused by the steric hindrance by the four aromatic groups. When the temperature was raised, to speed-up the complex formation process, the compound started to decompose.



Scheme 4. Synthesis of **CLaNP-10**. (a) DHP, PTTs, CH_2Cl_2 , RT, 16 h; (b) propargyl alcohol, ascorbate acid, CuSO_4 , THF/ H_2O solvent mixture, RT, 16 h; (c) i) MsCl , TEA, CH_2Cl_2 , 0°C , 1 h; ii) 10 equiv. LiCl , acetone, RT, 16 h; (d) K_2CO_3 , MeCN, reflux, 16 h; (e) i) TFA, CH_2Cl_2 , RT, 4 h; ii) 2-(chloromethyl) pyridine-*N*-oxide, K_2CO_3 , MeCN, reflux, 16 h; (f) dry MeCN, PPh_3Br_2 , at 0°C to RT, 16 h.

Probe attachment

^{15}N -enriched T4Lys N55C/V57C was activated with DTT, washed, and directly incubated with 10 equiv. of Ln-**CLaNP-9** at RT for 6 hours, after which the tagged protein was purified using an ion-exchange column. The ^{15}N - ^1H -HSQC spectra of tagged T4Lys were recorded in the presence of three lanthanoid ions (Lu^{3+} , Yb^{3+} and Tm^{3+}). The paramagnetic lanthanoid ions (Yb^{3+} and Tm^{3+}) caused changes in the resonance frequencies of the observed nuclei, which were identified as PCSs (Figure 4). The spectra of tagged T4Lys were identical in the presence and absence of DTT, indicating that the probe was stable under reductive conditions. Moreover, the spectra were the same after keeping the protein samples at 4°C for 2 weeks. The copper protein Paz mutant E51C/E54C was the second tested protein. Instead of DTT, TCEP was used to activate the protein because the copper ion is removed from the protein by a high concentration of DTT. The ^{15}N - ^1H -HSQC spectra of tagged

Cu Paz also exhibited single sets of PCSs. Both experiments indicated that the probe was attached rigidly to the protein and existed in one dominant conformation. To demonstrate the efficacy of this new probe, the Ln-**CLaNP-9** tagged Cu(II)-Paz was reduced to Cu(I)-Paz by using TCEP. As expected, the tagged probe was stable under reducing conditions and significant paramagnetic effects were observed (Figure 5). The $\Delta\chi$ -tensors values for Tm- and Yb-**CLaNP-9**, and **CLaNP-5** for comparison, are reported in Table 1 and the back-calculated PCSs are plotted versus the observed ones in Figures 6. The yield of labeling after purification was 50 ~ 80%, which estimated from the intensity of diamagnetic peaks in the spectra of samples with paramagnetic tags. The LC/MS results show that the diamagnetic peaks come from unlabeled protein and not one-arm attached tag. A simple explanation is that the probe concentration was insufficient to yield complete labeling. Theoretically, the probe was in 10-fold excess over the protein, but the accuracy of this number is questionable, due to the purification step. In the future, 20 or 30 excess fold of probe and longer incubation times could be tried to increase the labeling yield.

Table 1. PCSs-based $\Delta\chi$ -tensors of CLaNP-5¹¹ and CLaNP-9^{a,b}

Protein	probe	Ln	$\Delta\chi_{ax}$	$\Delta\chi_{rh}$	Restrains	Q
Paz Cu(I)	CLaNP-5	Yb	9.4 ± 0.2	1.9 ± 0.4	93	0.04
E51C/E54C		Tm	55.5 ± 0.8	10 ± 1	89	0.03
Paz Cu(II)	CLaNP-9	Yb	7.5 ± 0.4^c	2.3 ± 0.4^c	66	0.04
E51C/E54C		Tm	39.5 ± 1.1^c	10.6 ± 1.5^c	41	0.02
T4Lys	CLaNP-9	Yb	6.3 ± 0.8^c	2.2 ± 0.8^c	88	0.04
N55/V57C		Tm	32.5 ± 2.3	15.6 ± 1.5	62	0.03

^a The unit of axial and rhombic components ($\Delta\chi_{ax}$ and $\Delta\chi_{rh}$) is 10^{-32} m^3 .

^b The program Numbat¹⁶⁸ was used to calculate the $\Delta\chi$ -tensors.

^c The error is calculated by randomly removing 10% of the data and repeating the $\Delta\chi$ -tensor fit 100 times.

The $\Delta\chi_{ax}$ of Tm³⁺ and Yb³⁺ of **CLaNP-9** are smaller than those of **CLaNP-5**. For **CLaNP-9**, the functionalized pyridine-*N*-oxide was the site for attachment to the protein, which may cause a larger mobility of the probe relative to the protein. In the case of T4Lys, the mutant site was at the end of the elongated shape of the protein

and therefore only part of amide proton resonances experienced a significant PCS, which can explain the larger error in $\Delta\chi_{ax}$ as compared to Paz.

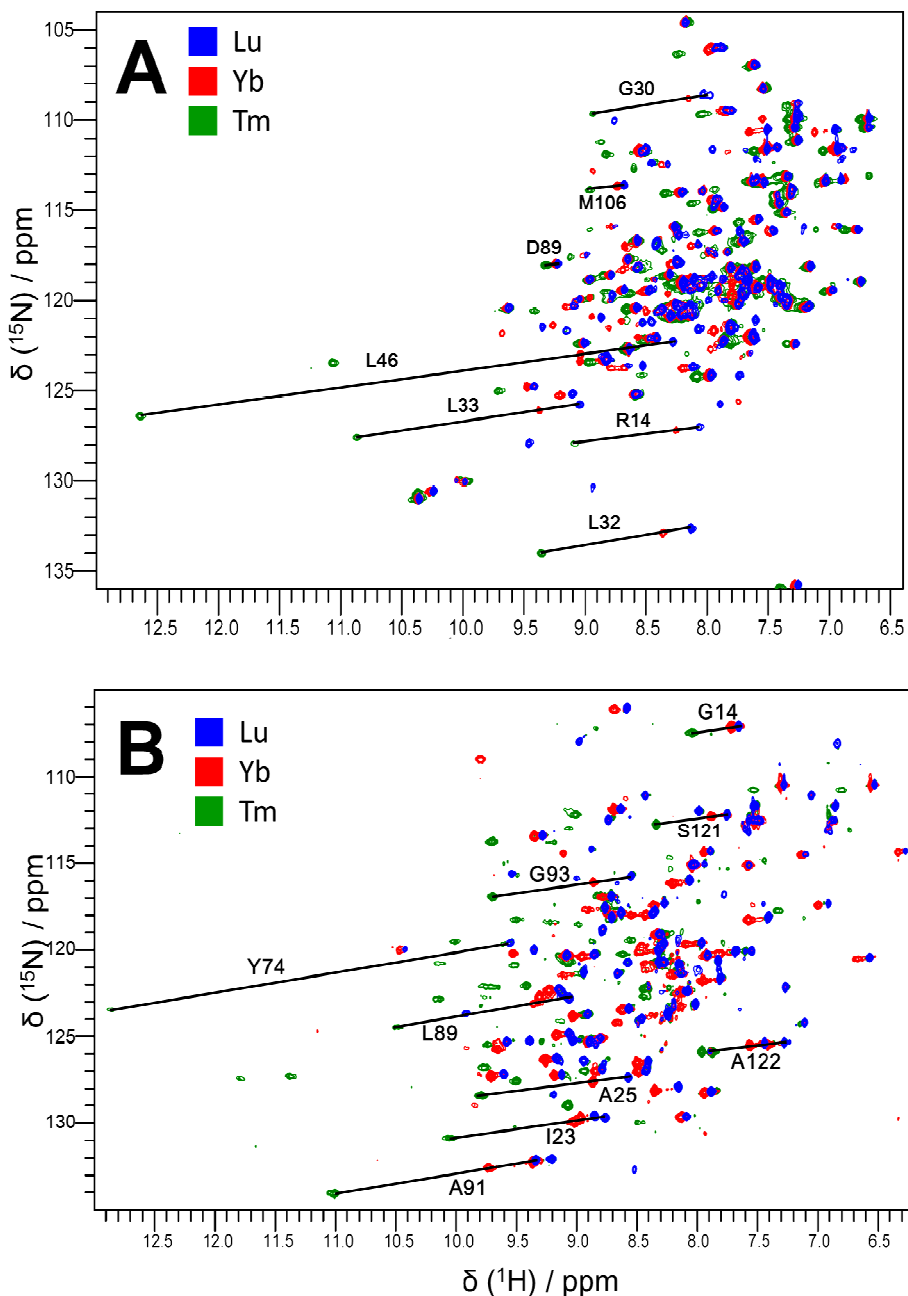


Figure 4. Overlay of $[\text{}^{15}\text{N}, \text{}^1\text{H}]$ -HSQC spectra of T4Lys N55C/V57C (A) and Paz-Cu(II) E51C/E54C(B) with **CLaNP-9**-Lu (blue), Yb (red) and Tm (green) attached. Several PCSs are indicated with solid lines.

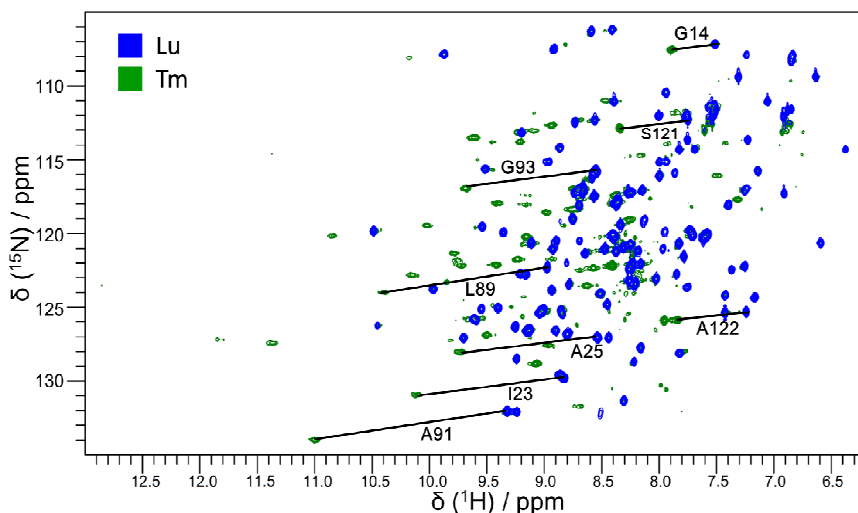


Figure 5. Overlay of [^{15}N , ^1H]-HSQC spectra of Paz-Cu(I) E51C/E54C (A) with CLaNP-9- Lu (blue) and Tm (green) attached. Several PCSs are indicated with solid lines.

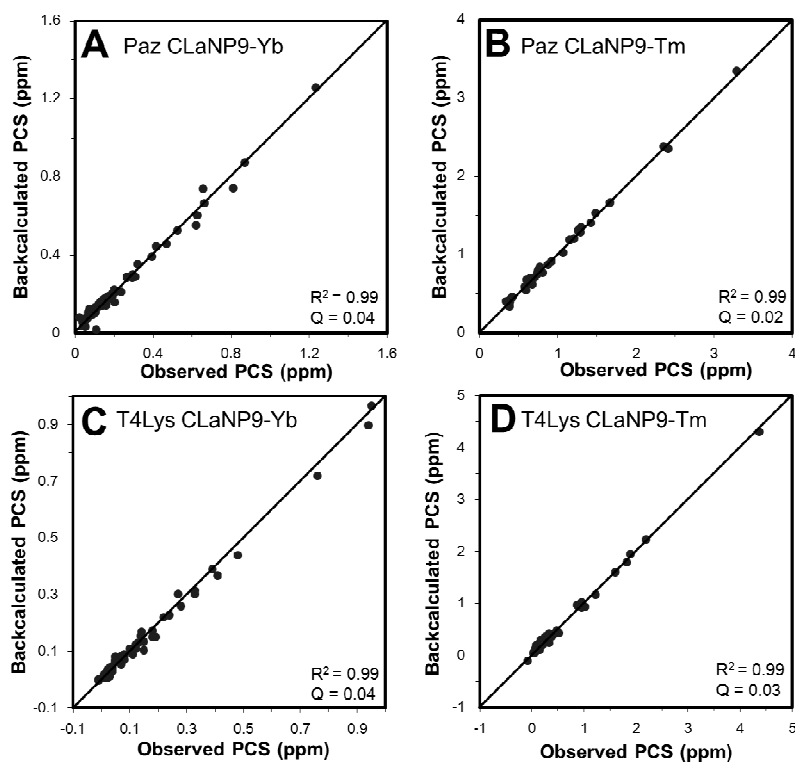
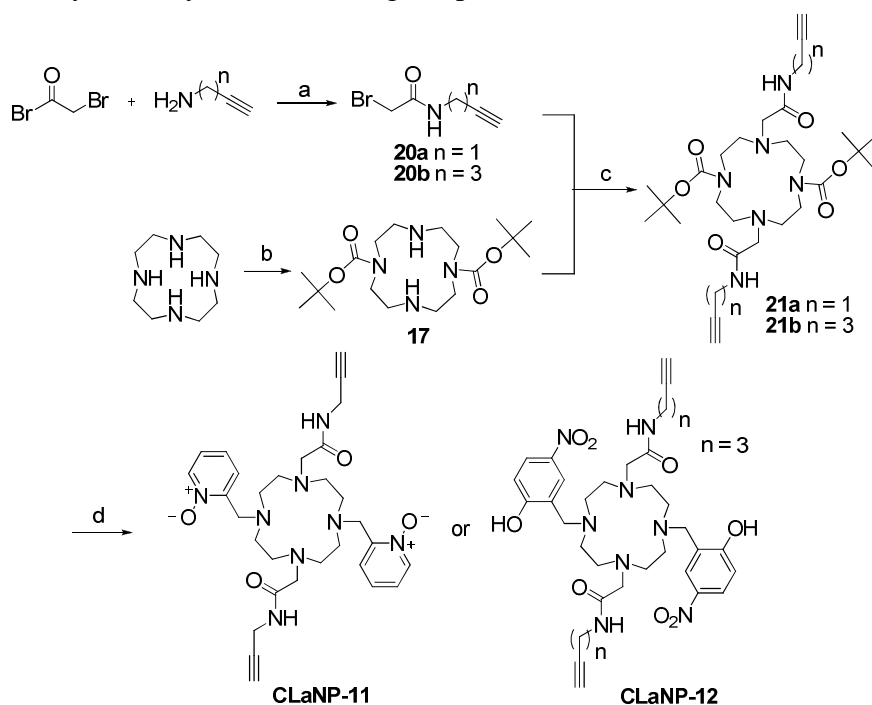


Figure 6. Experimentally observed amide proton PCSs of Paz Cu(II) E51C/E54C (A, B) and T4Lys N55C/V57C (C, D) Ln-CLaNP-9 plotted against the back-calculated PCSs. The solid lines represent the perfect correlation ($y=x$).

Bioorthogonal reactions: A potential method for site-specifically attaching lanthanoid probes

Synthesis of CLaNP-click

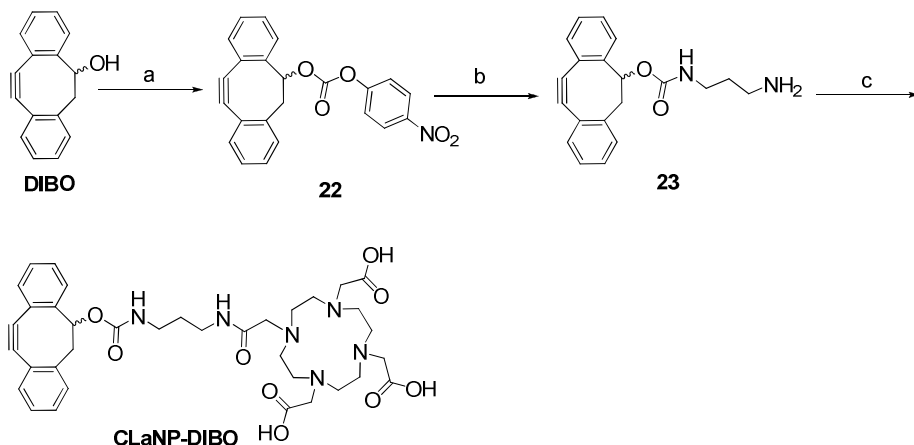
The structures of the CLaNP-click series are based on two successful probes, **CLaNP-5** and **CLaNP-7** (Chapter 1).^{11,42} In the design of the bioorthogonal probes, the two reactive groups on these CLaNP's are replaced with terminal alkynes to allow a bioorthogonal reaction. **CLaNP-11** and **CLaNP-12** were synthesized as depicted in Scheme 5. Compound **20a**, **20b** and **17** were prepared using previously published methods.^{42,169} To obtain **21a** and **21b**, **17** was functionalized with alkyl functional arms (**20a** or **20b**). Removal of the Boc protective group in **21a** and **21b**, alkylation with 2-(chloromethyl)pyridine-*N*-oxide or 2-(bromomethyl)-4-nitrophenol, and purification by HPLC yielded the designed products.



Scheme 5. Synthesis of CLaNP-11 & 12. (a) NaHCO₃, CH₂Cl₂, RT, 16 h; (b) BocOSu, dry CHCl₃, RT, 1 day; (c) **20a** or **20b** (2.5 equiv.), MeCN, K₂CO₃, 0 °C to RT, 16 h.; (d) i) TFA, CH₂Cl₂, RT, 4 h; ii) 2-(chloromethyl)pyridine-*N*-oxide or 2-(bromomethyl)-4-nitrophenol, MeCN, 80 °C, 16 h.

For the ring strain-promoted [3+2] cycloaddition, **CLaNP-DIBO** was synthesized (Scheme 6). Compound **DIBO**¹⁷⁰ was activated by *p*-nitrophenyl

chloroformate, then reacted with 1,3-diaminopropane yielding **23**.^{171,172} The final product was synthesized through EDC coupling of the free amine of **23** with a single carboxylic acid group of a DOTA ring yielding the desired compound.¹⁷³



Scheme 6. Synthesis of CLaNP-DIBO. (a) *p*-nitrophenyl chloroformate, CH₂Cl₂, pyridine, RT, 16 h; (b) 1,3-diaminopropane, dry CH₂Cl₂, TEA, RT, 1 h; (c) DOTA, DIPEA, EDC, water/MeOH, pH = 4.5-8.0, RT, 1 h, yield 20% (over 3 steps).

Protein labeling study

Copper-catalyzed azide-alkyne 1,3-dipolar cycloaddition (CuAAC)

Site-specific introduction of unnatural amino acids (uaa) into a protein system *in vivo* was first reported by Prof. P. Schultz and co-workers.¹⁷⁴ This method uses the stop codon, UAG, as the codon of uaa. In *Escherichia coli* the genes of complementary tRNA, the gene for a dedicated AzF-tRNA synthetase and the target gene with the UAG codon(s) introduced at the site(s) for AzF incorporation were expressed together. To demonstrate the utility of this new method, two AzF mutants of T4Lys were designed, N68AzF/D72AzF and N55AzF/V57AzF. However, the protein yield was low due to the presence of two UAG codons close together in the sequence. Therefore, single mutant proteins were also produced and used as test proteins. Protein expression and purification were performed by Mrs. Anneloes Blok (Leiden University, Inst. Chemistry).

In order to reduce the catalyst Cu(II) to Cu(I) and to stabilize the Cu(I), a reductor and a metal stabilizer (TBTA) are employed, respectively. In the labeling experiment, the probes were added in five-fold excess and the reaction was quenched

by EDTA after 30 min. This procedure was performed because it was found that Cu(I)-induced protein precipitation increases with time. Firstly, the amounts of CuSO₄ and TBTA were optimized. SDS-PA gel was used to detect the tagged protein. A weak second band indicative of the tagged protein was present at the highest concentration of CuSO₄ (Figure 7A). Tris(2-carboxyethyl)phosphine (TCEP), sodium ascorbate (NaAsc) and dithiothreitol (DTT) are commonly used to reduce Cu(II). TCEP gave the best results in our system (Figure 7B). The commercially available fluorescent probe, Tamra, was also used as a control to confirm that the employed reaction conditions allowed tagging of the protein. In the Tamra test, a second protein band was present in SDS-PA gels and showed intensive fluorescence, even though only a small portion of the protein was labeled (Figure 7C). The labeling yield increased with a higher concentration of TCEP. Using these conditions, T4Lys D72AzF was incubated with the Yb-CLaNP-11 and excess probe was removed using a HiTrapSP column.

[¹⁵N, ¹H]-HSQC spectra taken of the T4Lys D72AzF before and after the reaction are shown in Figure 8. Unexpectedly, the HSQC spectra before and after reaction are identical except for few residues. These residues are within 10 Å of the C-terminus, with has an additional His tag. The His tag could chelated Cu(II) resulting PREs. No PCSs were observed, indicating that the labeling reaction was unsuccessful.

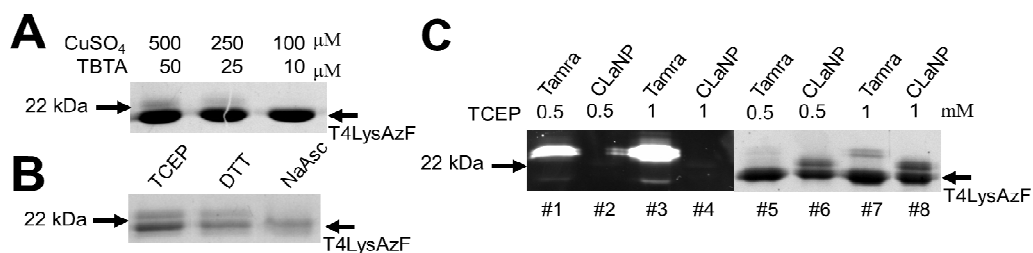


Figure 7. Optimization of the click reaction. (A) Influence of the amount of CuSO₄ used during the click reaction. (B) The effect of different reducers. (C) Influence of the amount of TCEP on the click labeling of Tamra and CLaNP to T4LysAzF. The reaction mixture contained CuSO₄ (500 μM), TBTA (50 μM), CLaNP or Tamra (250 μM), and T4Lys D72AzF (50 μM). Lanes 1-4 show the fluorescence and 5-8 the Coomassie stain of the SDS-PA gel.

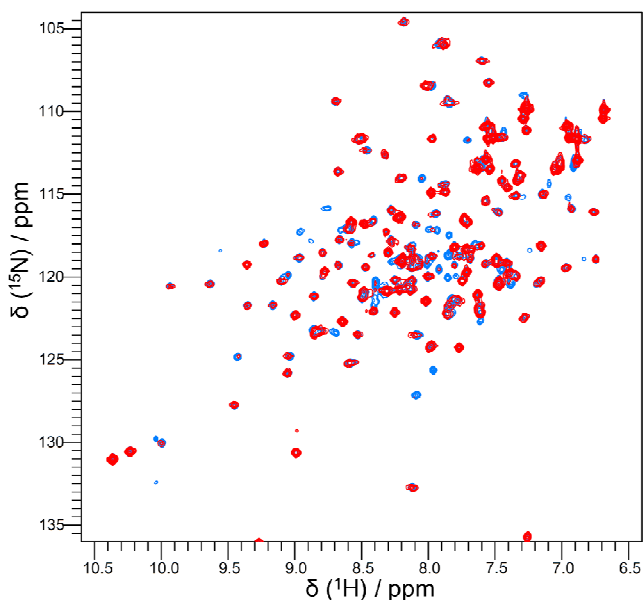


Figure 8. Overlay of [^{15}N , ^1H]-HSQC spectra of T4Lys D72AzF before (blue) and after the reaction with Yb-CLaNP-11 (red). No PCS are observed.

The low level of labeling may be caused by the short alkyl arms in **CLaNP-11**, and therefore, **CLaNP-12** was used for testing. **CLaNP-12** has an additional absorption band at 390 nm, which simplifies the detection of tagged protein compared with **CLaNP-11**. However, the poorly aqueous solubility of **CLaNP-12** was a serious problem and caused a low labeling yield. It was not pursued further.

Copper free click chemistry

For protein labeling, the yield of the tagging reaction could also be site-dependent. In T4Lys D72AzF a lysine and an arginine are close to the AzF, which is on an α -helix. The long side-chains of Lys and Arg could increase the steric hindrance and negatively influence the labeling efficiency. Moreover, the charges of those amino acids could repel the positive **CLaNP-11** complexes. For these reasons, another AzF mutant, T4Lys N55AzF, was selected as a model protein for **CLaNP-DIBO** labeling. To test the reactivity of **CLaNP-DIBO**, it was reacted with free AzF and product formation was monitored by LC/MS. The sample was incubated at 4 °C with continuous stirring, and **CLaNP-DIBO** was completely converted into the cycloaddition products and both isomers (Chart 2B) were present in a 1:1 ratio. Upon

linking **CLaNP-DIBO** to a protein, two products are expected and, therefore, two sets of PCS, which is not desired. However, **CLaNP-DIBO** can be loaded with Gd^{3+} , to obtain a PRE probe. The presence of diastereoisomers will not complicate the spectrum in that case. Following the same protocol, T4Lys N55AzF was incubated with the Ln-**CLaNP-DIBO** complexes and the labeling experiment was checked by SDS-PA gel (Figure 9). The gel suggests that a fraction of the protein is labeled with the probe. The excess probe was removed and the protein sample was concentrated and analyzed without further purification. The HSQC spectra of T4Lys N55AzF reacted with Lu^{3+} and Gd^{3+} complexes are shown in Figure 10. The peak intensity ratios of $\text{Gd}^{3+}/\text{Lu}^{3+}$ samples is close to 1 (data not shown), indicating that the Gd^{3+} -containing probe was not attached onto the protein in sufficient quantity to cause substantial PRE.



Figure 9. Detail of the SDS-PA gel showing the results of the CLaNP-DIBO labeling experiment.

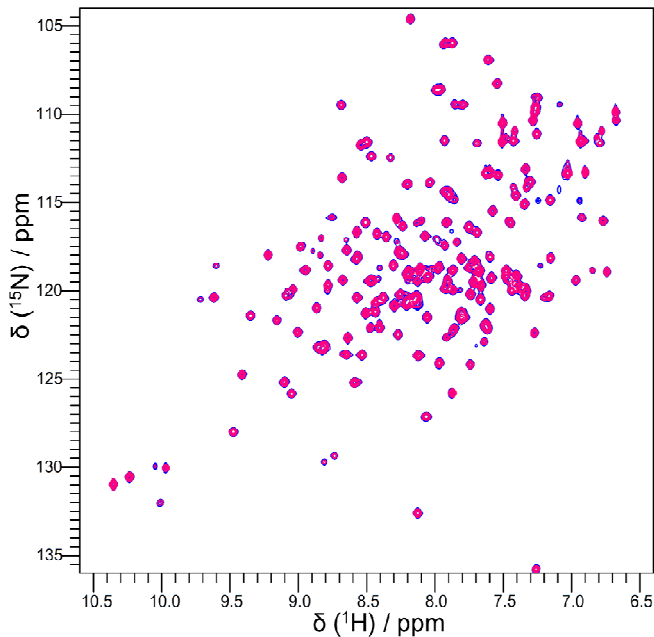


Figure 10. Overlay of $[\text{}^{15}\text{N}, \text{}^1\text{H}]$ -HSQC spectra of T4Lys N55AzF reacted with Lu-CLaNP-DIBO (blue) and Gd-CLaNP-DIBO (red).

The application of copper-catalysed 1,3-dipolar azide-alkyne cycloaddition (CuAAC) to obtain a modified protein amenable to NMR spectroscopy is a challenge, as compared to fluorescent studies, because high tagging yields are required. In Figure 7, the SDS-PA gel showed an intense fluorescent band indicating the tagged protein, yet, only a small fraction of the protein was actually labeled. To deduce the reason for the low labeling yield, the quality of T4LysAzF protein was assessed by mass spectroscopy. The MS results demonstrate that incorporation of the unnatural amino acid is 100%, but the results always had a mass of 28 Da less than the theoretical value indicating the loss of two nitrogens from the azide group. The degradation of AzF might be caused by the chemical reactivity and photoinstability of the aryl-azide group, which could have decomposed either during the MS analysis or the protein synthesis and purification.¹⁷⁵ Hence, the quality of protein samples could not be accurately assessed. The NMR spectra showed that there were no paramagnetic effects, even though the SDS-PA gel showed that a small fraction of the protein was modified. A similar result was observed in the **CLaNP-DIBO** labeling experiments.

Recently, site-specifically labeling *via* a UAA was demonstrated by a similar approach.⁵⁰ A terminal alkyne functionalized DOTA-base probe was attached to a protein using CuAAC. These researchers faced similar problems to obtain high reaction yields. For example, the protein precipitated during the reaction and a His tag poisoned the Cu(I) yielding lower labeling efficiency.¹⁷⁶ Instead of TBTA, a new Cu(I)-stabilizing ligand, BTAA (2-[4-((bis[(1-tert-butyl-1H-1,2,3-triazol-4-yl)methyl]-amino)methyl)-1H-1,2,3-triazol-1-yl]acetic acid), was employed. The new stabilizing ligand performs significantly better and the solubility is higher than commercially available TBTA.¹⁷⁷ Instead of TCEP, NaAsc was employed to reduce the Cu(II). Glycerol and aminoguanidine were also added into the reaction mixture because they prevent protein aggregation caused by the oxidized NaAsc.^{176,178} Additionally, the reaction was performed in a glovebox under N₂ with continuous stirring for 16 h at RT. Although the alkyne functionalized probe was successfully attached to protein, the complicated protocol limits the application of this method to very stable proteins. Moreover, the application of CuAAC appears to require optimized reaction conditions for each protein.¹⁷⁹ Consequently, a general protocol is difficult to develop.

Conclusion

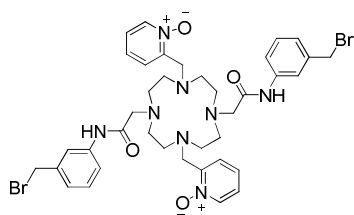
A new thioether paramagnetic NMR probe, **CLaNP-9**, has been reported. It provides stable tagged products under reducing conditions creating the possibility of studying reductive proteins and produces large single PCSs. The charge of **CLaNP-9** complexes is the same as that of **CLaNP-7** (Chapter 2), but is far more soluble under aqueous conditions. The $\Delta\chi$ -tensors for Yb^{3+} and Tm^{3+} were also defined using two different model proteins. It is therefore an attractive probe for paramagnetic NMR.

AzF containing T4Lys was successfully produced, however, the reactivity of protein is questionable in the light of the results of MS. Azide reactive probes have been produced and ligated with AzF functionalized protein. However, the attachment experiments showed that it is very difficult and impractical to obtain yields sufficient for NMR spectroscopy.

Experimental Section

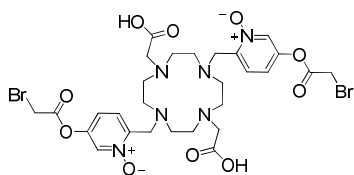
General Procedures:

Compound **1**¹¹, **3**¹⁶⁴, **6**⁴², **9**^{165,166} and **13**¹⁶⁷, **17**⁴², **20a**, **22b**¹⁶⁹, and **DIBO**¹⁷⁰ were prepared according to methods published in the literature. All other chemicals were used as purchased without further purification. TLC-analysis was conducted on DC-alufolien (Merck, Kieselgel60, F254) with detection by UV-absorption (254 nm). Flash chromatography was performed on Screening Devices silica gel 60 (0.04-0.063 mm). A Biocad Vision HPLC (PerSeptive Biosystems, inc.) and an Äkta Basic FPLC (GE Healthcare Inc.) were used for purification. Semipreparative and preparative reversed phase C18 columns were obtained from Phenomenex (Torrance, CA). Superdex 75, CM sepharose and HiTrap SP columns were obtained from GE Healthcare. NMR spectra were recorded on a Bruker AV-400 (400/100 MHz) and Bruker Avance-III 600 (600/150 MHz) spectrometer equipped with a TCI-Z-GRAD cryoprobe. A LCQ LCMS system and a Finnigan LTQ Orbitrap system were used for HRMS and protein conjugation analysis. FTIR was performed on a Perkin-Elmer (Shelton, CT) Paragon 1000 FTIR spectrometer. Melting points were obtained using a SMP3 scientific melting apparatus (Stuart, Bibby Sterlin Ltd.)



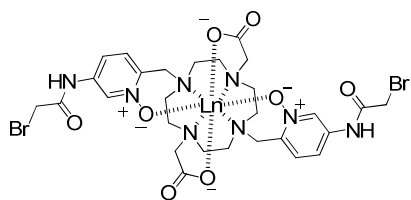
Towards CLaNP-6

The compound **1**¹¹ (1 g, 1.6 mmol) was dissolved in a mixture of TFA/CH₂Cl₂ (3/1, v/v, 8 mL). After 4 h stirring at RT, the reaction mixture was concentrated by coevaporating with toluene. The crude residue obtained was redissolved in 10 mL DMF and triethylamine was added until the pH was neutral. Subsequently, HATU (1.3 g, 3.4 mmol) and 3-aminobenzyl alcohol (0.4 g, 3.4 mmol) were added and stirring was continued for 16 h at RT. Concentration of the reaction mixture, redissolving the residue in mini-Q water, filtering out the solids and concentration of the aqueous layer resulted in crude compound **2**, after which crude **2** (90 mg, 0.13 mmol) was dissolved in 0.5 mL dry MeCN and added into a 2.5 mL dry MeCN solution containing PPh₃Br₂ (531 mg, 1.3 mmol) under argon. The reaction mixture was stirred at 0 °C for 1 h and was quenched with 0.5 mL demi water. During the reaction, the product formation was monitored by LC/MS. The result showed that the **CLaNP-6** decomposed after quenching with water.



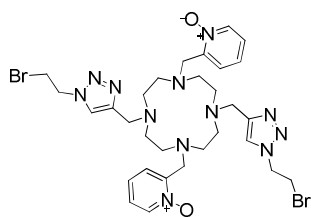
Towards CLaNP-8

Compound **5** (398 mg, 1.92 mmol), **6** (276 mg, 0.87 mmol) and K₂CO₃ (361 mg, 2.61 mmol) were dissolved in 6 mL MeCN, heated to 50 °C and stirred for 16 h. Filtering out the excess K₂CO₃ and concentration of the reaction mixture resulted in crude **7**. Redissolving crude **7** in a mixture of 1,4-dioxane (final concentration is 15 mM) and NaOH (final concentration 0.4 M) and stirring for 3 h at RT yielded compound **7**. Acid-resin was added until the pH ~ 7, and this was then removed by filtration. The filtrate was concentrated *in vacuo* and redissolved in a TFA (6 mL) and CH₂Cl₂ (2 mL) solution mixture. Stirring for 4 h, the reaction mixture was coevaporated with toluene twice. The crude compound **8** (100 mg, 0.19 mmol) obtained and K₂CO₃ (65.5 mg, 0.47 mmol) were dissolved in 1 mL dry MeCN. Bromoacetyl bromide (94.8 mg, 0.47 mmol) was added into the reaction mixture with continuous stirring at RT. Product formation was monitored by LC/MS. When all of the starting material was converted to the desired **CLaNP-8**, the reaction was quenched by adding water, to hydrolyze the excess-reagent(s), which resulted in degradation of the target compound.



Ln-CLaNP-9

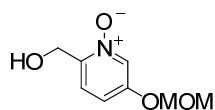
To a solution of **12** (100 mg, 0.187 mmol) in 100 μ L DMF 1.1 equiv. $\text{Lu}(\text{OAc})_3$ was added. The solution mixture was stirred at RT 16 h and the formation of lanthanoid complex was checked by LC/MS. The previously mentioned solution mixture was added into 6.5 mL dry MeCN. Subsequently, NaHCO_3 (15 equiv.) and bromoacetyl bromide (15 equiv.) were added to the reaction mixture. The reaction mixture was stirred at RT for 30 mins and monitored by LC/MS. When the starting material was completely converted to product, the reaction was quenched by few drops of water and run through a PrevailTM C18 column (Alltech[®] Etract-CleanTM) with a 10-50% acetonitrile gradient. The acetonitrile was removed *in vacuo* and the remained aqueous solution was directly used for protein labeling experiment. HR-MS m/z : 947.0408 $[\text{M}]^+$, calcd $[\text{C}_{28}\text{H}_{36}\text{Br}_2\text{LuN}_8\text{O}_8]$: 947.0407.



CLaNP-10

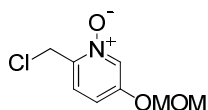
Compound **16** (1.6 g, 6.4 mmol), **17** (1.1 g, 2.9 mmol) and K_2CO_3 (1 g, 7.3 mmol) were dissolved in 30 mL MeCN and the solution mixture was stirred at 50 $^\circ\text{C}$ for 2 days. The excess K_2CO_3 was removed by filtration and the filtrate was concentrated under reduced pressure. The obtained crude compound **18** was redissolved in a solution mixture containing 6 mL TFA and 2 mL CH_2Cl_2 . After 4 h stirring at RT, the TFA was removed by coevaporation with toluene (twice), and then dissolved in 30 mL MeCN. 2-(chloromethyl) pyridine-*N*-oxide (2.3 g, 16 mmol) and K_2CO_3 (2.2 g, 16 mmol) were added to the previously described solution with continuous stirring at 80 $^\circ\text{C}$ for 1 day. The mixture was filtered and concentrated *in vacuo* yielding crude **19**. Crude compound **19** (100 mg) was dissolved in 2 mL dry MeCN and PPh_3Br_2 (20 equiv.) was added at 0 $^\circ\text{C}$. The reaction mixture was allowed to warm up from 0 $^\circ\text{C}$ to RT with continuous stirring for 16 h, and then which was extracted with CH_2Cl_2 . Removing the organic layer, the water layer was purified by HPLC (0.1% TFA and a 10-30% acetonitrile gradient on C18 preparative column) yielding **CLaNP-10** (6 % yield over 3 steps). ^1H NMR (600 MHz, D_2O , 323 K): δ = 8.77 (d, 2H, J = 6.6 Hz), 8.54 (s, 2H), 8.21 (d, 2H, J = 7.8 Hz), 8.05 (t, 2H, J = 7.8 Hz), 7.90 (t, 2H, J = 7.2 Hz), 5.14 (t, 4H, J = 6 Hz), 4.54 (s, 4H), 4.39 (s, 4H), 4.14

(s, 4H, $J = 6$ Hz), 3.87-3.56 (br, 8H), 3.50 (br, 8H). ^{13}C NMR (150 MHz, D_2O , 323 K): $\delta = 144.72, 140.35, 135.67, 131.05, 128.96, 127.56, 127.14, 51.89, 51.55, 49.53, 47.96, 47.28, 30.25$. HR-MS m/z : 834.2380 $[\text{M}]^+$, calcd $[\text{C}_{36}\text{H}_{42}\text{Br}_2\text{N}_{12}\text{O}_2]$: 834.1894.



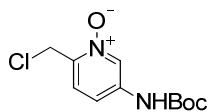
(5-methoxymethoxy-2-hydroxymethyl)pyridine-*N*-oxide (**4**)

To a solution of **3** (900 mg, 5.3 mmol) in 25 mL chloroform *m*CPBA (1.6 g, 6.4 mmol) was added and the reaction mixture was stirred at RT for 16 h. The mixture was quenched with saturated aqueous $\text{Na}_2\text{S}_2\text{O}_3$, extracted with CH_2Cl_2 , dried over MgSO_4 and concentrated *in vacuo*. Purification by silica column chromatography afforded **4** (689 mg, 70%) as a white solid. $R_f = 0.16$ (5% methanol in ethyl acetate). m.p. = 81-82 °C. ^1H NMR (400 MHz, CDCl_3): $\delta = 8.11$ (d, 1H, $J = 2.4$ Hz), 7.19 (d, 1H, $J = 8.8$ Hz), 7.03 (dd, 1H, $J = 8.8$ Hz, $J = 2.4$ Hz), 5.14 (s, 2H), 4.71 (s, 2H), 3.44 (s, 3H). ^{13}C NMR (100 MHz, CDCl_3): $\delta = 154.83, 143.54, 129.79, 124.33, 115.86, 94.96, 60.95, 56.44$. FTIR: 3140.2, 3056.3, 2920.3, 1620.3, 1555.6, 1501.6, 1393.6, 1269.2, 1157.3, 1066.7, 1003.0, 917.2, 825.6 cm^{-1} . HR-MS m/z : 186.0765 $[\text{M}+\text{H}]^+$, calcd $[\text{C}_8\text{H}_{12}\text{NO}_4]$: 186.0761.



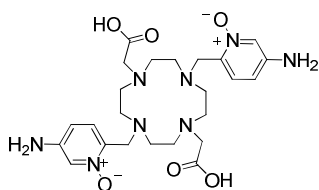
2-(chloromethyl)-5-(methoxymethoxy)pyridine-*N*-oxide (**5**)

Compound **4** (100 mg, 0.54 mmol) was dissolved in 2 mL dry CH_2Cl_2 and cooled with an ice bath. To this cooled solution MsCl (74.5 mg, 0.65 mmol) and TEA (84.0 mg, 0.65 mmol) were added and the reaction was stirred for 1 h at 0 °C. Lithium chloride (226.8 mg, 5.4 mmol) was added into the solution with continuous stirring at RT for 16 h. The white solid and the excess lithium chloride were filtered off, the filtrate was diluted with CH_2Cl_2 and extracted with brine. The organic layer was dried with MgSO_4 and concentrated *in vacuo*. Purification by silica column chromatography afforded **5** (109.7 mg, 91%) as light yellow solid. $R_f = 0.41$ (5% methanol in ethyl acetate). ^1H NMR (400 MHz, CDCl_3): $\delta = 8.12$ (d, 1H, $J = 2$ Hz), 7.38 (d, 1H, $J = 8.8$ Hz), 6.99 (dd, 1H, $J = 8.8$ Hz, $J = 2$ Hz), 5.12 (s, 2H), 4.72 (s, 2H), 3.41 (s, 3H). ^{13}C NMR (100 MHz, CDCl_3): $\delta = 155.11, 140.84, 129.66, 125.44, 114.75, 94.79, 56.37, 39.26$. FTIR: 3038.9, 2966.6, 1622.2, 1557.6, 1501.6, 1432.2, 1398.4, 1304.9, 1259.6, 1183.4, 1148.7, 1015.6, 992.4, 915.3 cm^{-1} . HR-MS m/z : 204.1384 $[\text{M}+\text{H}]^+$, calcd $[\text{C}_8\text{H}_{11}\text{ClNO}_3]$: 204.0422.



5-(tert-butoxycarbonylamino)-2-(chloromethyl)pyridine-*N*-oxide (10)

To a solution of **9** (140 mg, 0.57 mmol) in 6 mL chloroform was added *m*CPBA (169.3 mg, 0.69 mmol). After 4 h stirring at room temperature, the reaction mixture was diluted with 10 mL chloroform and quenched with Na₂S₂O₃. The crude reaction mixture was washed with brine and the organic layer was dried with MgSO₄ and concentrated *in vacuo*. Silica column chromatography afforded title compound **10** (90%, 132.3 mg, 0.51 mmol) as a white solid. The compound decomposed above 194 °C. *R*_f = 0.2 (EtOAc/PET : 2/1 (v/v)). ¹H NMR (400 MHz, d⁶-DMSO): δ = 9.87 (s, 1H), 8.50 (s, 1H), 7.58 (d, 1H, *J* = 8.8 Hz), 7.38 (d, 1H, *J* = 8.8 Hz), 4.79 (s, 2H), 1.47 (s, 9H). ¹³C NMR (100 MHz, d⁶-DMSO): δ = 152.3, 139.8, 138.9, 129.0, 126.8, 114.8, 80.5, 39.5, 27.9. FTIR: 3146.4, 3029.3, 2977.3, 1725.4, 1573.9, 1509.4, 1382.0, 1252.8, 1172.8, 1054.1, 988.6, 871.9 cm⁻¹. HR-MS *m/z*: 259.1905 [M+H]⁺, calcd [C₁₁H₁₆ClN₂O₃]: 259.0844.

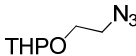


6,6'-(4,10-bis(carboxymethyl)-1,4,7,10-tetraazacyclododecane-1,7-diyl)bis(methylene)bis(3-aminopyridine-*N*-oxide) (12)

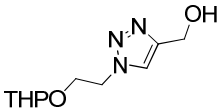
Compound **10** (200 mg, 0.39 mmol), **6** (219 mg, 0.85 mmol) and NaHCO₃ (71 mg, 0.85 mmol) were dissolved in 4 mL DMF. The solution mixture was heated to 50 °C with continuous stirring for 2 days and product formation was monitored by LC/MS. When the reaction was complete, the excess NaHCO₃ was filtered off and the reaction mixture was concentrated *in vacuo* without further purification giving crude compound **11**. Crude compound **11** was taken up in a TFA/CH₂Cl₂ (3/1, v/v, 2 mL) solution mixture. After 4 h stirring at RT, the TFA was removed by coevaporating with toluene (twice) and the crude mixture was redissolved in a 1,4-dioxane and NaOH solution mixture (The final concentration of starting material was 15 mM and 0.4 M for NaOH). The reaction was stirred for 4 h at RT, after which it was neutralized by acid resin, followed by filtrating off the resin, concentration, and purification by HPLC (0.1% TFA and a 0-10% acetonitrile gradient on C18 preparative column) yielding **12** (60%, over 3 steps). ¹H NMR (600 MHz, D₂O, 323 K): δ = 8.24 (d, 2H, *J* = 2.4 Hz), 7.81 (d, 2H, *J* = 9 Hz), 7.36 (dd, 2H, *J* = 9 Hz, *J* = 2.4 Hz), 4.91 (s, 4H), 3.68 (br, 8H), 3.60 (s, 4H), 3.48 (br, 8H). ¹³C NMR (150 MHz, D₂O, 323 K): δ = 174.7, 163.8, 149.8,

131.4, 129.0, 128.2, 118.6, 116.7, 54.9, 54.1, 52.5, 49.6. FTIR: 3344.7, 3203.9, 3065.9, 1666.5, 1611.6, 1425.5, 1169.9, 1126.5, 1085.9, 978.9, 829.4 cm^{-1} . HR-MS m/z : 532.4383 $[\text{M}]^+$, calcd $[\text{C}_{24}\text{H}_{36}\text{N}_8\text{O}_6]$: 532.2758.

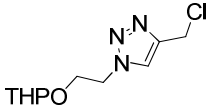
2-(2-azidoethoxy)-tetrahydro-2H-pyran (**14**)

 To a solution of **13** (1 g, 11.5 mmol) in 38 mL dry CH_2Cl_2 DHP (1.3 mL, 13.8 mmol) and PTTs (288 mg, 1.15 mmol) were added. After 16 h stirring at RT, the reaction mixture was washed with NaHCO_3 , dried by MgSO_4 , concentrated *in vacuo* and purified by column chromatography yielding compound **14** (95%, 1.9 g). R_f = 0.38 (EtOAc/PET = 1:1 (v/v)). ^1H NMR (400 MHz, CDCl_3): δ = 4.64 (t, 1H), 3.92-3.82 (m, 2H), 3.59-3.50 (m, 2H), 3.42-3.33 (m, 2H), 1.86-1.58 (m, 6H). ^{13}C NMR (100 MHz, CDCl_3): δ = 98.8, 66.4, 62.0, 50.9, 30.4, 25.4, 19.1. FTIR: 2941.4, 2870.0, 2098.5, 1440.8, 1282.7, 1122.6, 1033.8, 977.9, 871.8, 813.9 cm^{-1} . HR-MS m/z : 172.0969 $[\text{M}+\text{H}]^+$, calcd $[\text{C}_7\text{H}_{14}\text{N}_3\text{O}_2]$: 172.1081.

(1-(2-(tetrahydro-2H-pyran-2-yloxy)ethyl)-1H-1,2,3-triazol-4-yl)methanol (**15**)

 Compound **14** (856 mg, 5 mmol) was dissolved in a solvent mixture of THF (7 mL) and H_2O (3 mL). Propargyl alcohol (321 μL , 5.5 mmol), 100 μL of 500 mM CuSO_4 (aq.) and 1 mL of 1 M ascorbate acid (aq.) were added to the solution mixture. The reaction mixture was stirred at RT for 16 h, and then it was extracted with ethyl acetate. The organic layer was dried using MgSO_4 , concentrated *in vacuo* and purified by column chromatography giving product **15** (96%, 1.09 g). R_f = 0.15 (Ethyl acetate). ^1H NMR (400 MHz, CDCl_3): δ = 7.65 (s, 1H), 4.69 (s, 2H), 4.55-4.43 (m, 3H), 4.30 (s, 1H), 4.04-3.99 (m, 1H), 3.73-3.67 (m, 1H), 3.62-3.56 (m, 1H), 3.41-3.36 (m, 1H), 1.72-1.39 (m, 6H). ^{13}C NMR (100 MHz, CDCl_3): δ = 147.8, 122.9, 98.9, 65.7, 62.3, 55.9, 50.4, 30.3, 25.1, 19.3. FTIR: 3375.4, 2941.4, 2870.0, 1734.0, 1440.8, 1348.2, 1122.6, 1031.9, 869.9, 812.0 cm^{-1} . HR-MS m/z : 227.1278 $[\text{M}+\text{H}]^+$, calcd $[\text{C}_{10}\text{H}_{17}\text{N}_3\text{O}_3]$: 227.1264.

4-(chloromethyl)-1-(2-(tetrahydro-2H-pyran-2-yloxy)ethyl)-1H-1,2,3-triazole (**16**)

 To a dry solution of **15** (9.58 g, 42.2 mmol) in 125 mL CH_2Cl_2 at 0 $^\circ\text{C}$ MsCl (3.94 mL, 50.6 mmol) and triethylamine (7.2 mL, 50.6 mmol) were added

with continuous stirring for 3 h. The reaction was extracted with brine, dried using MgSO_4 and concentrated *in vacuo*. The crude mixture was dissolved in 20 mL dry acetone and lithium chloride (10 equiv.) was added. The reaction was stirred 16 h at RT. Concentration *in vacuo*, redissolving in CH_2Cl_2 , extraction with brine, drying (MgSO_4), concentrating, and purifying by silica chromatography gave product **16** (85%, 8.81 g). $R_f = 0.22$ (EtOAc/PET = 1:1 (v/v)). ^1H NMR (400 MHz, CDCl_3): $\delta = 7.73$ (s, 1H), 4.69 (s, 2H), 4.59-4.51 (m, 2H), 4.09-4.05 (m, 1H), 3.76-3.73 (m, 1H), 3.59-3.56 (m, 1H), 3.44-3.42 (m, 1H), 1.76-1.64 (m, 2H), 1.56-1.53 (m, 4H). ^{13}C NMR (100 MHz, CDCl_3): $\delta = 144.6, 123.9, 99.0, 65.6, 62.4, 50.6, 36.3, 30.4, 25.2, 19.3$. FTIR: 2943.4, 2870.1, 1734.0, 1352.1, 1228.7, 1122.6, 1033.8, 964.4, 869.9, 813.9, 729.1 cm^{-1} . HR-MS m/z : 246.0782 $[\text{M}+\text{H}]^+$, calcd $[\text{C}_{10}\text{H}_{17}\text{ClN}_3\text{O}_2]$: 246.1004.

General method for protein labeling experiment

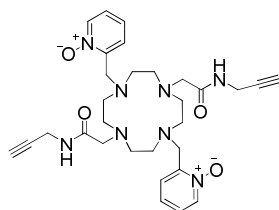
Both of the ^{15}N enriched Paz and T4Lys were kindly performed by Mrs. Anneloes Blok and Dr. Monika Timmer (Leiden University, Inst. Chemistry). To attach Ln-**CLaNP-9** to T4Lys N55C/V57C and Paz E51C/E54C, protein sample (1 mL, 150-300 μM) was treated with DTT (final concentration 5 mM) at 0 $^\circ\text{C}$ for 1 h to remove possible dimers. The reaction mixture was loaded on a PD-10 column (GE Healthcare) pre-equilibrated with labeling buffer (20 mM Tris, 150 mM NaCl and pH 8.0) to remove DTT. To avoid any reoxidation by air, the buffer was degassed and the PD-10 column kept under an argon atmosphere. To the eluted protein eight equivalents Ln-**CLaNP-9** were added. For T4Lys N55C/V57C, the labeling reaction was stirred at RT for 6 h, after which the tagged protein was purified on a HiTrap-SP column. The mass of the resulting ^{15}N T4Lys Lu-**CLaNP-9** (20478 ± 2 Da) agreed with the expected mass of 20478 Da assuming 98% ^{15}N enrichment. In the case of Paz E51C/E54C, the protein was activated with TCEP, after which the probe attached Paz sample was concentrated to 500 μL , $\text{K}_3[\text{Fe}(\text{CN}_6)]$ was added until 1 mM, and purified over a Superdex 75 gel filtration column. The mass of ^{15}N Paz Yb-**CLaNP-9** (14410 ± 2 Da) also agreed with expected mass 14411 Da. The yield of labeling after purification was 50 ~ 80%, which estimated from the intensity of diamagnetic peaks in the spectra of samples with paramagnetic tags.

PCS analysis

The PCS analysis, $\Delta\chi$ -tensor calculation and Q factor are based on published method (Chapter 2). Instead of NIH-XPLOR, a program NUMBAT¹⁶⁸ was used to calculate the $\Delta\chi$ -tensor. The structures of Paz and T4Lys were taken from PDB entries 1PY0 and 3DKE and hydrogens were added. The variation in the Ln positions was calculated by randomly removing 10% PCS data and repeating the $\Delta\chi$ -tensor fit 100 times.

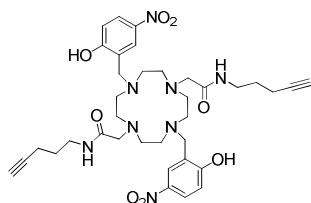
General protocol for CLaNP-click series

To a solution of **17** (100 mg, 0.31 mmol) in 5 mL MeCN **20a** or **20b** (2.5 equiv.) and K₂CO₃ (106.9 mg, 0.77 mmol) were added with continuous stirring at RT for 16 h. The excess K₂CO₃ was filtered off and the filtrate was concentrated *in vacuo* without any purification. The concentrated crude compounds were re-dissolved in 10 mL MeCN. To synthesize **CLaNP-11** and **CLaNP-12**, K₂CO₃ (2.5 equiv.), 2-(chloromethyl)pyridine-N-oxide and 2-(bromomethyl)-4-nitrophenol (2.5 equiv.), respectively, were added and the reaction mixture was stirred at 80 °C. After 16 h stirring, the reaction was allowed to cool to RT, the excess K₂CO₃ was filtered off, concentrated, and purified by HPLC.



CLaNP-11

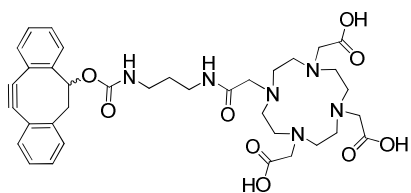
Purification by HPLC (0.1% TFA and a 5-30% acetonitrile gradient on C18 preparative column) yielded **CLaNP-11** (41.6 %). ¹H NMR (600 MHz, D₂O, 323 K): δ = 8.75 (d, 2H, J = 6.6 Hz), 8.13 (d, 2H, J = 7.8 Hz), 8.06 (t, 2H, J = 7.8 Hz), 8.00 (t, 2H, J = 7.8 Hz), 4.99 (s, 4H), 4.35 (s, 4H), 3.65-3.62 (br, 8H), 3.54-3.47 (br, 12H), 2.85 (t, 2H, J = 2.4 Hz). ¹³C NMR (150 MHz, D₂O, 323 K): δ = 170.29, 139.76, 132.18, 129.93, 128.44, 117.16, 115.22, 79.70, 71.65, 56.77, 53.80, 50.40, 49.02, 28.69. FTIR: 3556.7, 3408.2, 3244.3, 2985.8, 2125.1, 1654.8, 1124.5, 829.4 cm⁻¹.



CLaNP-12

Final product was purified by HPLC (0.1% TFA and a 0-50% acetonitrile gradient on C18 preparative column). ¹H NMR (600 MHz, d⁶-DMSO, 323 K): δ = 8.50 (s, 2H),

8.21-8.19 (m, 4H), 7.12 (d, 2H, $J = 6$ Hz), 4.35 (s, 4H), 3.67 (br, 2H), 3.26-3.30 (m, 16H), 3.09 (s, 8H), 2.67 (t, 2H, $J = 2.4$ Hz), 2.19 (t, 4H, $J = 7.2$ Hz), 1.66-1.62 (m, 4H). ^{13}C NMR (150 MHz, $\text{d}^6\text{-DMSO}$, 323 K): $\delta = 169.58, 163.81, 139.24, 129.31, 127.02, 116.31, 83.67, 71.02, 54.33, 51.14, 49.65, 48.97, 37.77, 27.72, 15.29$. FTIR: 3304.1, 3115.0, 2958.8, 2112.0, 1647.2, 1338.6, 1197.8, 1080.1, 717.5 cm^{-1} . HR-MS m/z : 721.3672 $[\text{M}+\text{H}]^+$, calcd $[\text{C}_{36}\text{H}_{49}\text{N}_8\text{O}_8]^+$: 721.3668.



CLaNP-DIBO

Pyridine (0.36 mL, 4.55 mmol) and *p*-nitrophenyl chloroformate (362 mg, 7.28 mmol) were added into a CH_2Cl_2 (27 mL) solution containing **DIBO** (200 mg, 0.91 mmol). The reaction was stirred 16 h, and then quenched with brine (3 mL). The solution mixture was extracted with CH_2Cl_2 and the organic layer was washed with brine, dried by MgSO_4 , concentrated under reduced pressure to provide crude **22**. To the solution of **22** in 5 mL CH_2Cl_2 was added dry TEA and 1,3-diaminopropane and the reaction was stirred at room temperature. After being stirred for 30 min, the reaction was diluted with CH_2Cl_2 (10 mL), washed with 1 M NaOH (10 mL x 2) and brine (10 mL). The organic phase was dried (MgSO_4), filtered, and evaporated. The crude residue was dissolved in MeOH (2.3 mL) and added into a water solution mixture (6.9 mL) containing DOTA (232 mg, 0.91 mmol) and HOBT (61 mg, 0.91 mmol). The reaction mixture was cooled on ice and pH was adjusted to 4.5-5.0 using *N,N*-diisopropylethylamine. EDC (130 mg) in water (2.3 mL) was added slowly into the mixture which was then stirred with cooling. After a 30 min stirring, the pH was elevated to 8 by adding *N,N*-diisopropylethylamine and the solution was stirred for a further 30 min at room temperature. The reaction was monitored by LC/MS and the title compound was purified by HPLC (0.1% TFA and a 35-55% acetonitrile gradient on C18 preparative column). ^1H NMR (600 MHz, D_2O , 323 K): $\delta = 7.76$ (d, 1H, $J = 7.8$ Hz), 7.73-7.64 (m, 7H), 5.58 (m, 1H), 4.07-3.96 (m, 8H), 3.55-3.47 (m, 24H). ^{13}C NMR (150 MHz, D_2O , 323 K): $\delta = 158.7, 152.49, 150.26, 133.34, 132.95, 131.43, 129.88, 128.86, 127.74, 127.70, 126.62, 125.03, 124.30, 121.76, 114.21, 111.14, 78.46, 70.90, 56.36, 55.43, 51.13, 50.83, 46.79, 39.4, 38.1$. FTIR: 3352.3, 3068.7, 2856.6, 1674.2, 1199.2, 1134.1 cm^{-1} . HR-MS m/z : 707.2844 $[\text{M}+\text{H}]^+$, calcd $[\text{C}_{36}\text{H}_{47}\text{N}_6\text{O}_9]^+$: 707.3399.

Protein production and purification

The production and purification of the ^{15}N enriched bacteriophage T4 Lysozyme (T4Lys) single AzF mutant, N55AzF and D72AzF, double Cys mutant N55C/V57C and the ^{15}N enriched double Cys mutant Paz E51C/E54C were performed by Ms. Anneloes Blok and Dr. Monika Timmer (Leiden University, Inst. Chemistry). The expression and purification of Paz E51C/E54C were followed by published protocol (Chapter 2).

Double Cys mutation T4Lys N55C/V57C were prepared by the WHOPS method¹⁸⁰ using the expression plasmid pET28-T4Lys as a template. The oligonucleotides 5'-GGTCGTAATGCCTGTGGTTGCATTACCAAAGATGAAG CCG-3' and its complement were used as the forward and reverse primers, respectively. *Escherichia coli* BL21 (DE3) was used to express the mutant gene. The transformed cells were incubated overnight in 10 mL ^{15}N rich M9 medium with kanamycin (final concentration 50 $\mu\text{g/mL}$) at 37 °C, 250 rpm. Overnight pre-cultures were diluted 100 times and incubated at 37 °C, 250 rpm. When the OD₆₀₀ value was around 0.8, cultures were induced by adding 1 mM IPTG. The temperature was reduced to 30 °C and cells were harvested 18 h after induction by centrifugation. Cells were lysed with a French pressure cell, and the lysates cleared by centrifugation (45 minutes, 2,500 rpm). Cleared lysate was loaded on a 5 mL HisTrap column (equilibrated in 20 mM Tris pH 7.5, 500 mM NaCl) and eluted with a 0 to 500 mM linear imidazole gradient. After a Ni²⁺-column, EDTA (1 mM) was added to the concentrated protein and the protein was purified over a Superose 12 column (equilibrated in 20 mM Tris pH 7.5, 150 mM NaCl, 1 mM DTT).

In the case of AzF mutant, single AzF mutations T4Lys N55AzF and T4Lys D72AzF were prepared by the WHOPS method¹⁸⁰ using the expression plasmid of wt T4Lys as a template. The oligonucleotides 5'-GGTCGTAATGCCTAGGGT GTGATTACCAAAGATGAGGCCG-3' and its complement were used as the forward and reverse primers, respectively, for N55AzF. Similarly, the oligonucleotides 5'-CTGTTTAATCAGGATGTTTAGGCAGCCGTTTCGTGGAAT TCTGC-3' and its complement were used as the forward and reverse primers, respectively, for D72AzF. pEVOL-AzF (coding for the AzF-tRNA transferase and AzF-tRNA, CAMr) were kindly provided by Prof. Peter Schultz, Scripps Research Institute (California) and was first transformed to *Escherichia coli* BL21 (DE3) and cells were made chemically competent. Then, the pEVOL containing BL21 (DE3)

were transformed with the KANr plasmid coding for the T4Lys AMBER mutant. The doubly transformed cells were grown overnight in 10 mL ^{15}N rich M9 Medium with kanamycin (final concentration is 50 $\mu\text{g/mL}$) and chloramphenicol (final concentration is 34 $\mu\text{g/mL}$). Overnight pre-cultures were diluted 100 times, grown for approximately 3 h at 37 $^{\circ}\text{C}$, 250 rpm, after which the temperature was reduced to 30 $^{\circ}\text{C}$. When the OD_{600} value was around 1.4, cultures were induced by adding 1 mM IPTG, 0.02% (w/v) arabinose and 1, 2 or 5 mM Paz. Cells were harvested 24 h after induction by centrifugation, resuspended in 20 mM Tris pH7.5, 500 mM NaCl). Cells were lysed by French press, cleared by centrifugation (45 minutes, 9,000 rpm). Cleared lysate was loaded on a 5 mL HisTrap column (equilibrated in 20 mM Tris pH 7.5, 500 mM NaCl) and eluted with a 0 to 500 mM linear imidazole gradient. The final yields were 96 mg/L and 112 mg/L of N55AzF and D72AzF culture, respectively.

Protein labeling experiment

The CuAAC reaction was performed in 20 mM HEPES buffer containing 150 mM NaCl (pH = 7.4). A solution mixture of T4LysAzF (50 μM) and paramagnetic NMR probe (250 μM) was treated with 1 mM TCEP, and then 500 μM of CuSO_4 and 50 μM of TBTA in 1:4 DMSO/tBuOH were added. After incubation for 30 min at room temperature, the reaction was stopped by adding 1 μL of 1 M EDTA. All the reactions were checked by SDS-PA gel and excess probe was removed by gel filtration chromatography.

For the ring strain-promoted [3+2] cycloaddition, CLaNP-DIBO coordinated to Gd^{3+} was prepared in DMF and was added to a protein solution, which was in 20 mM HEPES buffer containing 150 mM NaCl (pH = 7.4). The final concentration of the protein was 50 μM and the probe was in five time excess. After 16 h stirring at 4 $^{\circ}\text{C}$, the reaction mixture was concentrated to 1 mL and applied to a PD10 column to remove the unreacted probe. The filtrate was concentrated without further purification and prepared for NMR spectroscopy.

NMR spectroscopy on proteins

The NMR samples of Paz Ln-CLaNP-9 (80-150 μM) were prepared in 20 mM sodium phosphate, 150 mM NaCl buffer and 6% (v/v) D_2O at pH = 7. The Cu(II) was reduced by 5 equiv. TCEP. All T4Lys samples (100-200 μM) contained 20 mM

HEPES, 150 mM NaCl buffer and 6% (v/v) D₂O at pH 7.2. All [¹⁵N, ¹H]-HSQC were recorded at 298 K on a Bruker Avance III 600 MHz spectrometer. Data were processed with NMRPipe and analyzed with CCPNMR Analysis version 2.1. Assignments of the resonances were based on previous work¹⁸¹ and kindly provided by Mr. Simon P. Skinner (Leiden University, Inst. Chemistry).

Chapter IV

CLaNP-5 derivatives: An approach to obtain multiple paramagnetic restraints sets from a single mutation site

Abstract

Site-specific labeling *via* disulfide bridges or thioether linkages are widely employed for paramagnetic probe attachment because cysteine residues can be selectively incorporated in protein. In order to investigate protein-protein and protein-ligand interactions, multiple paramagnetic data sets are required; however, finding suitable mutation sites is sometimes difficult, especially for small proteins. An alternative is to attach different paramagnetic probes to same site. Several CLaNP-5 derivatives have been synthesized for this purpose and one of them was tagged to a model protein. The HSQC spectra of methoxyl functionalized CLaNP-5 showed two sets of PCSs. This phenomenon could be explained by an interaction with a neighboring amino acid with the methoxyl group.

Introduction

Lanthanoid complexes have been widely used as paramagnetic centers in high resolution NMR spectroscopy, because the interaction of an unpaired electron provided by lanthanoids with protein nuclei yields significant structural information (Chapter 1). To generate unique paramagnetic effects, lanthanoid probes have to be rigidly and site-specifically attached to proteins. So far, most synthetic probes are tagged to proteins *via* disulfide bonds or thiol alkylation. The advantages of these methods are that the cysteine residues can be selectively incorporated into proteins and these residues react specifically with thiol-reactive groups, avoiding undesired side-products. Multiple unique paramagnetic restraints are required for evaluating protein-protein and protein-ligand interactions. However, finding ideal mutation sites is not easy in many cases, especially for small proteins. Hence, the development of alternative approaches is desirable.

The 12-membered macrocyclic DOTA, an octadentate ligand, is used as a complexing agent, especially for lanthanoid ions. The coordination of DOTA and its analogs to lanthanoid ions is such that two stable enantiomer pairs are formed, namely, capped square antiprism (SA) and twisted capped square antiprism (TSA). These two forms inter-convert slowly on the NMR time scale in solution (Chapter 1). In 2004, pyridine-*N*-oxide was first introduced into DOTA ring and it coordinated to lanthanoid ions *via* a six-membered ring yielding a single conformation, the SA form, in solution.^{39,182} Subsequently, two pyridine-*N*-oxides were substituted the opposite acetate arms of a DOTA ring to give *C*₂-symmetry forming a powerful paramagnetic NMR probe, **CLaNP-5**. The replacement of pyridine-*N*-oxide with *para*-nitrophenol resulted in a next generation probe, **CLaNP-7**. Both of these probes yielded a single set of PCSs and were used for the study of protein-protein interactions (Chapter 1). They exhibit different magnetic susceptibilities at the same attachment site. Therefore, using different paramagnetic probes at single attachment site could be an alternative approach to obtain multiple data sets.

To demonstrate this idea, several **CLaNP-5** derivatives as well as a model system, the **AMC5**-series, were designed and synthesized (Chart 1). The proton at the *para*-position of the pyridine-*N*-oxide ring was replaced with different functional groups to modify the magnetic susceptibility of the probes. The ¹H NMR spectra of Ln³⁺ **AMC5**-series complexes indicate that only a single enantiomeric pair is present in solution and the magnetic susceptibilities depend on the substituents. However,

two sets PCSs were observed in the HSQC spectrum of **CLaNP-5-OMe** tagged protein and the relative intensity was temperature dependent. Possible explanations and the implications for deriving multiple paramagnetic data sets from a set of related probes are discussed.

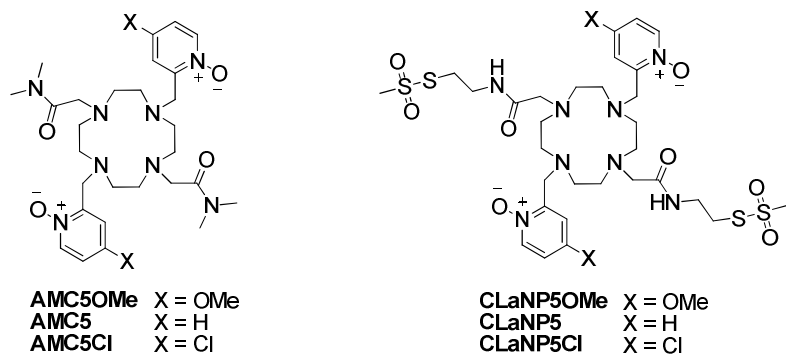
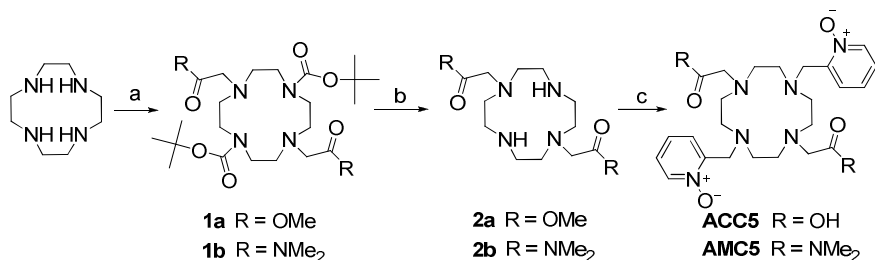


Chart 1. Structures of AMC5 and CLaNP-5 analogs.

Results and discussion

Synthesis of caged lanthanoid NMR probe-5 (CLaNP-5) analogs

The *para*-position in the pyridine-*N*-oxide core is relatively far from the lanthanoid and the substitutions do not have side effect on the overall structure of Ln^{3+} complexes.^{39,145} Consequently, the proton could be replaced with different functional groups. The synthesis of **AMC5** is shown in Scheme 1. The commercially available cyclen was converted to selectively protected **1a** and **1b** using a published protocol.⁴² The protective groups in **1a** and **1b** were fully removed using TFA and the crude compounds were then reacted with 2-(chloromethyl)pyridine-1-oxide at 80 °C to obtain **AMC5**.



Scheme 1. Synthesis of AMC5. (a) i) BocOSu, CHCl₃, RT, 1 day; ii) methyl bromoacetate or 2-chloro-*N,N*-dimethylacetamide, K₂CO₃, MeCN, RT, 16 h; (b) TFA, CH₂Cl₂, RT, 4 h; (c) K₂CO₃, 2-(chloromethyl)pyridine-*N*-oxide, MeCN, 80 °C, 12 h.

and the vicinal protons of the cyclen ring. The most shifted axial cyclen ring proton resonances of all of the Eu^{3+} -complexes were near 20-30 ppm, typical of SA structures,¹⁸⁴ indicating that there is only one enantiomer pair in solution. Moreover, the proton resonances differ between the samples with the different substituents for both lanthanoid complexes, indicating that the magnetic susceptibility is affected by the substituents, although not to a large extent. The lanthanoid induced shift (LIS) is the sum of three contributions: diamagnetic, contact, and pseudocontact shifts (eq 1).

$$\delta_{LIC} = \delta_{dia} + \delta_{con} + \delta_{pcs} \quad (\text{eq 1})$$

The diamagnetic shift is usually caused by conformational changes, inductive effects, and electric field effects and its value are usually determined using diamagnetic lanthanoid ions (La^{3+} , Lu^{3+}), because that they provide isostructural complexes for the early and the late lanthanoid of the series, respectively. Contact shifts (CS) are through-bond interactions of the unpaired 4f electron spin with the coordinated nucleus, and they decrease rapidly as the number of bonds between the lanthanoid and observed nucleus increases. The pseudocontact shift (PCS) originates from a through-space dipolar interaction between the unpaired electron and observed nucleus. PCS is relevant for protein-protein and protein-ligand interaction. CS is not because the nuclei are too far away or even not bonded in such systems. In the case of Yb^{3+} , the contact shift is usually negligible because it has greatest charge density in the paramagnetic lanthanoid series. As a result, the LIS of Yb^{3+} is dominated by PCSs. As shown in Figure 1, the proton resonances of Yb^{3+} complexes were shifted by changing functional groups, suggesting that the magnetic susceptibilities are different.

To demonstrate the feasibility of our hypothesis, **CLaNP-5-OMe** as well as **CLaNP-5** coordinated to diamagnetic Lu^{3+} and paramagnetic Yb^{3+} were attached to a model protein, ubiquitin (Ub) A28C/D32C and the $[\text{}^{15}\text{N}, \text{}^1\text{H}]$ -HSQC spectra of labeled proteins are shown in Figure 2. Surprisingly, two sets of PCSs were observed in the case of **CLaNP-5-OMe**, but a single set for **CLaNP-5**. One of these two sets of PCSs was similar to the one of **CLaNP-5** and most of the paramagnetic peaks were merged to “CLaNP5-like” peaks when the temperature was increased. Some resonances showed PCSs of the opposite sign compared to the shift observed with “CLaNP5-like”. Those amide resonances with different sign are located in the same area of protein, as showed in Figure 3. This is indicative of the fact that these two sets of PCSs had differently orientated magnetic susceptibility tensors, the

“CLaNP5-like” state and the “additional” state. The $\Delta\chi$ -tensors and metal positions of **CLaNP-5** and the two states of **CLaNP-5-OMe** were calculated using NUMBAT¹⁶⁸. The axial ($\Delta\chi_{ax}$) and rhombic ($\Delta\chi_{rh}$) components are reported in Table 1 and the back-calculated PCSs are plotted versus the observed ones in Figure 4. The $\Delta\chi_{ax}$ and $\Delta\chi_{rh}$ of **CLaNP-5-OMe** are similar to those of **CLaNP-5**. The metal positions of the “additional” state and “CLaNP5-like” state based on calculated $\Delta\chi$ -tensors are slightly different (2.3 Å) and $\Delta\chi$ -tensors show a 40° difference in β angle and 30° in γ Euler angles (Table 1). In the case of **CLaNP-7**, a histidine sits close to the attachment site and forms a hydrogen bond with a proposed ninth coordinating ligand, namely water. As a result, the symmetry of probe was broken, yielding two sets of PCSs (Chapter 2). Here, the attachment site is located on an α -helix and a glutamine, Gln31, is close to it. So, in analogy with **CLaNP-7**, the side-chain amide could form a hydrogen bond with the methoxyl oxygen atom of **CLaNP-5-OMe**, twisting the probe and yielding “additional” state. However, in a model of the probe the distance between the side-chain amide proton of Gln31 and the oxygen atom of methoxyl is too long to form a proper hydrogen bond (Figure 5A).

It is worth noting that the amide resonance of residue Glu34, which is close to that attachment site, shows a small shoulder in the HSQC spectrum of Lu-**CLaNP-5** and these peaks become two clear peaks in the case of Lu-**CLaNP-5-OMe** tagged protein. This suggests also in the **CLaNP-5** case there is a minor second state and that in the methoxyl functionalized **CLaNP-5** the population of this state is enhanced to give the “additional” state. DOTA-based lanthanoid complexes such as Eu-**CLaNP-5** are known to undergo enantiomerization with an exchange rate of 200 s⁻¹ at 298 K.¹¹¹ The ¹H NMR spectrum of Yb-**CLaNP-5-OMe** complex shows a single enantiomeric pair in solution (Figure 6). This symmetry is broken when the probe is bound to a chiral protein, resulting in a pair of diastereoisomers. However, the paramagnetic probe may still present a single set of PCSs if both diastereoisomers are similar enough to have identical $\Delta\chi$ -tensors or if one of the diastereoisomers is much more stable than the other. The former seems to be usually the case for **CLaNP-5**. If the diastereoisomers are sufficiently different or if the disulphide bridges can assume two conformations¹⁸⁵, more than a single set of peaks may result. In the present case, the attachment site A28C/D32C is surrounded by several amino acids with long side-chains (Figure 5B), which may interact sterically with the probe

and more strongly with the methoxyl group, yielding two clear sets of PCSs, by either of these mechanisms.

Table 1. PCSs-based $\Delta\chi$ -tensors of Ub A28C/D32C tagged with Yb-CLaNP-5¹¹ and Yb-CLaNP-5-OMe.

	CLaNP5	CLaNP5-OMe (CLaNP5-like state)	CLaNP5-OMe (External state)
$\Delta\chi_{ax}^a$	9.2±0.5	8.0±0.5	9.5±0.6
$\Delta\chi_{rh}^a$	2.4±0.7	2.7±0.6	3.3±0.5
α	142±4	139±4	147±3
β	87±2	90±2	54±2
γ	91±8	100±8	71±7
Restraints	45	38	33
Q	0.01	0.02	0.01

^a The unit of axial and rhombic components ($\Delta\chi_{ax}$ and $\Delta\chi_{rh}$) is 10^{-32} m^3 .

Conclusion

To develop an alternative method for getting multiple data restraints from a single mutant site, two **CLaNP-5** derivatives as well as a model system were synthesized. The ¹H NMR spectra showed that the paramagnetic shift was affected in the derivatives and all presented a single enantiomeric pair in solution. However, the $\Delta\chi_{ax}$ and $\Delta\chi_{rh}$ based on protein data show that **CLaNP-5-OMe** and **CLaNP-5** have similar magnetic susceptibility tensors. It is concluded that remote changes in the coordination system yield changes in the $\Delta\chi$ -tensor that are too small to be of practical use. The functional group does affect the physical behavior of the probe after attachment. The HSQC spectra of **CLaNP-5-OMe** tagged protein presented two sets of PCSs, but a single set for **CLaNP-5**. This could be explained by interactions of the probe with the surrounding amino acids, because of the increased bulkiness of the **CLaNP-5-OMe**.

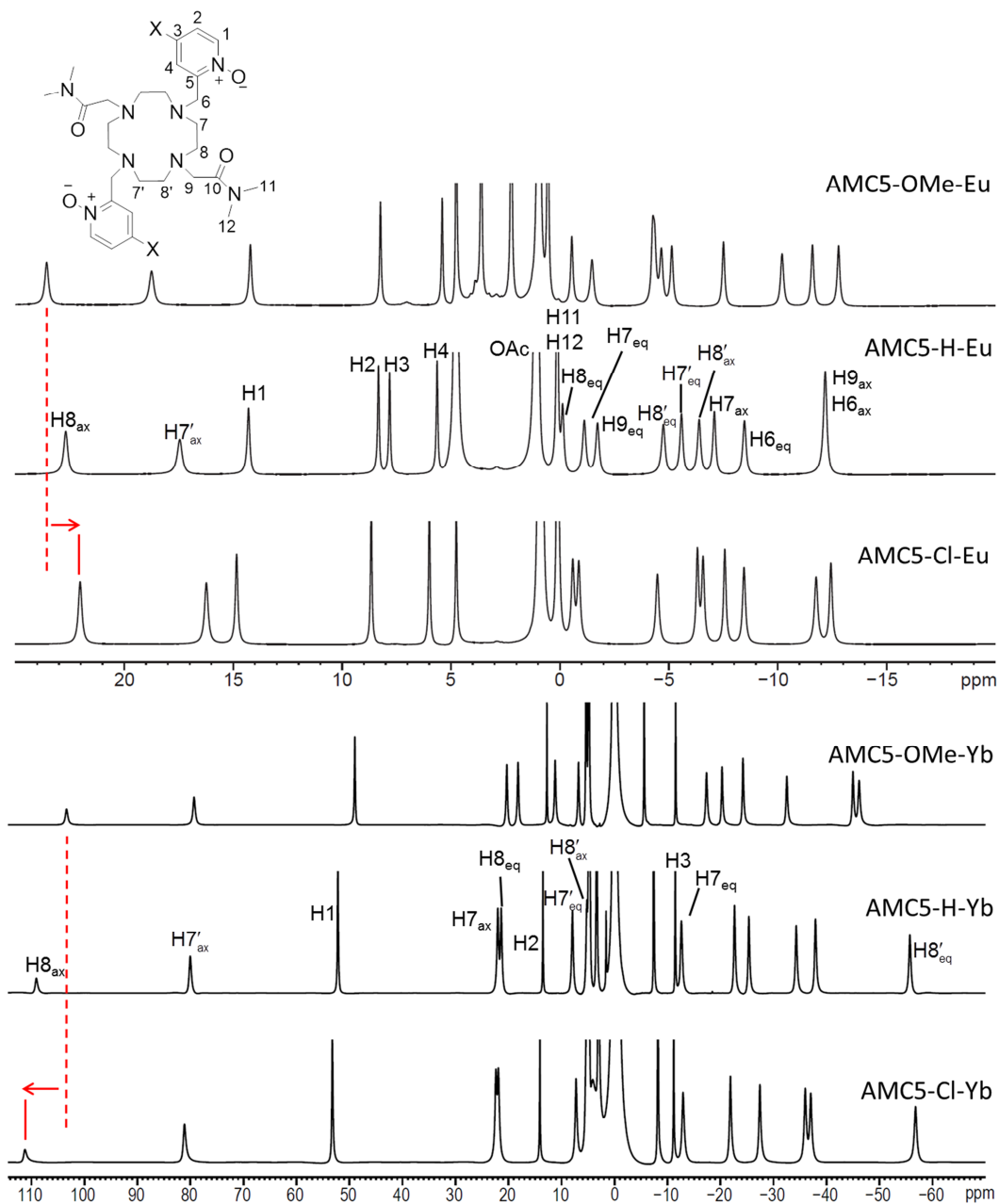


Figure 1. The ^1H NMR spectra of Yb $^{3+}$ and Eu $^{3+}$ complexes with AMC5-series. Proton assignments of AMC5-Eu are indicated by corresponding numbers on the structure. The red dashed and red solid lines indicate the positions of the axial ring proton of AMC5-OMe and AMC5-Cl complex resonances, respectively.

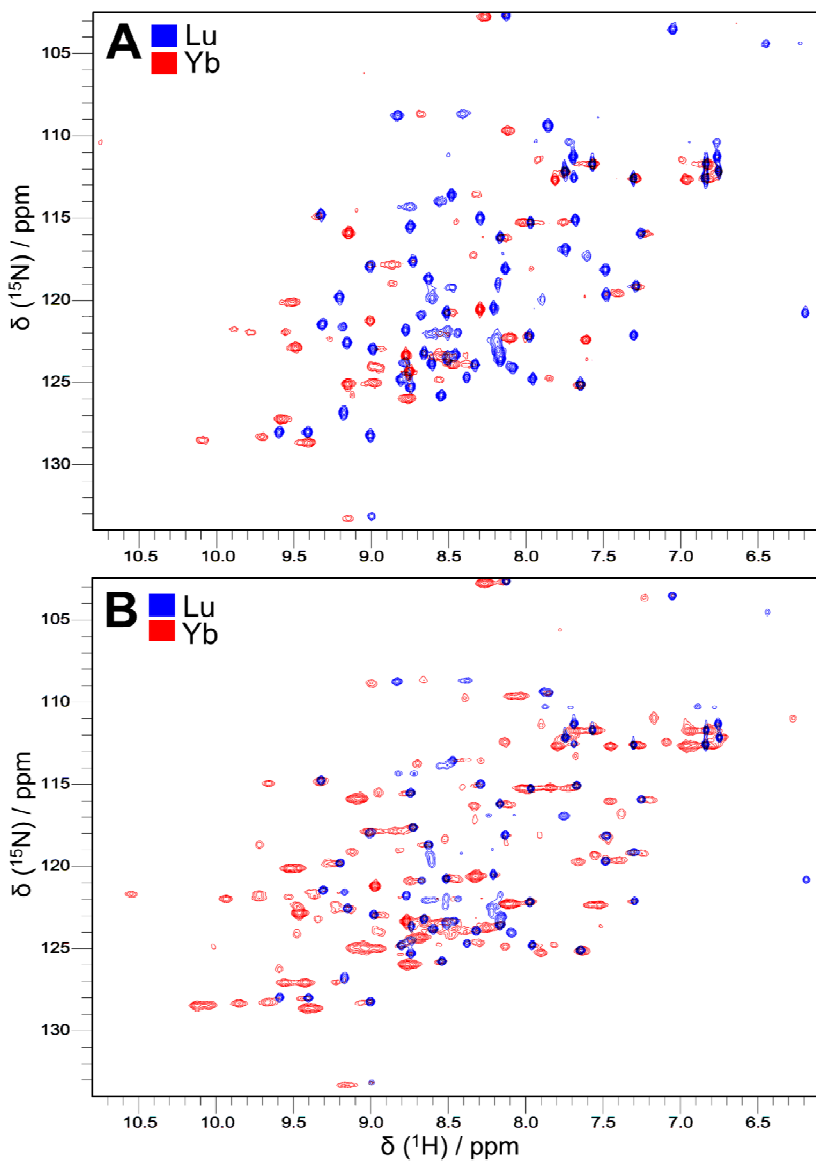


Figure 2. Overlay of ^{15}N , ^1H -HSQC spectra of Ub A28C/D32C attached to CLaNP-5 (A) and CLaNP-5-OMe (B) with diamagnetic Lu^{3+} (blue) and paramagnetic Yb^{3+} (red) at 296 K. Several PCSs are indicated with solid lines.

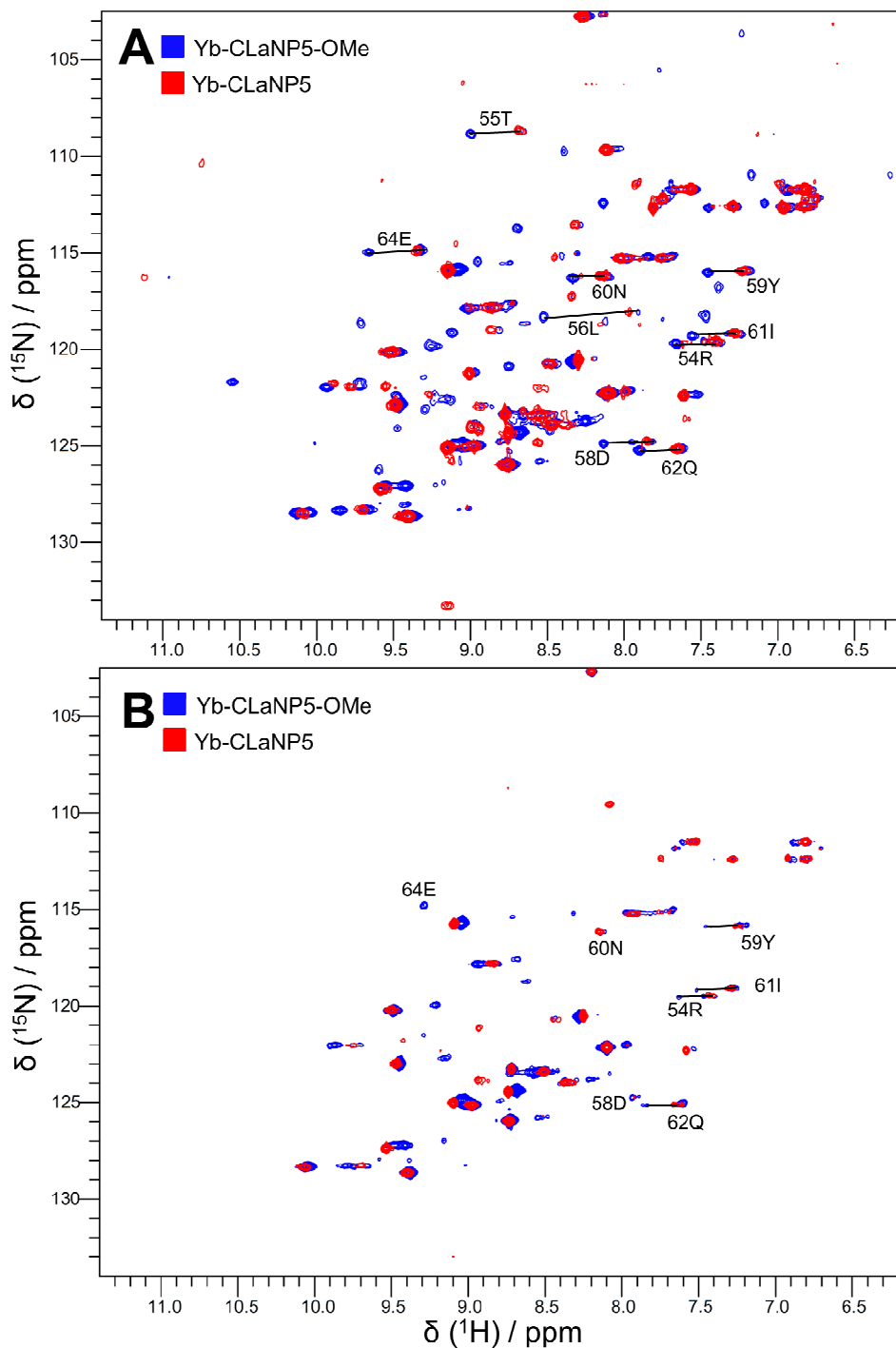


Figure 3. Overlay of $[\text{}^{15}\text{N}, \text{}^1\text{H}]$ -HSQC spectra of Ub A28C/D32C attached to Yb-CLaNP5-OMe (blue) and Yb-CLaNP5 (red) at 296 K (A) and 306 K (B). The assignment of amide proton resonances is indicated in solid line.

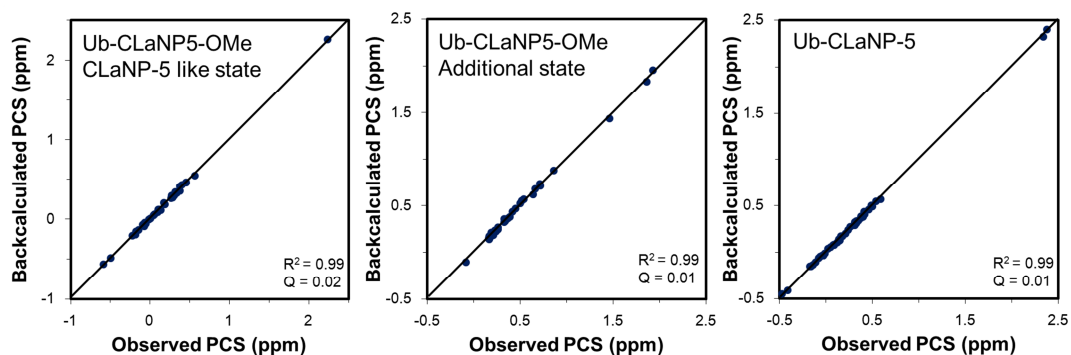


Figure 4. Experimentally observed amide proton PCSs of Ub A28C/D32C Yb-CLaNP-5-OMe and Yb-CLaNP-5 plotted against the back-calculated PCSs. The solid lines represent the perfect correlation ($y = x$).

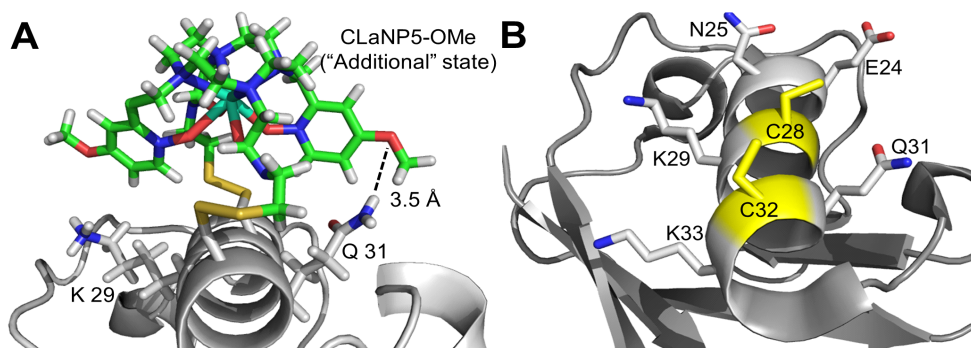


Figure 5. Structure of Ub A28C/D32C attachment site (PDB entry 1D3Z¹⁸⁶). The Cys residues at positions 56 and 58 were modeled. (A) Model of CLaNP-5-OMe attached to Ub A28C/D32C. The position of the Yb³⁺ (cyanine) is derived from a fit to the PCS data. The distance between the side-chain amide proton of Q 31 and the methoxyl oxygen atom is 3.5 Å. (B) The surrounding amino acids with long side-chains are shown. The protein main chain is shown in grey. The Ub (A28C/D32C) and the N 25, E 24, K 29, Q 31, and K 33 side-chains are shown in CPK colors. The carbon atoms from CLaNP-5-OMe are shown in green, nitrogen atoms in blue, oxygen atoms in red and sulfur atoms in yellow.

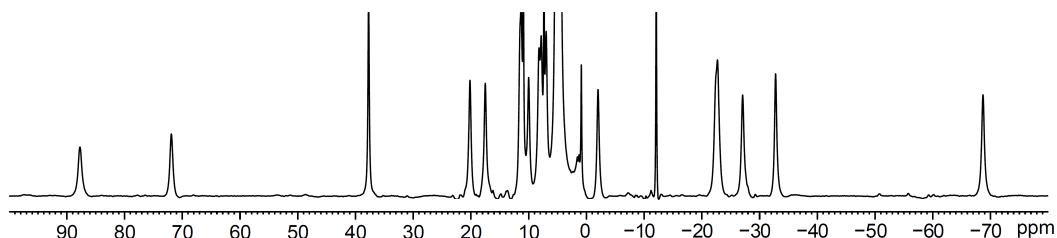


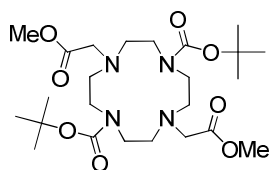
Figure 6. ^1H NMR spectra of Yb-CLaNP-5-OMe complex.

Materials and Methods

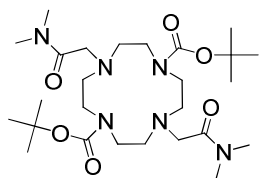
General

Compound **1a**⁴², **1b**⁴², **3**¹⁸⁷, **4**¹⁸⁸, **5**¹⁸⁸, **6**¹⁸³, and **7**¹⁸³ were prepared according to literature procedures and all other chemicals were used as purchased without further purification. TLC-analysis was conducted on DC-alufolien (Merck, Kieselgel60, F254) with detection by UV-absorption (254 nm). Flash chromatography was performed on Screening Devices silica gel 60 (0.04 - 0.06 mm). A Biocad Vision HPLC (PerSeptive Biosystems, inc.) and an Akta Basic FPLC (GE Healthcare Inc.) were used for purifications. Analytical, semipreparative, and preparative reversed phase C18 columns were obtained from Phenomenex (Torrance, CA). Superdex 75 was obtained from GE Healthcare. NMR spectra were recorded on a Bruker AV-400 (400/100 MHz) and Bruker Avance-III 600 (600/150 MHz) spectrometer. A LCQ LCMS system and a Finnigan LTQ Orbitrap system were used for HRMS and protein conjugation analysis. FTIR was performed on a Perkin-Elmer (Shelton, CT) Paragon 1000 FTIR spectrometer. Melting points were obtained using a SMP3 scientific melting apparatus (Stuart, Bibby Sterlin Ltd.)

The synthesis of protective cyclen (**1a**, **1b**)

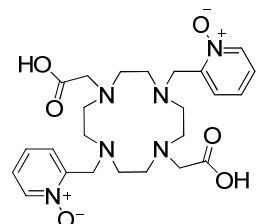


1a and **1b** were prepared according to literature procedures.⁴²
1a: ^1H NMR (400 MHz CDCl_3): δ = 1.27 (s, 18H), 2.69 (br, 8H), 3.21 (br, 8H), 3.28 (s, 4H), 3.51 (s, 6H). ^{13}C NMR (100 MHz CDCl_3): δ = 28.14, 46.21, 50.98, 54.36, 54.54, 79.05, 155.51, 171.39. HR-MS: m/z 517.3225 $[\text{M}+\text{H}]^+$, calcd $[\text{C}_{24}\text{H}_{45}\text{N}_4\text{O}_8]$ 517.3232.



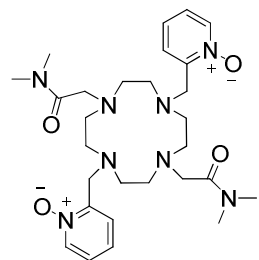
1b: ^1H NMR (400 MHz CDCl_3): δ = 1.36 (s, 18H), 2.79 (br, 8H), 2.84 (s, 6H), 2.96 (s, 6H), 3.37 (br, 12H) ^{13}C NMR (100 MHz CDCl_3): δ = 28.5, 35.4, 36.9, 46.3, 54.5, 56.7, 79.4, 155.9, 170.4. HR-MS: m/z 543.3857 $[\text{M}+\text{H}]^+$, calcd $[\text{C}_{26}\text{H}_{51}\text{N}_6\text{O}_6]$ 543.3864.

ACC5



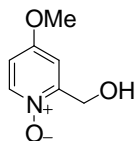
Compound **1a** (273 mg, 0.53 mmol) was dissolved in a 1.5 mL TFA/ CH_2Cl_2 (v/v, 3/1) solution mixture and the reaction was stirred at RT for 4 h. After removal the reaction solvent, the residue was co-evaporated with toluene twice and re-dissolved in 5 mL MeCN. 2-(chloromethyl)pyridine-*N*-oxide (167 mg, 1.16 mmol) and K_2CO_3 (167 mg, 1.2 mmol) were added into the solution mixture and it was stirred at 80 $^\circ\text{C}$ for 16 h. The excess K_2CO_3 was filtered off and the filtrate was concentrated *in vacuo*. The concentrated residue was dissolved in a solution mixture which contains 1,4-dioxane (final concentration was 15 mM) and 3 M NaOH (final concentration was 0.4 M) and was stirred at RT for 4 h. Neutralizing and removing the solvent, the crud compound was purified by HPLC (0.1% TFA and a 5-20% acetonitrile gradient on C18 preparative column) to give **ACC5** (160 mg, 60%). HR-MS m/z : 503.2610 $[\text{M}+\text{H}]^+$, calcd $[\text{C}_{24}\text{H}_{35}\text{N}_6\text{O}_6]$: 503.2613. The NMR data agree with literature reported.¹¹

AMC5



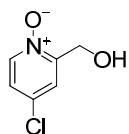
Compound **AMC5** was prepared using the same protocol with **ACC5** and purified by HPLC (0.1% TFA and a 5-20% acetonitrile gradient on C18 preparative column) in 9% yield. ^1H NMR (600 MHz, D_2O , 323 K): δ = 8.37 (d, 2H, J = 6.6 Hz), 7.87 (d, 2H, J = 7.8 Hz), 7.70 (t, 2H, J = 7.2 Hz), 7.59 (t, 2H, J = 6.9 Hz), 4.19 (s, 4H), 4.07 (s, 4H), 3.56 (br, 8H), 3.11-3.06 (br, 8H), 2.91 (s, 6H), 2.87 (s, 6H). ^{13}C NMR (150 MHz, D_2O , 323 K): δ = 165.6, 146.4, 141.1, 131.9, 130.2, 127.8, 54.9, 52.2, 51.7, 49.1, 36.6, 36.4. HR-MS m/z : 557.3559 $[\text{M}+\text{H}]^+$, calcd $[\text{C}_{28}\text{H}_{45}\text{N}_8\text{O}_4]$: 557.3558.

(4-methoxypyridin-2-yl)methanol-*N*-oxide (**8a**)



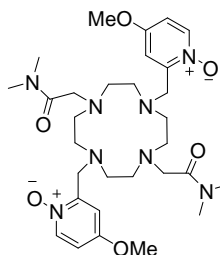
To a solution of **6** (139 mg, 1 mmol) in 5 mL CHCl_3 *m*CPBA (295 mg, 1.2 mmol) was added. The reaction was stirred at RT for 10 h and was directly concentrated *in vacuo* without extraction. Using silica column chromatography purified the crude residues yielding **11a** (148 mg, 96 %) as a white solid. R_f = 0.06 (10% MeOH in ethyl acetate). m.p. = 130 °C. ^1H NMR (400 MHz, CDCl_3): δ = 8.22 (d, 1H, J = 6.8 Hz), 7.78 (d, 1H, J = 2.4 Hz), 7.65 (dd, 1H, J = 6.8, 2.4 Hz), 2.49 (s, 3H), 1.56 (s, 9H). ^{13}C NMR (100 MHz, CDCl_3): δ = 162.4, 148.6, 138.9, 127.6, 126.1, 123.2, 82.1, 27.7, 17.4. FTIR: 3059.1, 2806.4, 1625.9, 1469.7, 1431.2, 1201.6, 1029.9, 736.8 cm^{-1} . HR-MS m/z : 156.0654 $[\text{M}+\text{H}]^+$, calcd $[\text{C}_7\text{H}_{10}\text{NO}_3]$: 156.0655.

(4-chloropyridin-2-yl)methanol-*N*-oxide (**8b**)



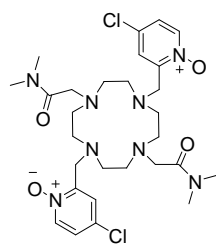
Compound **7** (500 mg, 3.5 mmol) and *m*CPBA (939 mg, 3.8 mmol) were dissolved in 25 mL CHCl_3 and the reaction mixture was stirred at RT. However, the starting material was hardly converted to desired product. After stirring for 16 h, the reaction mixture was concentrated *in vacuo* and purified by silica column chromatography. The title compound was obtained in 30% yield. R_f = 0.3 (10% methanol in ethyl acetate). Compound decomposed over 172 °C. ^1H NMR (400 MHz, $\text{d}^4\text{-MeOD}$): δ = 8.27 (d, 1H, J = 6.8 Hz), 7.71 (d, 1H, J = 2.8 Hz), 7.5 (dd, 1H, J = 6.8 and 2.8 Hz), 4.76 (s, 2H). ^{13}C NMR (100 MHz, $\text{d}^4\text{-MeOD}$): δ = 155.3, 141.4, 136.7, 125.9, 124.7, 59.4. FTIR: 3132.4, 3101.5 3072.6, 3028.2, 2918.3, 1850.8, 1606.7, 1423.4, 1211.3, 1055.0, 862.2 cm^{-1} . HR-MS m/z : 160.0158 $[\text{M}+\text{H}]^+$, calcd $[\text{C}_6\text{H}_7\text{ClNO}_2]$: 160.0159.

AMC5OMe



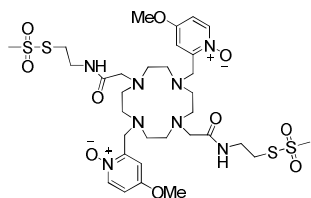
To a solution of **8a** (271 mg, 1.75 mmol) in 10 mL dry CH_2Cl_2 thionyl chloride (229 mg, 1.92 mmol) was slowly added at 0 °C with continuous stirring for 2 h. Few drops of MeOH were added to quench the excess thionyl chloride and the reaction solvent was dry *in vacuo*. The crude precursor without any purification was redissolved in a 10 mL MeCN solution containing K_2CO_3 (241 mg, 1.75 mmol) and **2b** (239 mg, 0.7 mmol) and the reaction was stirred at 50 °C for 1 day. After filtration with celite, the filtrate was concentration, diluted with

water and purified by HPLC (0.1% TFA and a 5-20% acetonitrile gradient on C18 preparative column) providing **AMC5OMe** in 10% yield. ^1H NMR (600 MHz, D_2O , 323 K): δ = 8.41 (d, 2H, J = 7.2 Hz), 7.66 (d, 2H, J = 3.6 Hz), 7.26 (dd, 2H, J = 7.2 Hz, 3.6 Hz), 4.14 (s, 4H), 4.09 (s, 4H), 4.04 (s, 6H), 3.59 (br, 8H), 3.09 (br, 8H), 2.94 (s, 6H), 2.88 (s, 6H). ^{13}C NMR (150 MHz, D_2O , 323 K): δ = 164.8, 164.6, 148.9, 142.8, 116.2, 113.2, 58.2, 55.4, 52.5, 51.6, 48.7, 36.5, 36.4. HR-MS m/z : 617.3768 $[\text{M}+\text{H}]^+$, calcd $[\text{C}_{30}\text{H}_{49}\text{N}_8\text{O}_6]$: 617.3769.



AMC5Cl

The title compound was prepared by following same protocol with **AM5OMe** and purified by HPLC (0.1% TFA and a 5-35% acetonitrile gradient on C30 preparative column) providing **AMC5Cl** in 48% yield. ^1H NMR (600 MHz, D_2O , 323 K): δ = 8.33 (d, 2H, J = 7.2 Hz), 7.97 (d, 2H, J = 3 Hz), 7.61 (dd, 2H, J = 7.2 Hz, 3Hz), 4.19 (s, 4H), 4.02 (s, 4H), 3.59 (t, 8H, J = 5.4 Hz), 3.06-3.01 (br, 8H), 2.92 (s, 6H), 2.90 (s, 6H). ^{13}C NMR (150 MHz, D_2O , 323 K): δ = 164.6, 148.4, 142.0, 137.8, 129.8, 127.8, 55.1, 52.5, 51.6, 48.8, 36.6, 36.4. HR-MS m/z : 625.2778 $[\text{M}+\text{H}]^+$, calcd $[\text{C}_{28}\text{H}_{43}\text{Cl}_2\text{N}_8\text{O}_4]$: 625.2779.

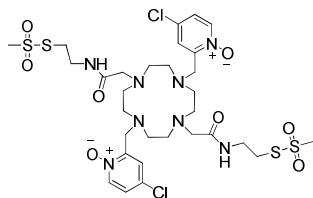


CLaNP-5-OMe

To a solution of **8a** (155 mg, 1 mmol) in 10 mL dry CH_2Cl_2 thionyl chloride (143 mg, 1.2 mmol) was dropwise added at 0 °C with continuous stirring for 2 h. Few drops of MeOH were added to quench the excess thionyl chloride and the reaction solvent was dry *in vacuo*. The crude precursor without any purification was redissolved in a 10 mL MeCN solution containing K_2CO_3 (207 mg, 1.5 mmol) and **2a** (126 mg, 0.4 mmol) and the reaction was stirred at 50 °C for 1 day. After filtration with celite, the filtrate was concentration under vacuo and dissolved in 66 mL of 3M NaOH/1,4-dioxane (v:v/3:20) solvent mixture. The crude reaction mixture was stirred for 4 h, neutralized with acid resin, filtered off, and the filtrate was co-evaporated with toluene twice. To a solution of crude residues (44 mg, 0.08 mmol) in 1mL *N,N*-dimethylformate NHS (36 mg, 0.3 mmol), EDC (60 mg, 0.3 mmol), and aminoethyl-MTS (46 mg, 0.2 mmol) were added. The reaction was stirred at RT for 16 h and

then diluted with 5 mL water. The crude aqueous solution was purified by HPLC (0.1% TFA and a 0-25% acetonitrile gradient on C18 preparative column) to provide title compound in 15% yield over 4 steps. ^1H NMR (600 MHz, D_2O , 323 K): δ = 8.40 (d, 2H, J = 7.2 Hz), 7.59 (d, 2H, J = 3.6 Hz), 7.26 (dd, 2H, J = 7.8 Hz and 3.6 Hz), 4.27 (s, 4H), 4.01 (s, 6H), 3.72 (s, 4H), 3.58 (t, 4H, J = 6.6 Hz), 3.48 (s, 8H), 3.44 (s, 6H), 3.43 (t, 4H, J = 6 Hz), 3.19 (br, 8H). ^{13}C NMR (150 MHz, D_2O , 323 K): δ = 146.1, 142.5, 116.4, 113.5, 58.0, 55.5, 53.0, 51.5, 50.4, 49.9, 39.6, 36.1. HR-MS m/z : 837.2762 $[\text{M}+\text{H}]^+$, calcd $[\text{C}_{32}\text{H}_{53}\text{N}_8\text{O}_{10}\text{S}_4]$: 837.2762.

CLaNP-5-Cl



The title compound was prepared by following the same protocol with **CLaNP-5-OMe** and purified by HPLC (0.1% TFA and a 0-25% acetonitrile gradient on C18 preparative column) providing **CLaNP-5-Cl** in 20% yield.

^1H NMR (600 MHz, D_2O , 323 K): δ = 8.38 (d, 2H, J = 6.6 Hz), 7.99 (d, 2H, J = 2.4 Hz), 7.67 (dd, 2H, J = 6.6 and 3 Hz), 4.19 (s, 4H), 3.87 (s, 4H), 3.60 (t, 4H, J = 6 Hz), 3.54 (s, 8H), 3.45 (s, 6H), 3.35 (t, 4H, J = 6 Hz), 3.17 (br, 8H). ^{13}C NMR (150 MHz, D_2O , 323 K): δ = 146.6, 142.0, 137.5, 129.9, 128.1, 55.4, 52.3, 51.8, 50.5, 49.4, 39.6, 36.1. HR-MS m/z : 845.1774 $[\text{M}+\text{H}]^+$, calcd $[\text{C}_{30}\text{H}_{47}\text{Cl}_2\text{N}_8\text{O}_8\text{S}_4]$: 845.1771.

Preparation of the lanthanoid complexes

To a solution of the **AMC5** derivatives (6 mg ~ 10 mg) in 100 μL D_2O was added 1.1 equiv of $\text{Ln}(\text{OAc})_3$. The solution mixture was stirred at RT for 12 h and monitored by LC/MS spectroscopy. When the free **AMC5** derivatives were completely converted to lanthanoid complexes, the solution mixture was diluted with 400 μL D_2O and the pD value was adjusted until 7 by using NaOD. The complexes without further purification were directly used for NMR experiments. The ^1H , 2D EXSY and COSY spectra were recorded on a Bruker Avance III 600 MHz spectrometer at 298 K.

Paramagnetic Probe Attachment

The lanthanoid complexes of **CLaNP-5** and **CLaNP-5-OMe** and attachment experiments were prepared according to reported protocol.^{11,42} The probe attached

Ub A28C/D32C sample was concentrated to 500 μ L and purified over a Superdex 75 gel filtration column. The yield of labeling, estimated from the intensity of diamagnetic peaks in the [^{15}N , ^1H]-HSQC spectra of samples with paramagnetic tags, was more than 90%. The mass of the resulting ^{15}N -Ub Yb-**CLaNP5-OMe** (9534 ± 1 Da) agreed with the expected mass of 9535 Da, assuming 95% ^{15}N enrichment. The Ub A28C/D32C protein expression and purification were kindly performed by Carlos Castaneda (University of Maryland). The NMR samples of Ub Ln-CLaNP5 and Ub Ln-CLaNP5-OMe (100-200 μM) were prepared in 20 mM HEPES, 100 mM NaCl buffer and pH = 7.2 with 6% (v/v) D_2O . All [^{15}N , ^1H]-HSQC were recorded on a Bruker Avance III 600 MHz spectrometer and data were processed with NMRPipe.

Chapter V

The application of spin labels

Abstract

Nitroxide radicals are commonly used as a paramagnetic center for electron paramagnetic resonance spectroscopy and nuclear magnetic resonance spectroscopy. Compared with other paramagnetic centers, such as lanthanoid chelating probes, the small size of nitroxide radicals is advantageous. Among all of the nitroxide radicals, *S*-(2,2,5,5-tetramethyl-2,5-dihydro-1H-pyrrol-3-yl)methyl methanesulfonothioate (MTSL) is the most widely used probe. However, the flexible linker complicates the data analysis. To overcome this drawback, a new doubled-armed nitroxide probe and a pyridyl-MTSL analog were synthesized. The results showed that the doubled-armed nitroxide was unstable after attaching to protein. Also, nitroxide radicals were introduced on an inhibitor of P450cam and the cocrystal structures were obtained. These results suggest that substrate/inhibitor functionalized nitroxide radicals might be a potential approach to study protein-ligand complexes.

Introduction

In recent years, nitroxide radicals have not only been used for determining protein topography, local and global structure and dynamics by electron paramagnetic resonance (EPR) spectroscopy,¹⁸⁹ but also for characterizing the dynamic complexes and low populated states of proteins by nuclear magnetic resonance (NMR) spectroscopy.¹⁹⁰ Among all of the nitroxide radical probes, MTSL is the most widely used (Chart 1). It can be site-specifically linked to a protein *via* a disulfide bridge to a Cys residue that is introduced by site-directed mutagenesis. The small size of MTSL is advantageous in comparison with other paramagnetic centers, such as lanthanoid chelating probes. The relatively small probe is unlikely to disturb the structure and the exposed hydrophobic surface of the labeled proteins. However, the mobility of the nitroxide group due to the rotatable bonds complicates the data analysis. It is for the reason that an ensemble of nitroxide positions has to be used to properly represent the paramagnetic center. To reduce the mobility of MTSL, two approaches have been developed. One of those is generating a second link between the nitroxide probe and a protein. Several bifunctional probes have been reported, as shown in Chart 1, and used for EPR studies.¹⁹¹⁻¹⁹³ The other approach is to introduce a bulky group next to the attachment site. Due to steric effects, the internal motion of the nitroxide probe is reduced and one of those derivatives, HO-3606, is shown in Chart 1.^{194,195} In this chapter the synthesis of a new double-armed spin label (DASL), HO-3606 and several inhibitor-based nitroxide probes is described. These probes offer new approach for paramagnetic NMR studies on protein-protein and protein-ligand complexes.

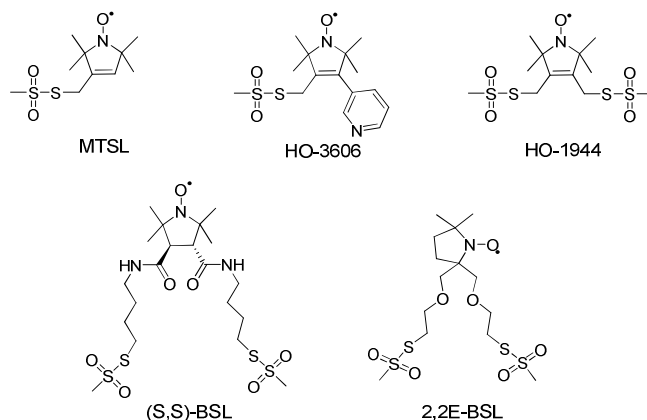
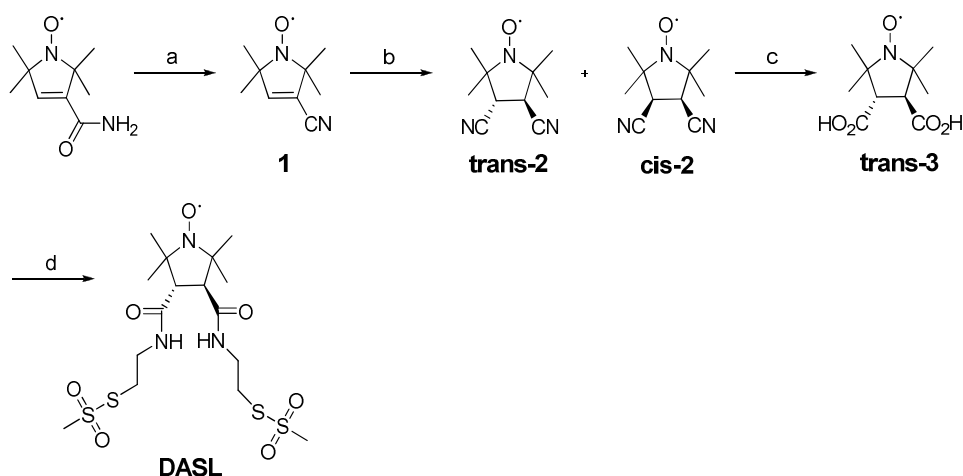


Chart 1. Structures of published spin label probes. Single-armed probes: MTSL¹⁹⁶, HO-3606¹⁹⁵; double-armed probes: HO-1944¹⁹², (S,S)-BSL¹⁹¹ and 2,2E-BSL¹⁹³.

Results and Discussion

Synthesis of double armed spin label (DASL)

According to the literature, several bifunctional nitroxide probes have been developed (Chart 1). However, those probes have some drawbacks. For example, **2,2E-BSL** is a water-soluble bifunctional probe, but two diastereoisomers are generated when it is attached to a protein.¹⁹³ In contrast to **2,2E-BSL**, the other two bifunctional probes, **HO-1944** and **(S,S)-BSL**, have a C_2 -symmetry. The C_2 -symmetric **HO-1944** circumvents the problem of diastereoisomers, but the structure of the attachment site is slightly altered when this rigid probe is linked to a protein.¹⁹² For **(S,S)-BSL**¹⁹¹, the inefficient labeling results in single- or double-armed attachment. The single-armed labeled protein has to be removed by an additional thiol reactive column, which complicates the purification and reduces the yield. Moreover, the long linker might be a potential drawback of bifunctional nitroxide probes due to their flexibility. To enhance the rigidity and labeling efficiency, a modified double-armed spin label (**DASL**) was designed and the synthesis of **DASL** is depicted in Scheme 1. A commercially available radical compound 3-Carbamoyl-2,2,5,5-tetramethyl-3-pyrrolin-1-oxyl was treated with TsCl in pyridine to yield the cyanide **1**. The treatment of **1** with potassium cyanide gave di-functionalized **2**. After hydrolyzing the cyano groups, the di-carboxylic acid **3** was obtained. Finally, the carboxylic acid was coupled with aminoethyl-MTS yielding **DASL**. EPR was used to determine the amount of radical in the **DASL** samples.



Scheme 1. Synthesis of DASL. (a) TsCl, pyridine, RT, 36 h; (b) KCN; (c) i) NaOH; ii) HCl; (d) aminoethyl-MTS, NHS, EDC, DMF, RT, 30 h.

To demonstrate the rigidity of double-armed labeling, **DASL** was attached to a model protein, Paz E51C/E54C. Paz was reduced with DTT in an ice bath for 1 h, washed, reacted with 10 equiv. excess **DASL** for 1 h, and purified by Superdex 75 column (GE Healthcare). For comparison MTSL was attached to Paz E51C. Both proteins were kindly provided by Dr. Monika Timmer (Leiden University, Inst. Chemistry). HSQC and EPR spectra of the tagged proteins were immediately recorded after labeling. In Figure 1, the [^{15}N , ^1H]-HSQC spectra of MTSL and **DASL** labeled Paz as well as the ratio of paramagnetic and diamagnetic peaks are presented. MTSL shows a stronger PRE effect than **DASL**. This unexpected result might arise from the low labeling efficiency or the instability of the probe itself. In order to quantify the degree of labeling, the protein sample was checked by EPR (Figure 2) and LC/MS. The EPR spectra were kindly measured by Mr. Martin von Son. The EPR experiments showed that only 30% of the sample was paramagnetic, whereas the LC/MS showed that the labeling was more than 95% (data now shown). The MS data rule out the possibility of inefficient labeling and show that **DASL** was attached *via* both arms. Further tests demonstrated that, the nitroxide radical of free **DASL** slowly decomposed when it was prepared as a stock solution in DMSO and stored in a fridge. Also, the excess DTT coming from the activation step might reduce the radical. To avoid those possibilities, **DASL** solution was prepared freshly and the excess DTT was removed carefully (see protein labeling experiment). However, the EPR results had no significant improvement. The scaffold of **DASL** is a saturated five-membered ring, pyrrolidine, and it presents significantly higher mobility compared with an unsaturated five-membered ring, pyrroline.¹⁹⁷ Several pyrrolidine ring based spin label probes have been studied and tested with proteins, suggesting that such probes are still stable, although information about the stability was not reported explicitly. The degradation of **DASL** attached to Paz could be a consequence of decreased stability of the mobile five-membered ring. In Paz E51C/E54C, the attachment site is located in a loop region and the distance between the two cysteines is around 10 Å, which could cause strain in **DASL** attachment because the maximum distance that can be spanned by the arms is around 10 Å. Although **DASL** was successfully tagged on the test protein *via* two arms, the flexible saturated pyrrolidine may be further twisted by the attachment, which could result in a more reactive nitroxide. Hence, another test protein with two cysteines closer together could be tested to check whether that yields a more stable probe.

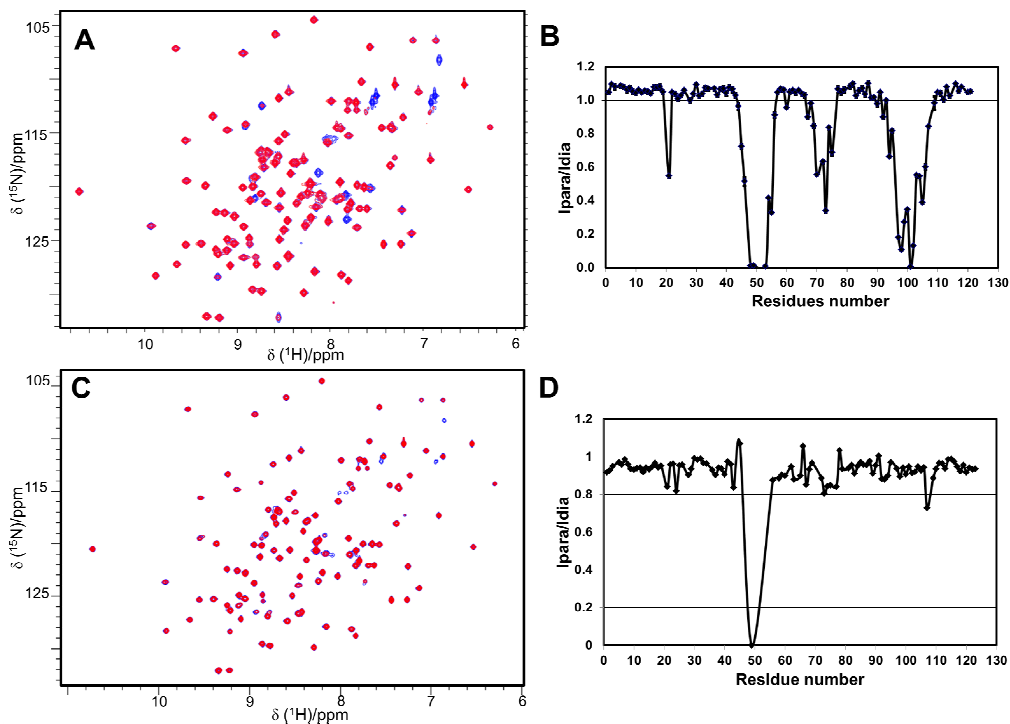


Figure 1. The HSQC spectra and PREs effect of MTSL (A, B) and DASL labeled Paz (C, D). (A, C) Overlay of $^{15}\text{N}, ^1\text{H}$ -HSQC spectra of MTSL (Red) and 1-Acetyl-2,2,5,5-tetramethyl- Δ^3 -pyrroline-3-methyl methanethiosulfonate (Blue) tagged Paz E51C (A) and DASL (Red) and reduced DASL (Blue) tagged Paz E51C/E54C (C). (B, D) $I_{\text{para}}/I_{\text{dia}}$ plots of the spectra in panel A (B) and C (D). MTS and DAS are the diamagnetic controls of MTSL and DASL, respectively.

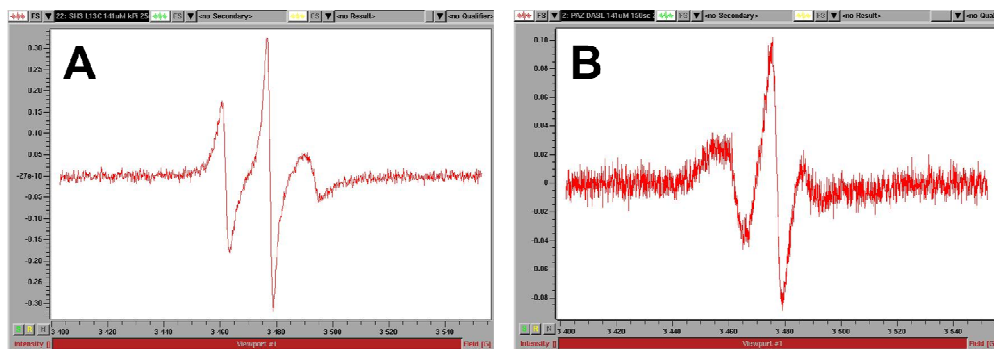
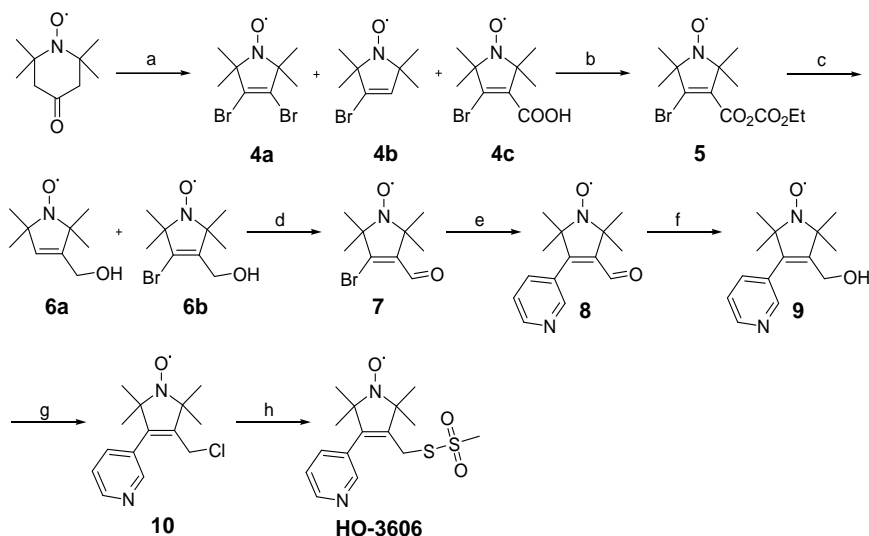


Figure 2. The EPR spectra of MTSL labeled Paz E51C (A) and DASL E51C/E54C (B). The EPR spectra were recorded at ambient temperature.

Synthesis of functionalized spin label

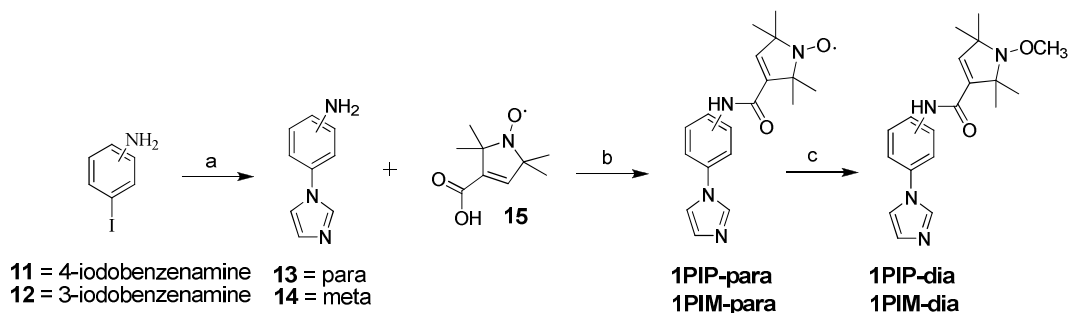
In 2011, Prof. Hubbell and co-workers published a rigid spin label, **HO-3606**, which is a 4-pyridyl analog of MTSL.¹⁹⁵ This substituted probe displays highly restricted motion and the EPR spectra were similar to the 4-phenyl analog of MTSL,¹⁹⁴ for which a single rotamer was found in the crystal structure of tagged protein (PDB code 1ZUR). In contrast, two rotamers were found in the crystal structure of MTSL tagged protein.¹⁹⁸ The observed PRE effects agreed with the theoretically predicted result using a single nitroxide position instead of an ensemble. Consequently, the data analysis can be simplified by using **HO-3606**. The synthesis of **HO-3606** is depicted in Scheme 2. Following the literature protocol, commercially available 4-Oxo-TEMPO was treated with NaOBr yielding the Favorskii rearranged product **4c**. The carboxylic acid group of **4c** was activated with ethyl chloridocarbonate and reacted with NaBH₄ to obtain **6b**. Oxidation of **6b** with CrO₃ in pyridine gave aldehyde **7**. Compound **7** was submitted to Suzuki condition to yield **8**. Treatment of **8** with NaBH₄ in ethanol and conversion of the hydroxyl group in **9** into a chloride yielded **10**. Finally, the chloride **10** was transformed with NaSSO₂CH₃ in a solution mixture of acetone and water, yielding **HO-3606**.



Scheme 2. Synthesis of HO-3606. (a) NaOBr, water/1,4-dioxane; (b) ClCO₂Et, Et₃N, Et₂O, 0 °C to RT, 3 h; (c) NaBH₄, EtOH, 0 °C, 4 h; (d) CrO₃, pyridine, 0 °C, 30 mins; (e) Pd(PPh₃)₄, dioxane, 3-pyridineboronic acid; (f) NaBH₄, EtOH, 0 °C, 4 h; (g) i) MsCl, CH₂Cl₂, 0 °C; ii) LiCl, acetone; (h) NaSSO₂CH₃, acetone/water, 40 °C.

Synthesis of 1-phenylimidazole analogs

A new approach to use paramagnetic centers to study protein complexes is to label enzyme ligands or inhibitors with a paramagnetic center that highlights the active site and interaction surface of the enzyme upon formation of the protein-ligand complex. 1-phenylimidazole (1PI) is a known inhibitor of P450cam and the co-crystal structure was solved by Poulos and Howard.¹⁹⁹ The crystal structure (PDB code 1PHD) shows that the imidazole ring of 1PI sits above the haem and the phenyl group occupies the camphor binding site (Figure 3A). Based on the co-crystal structure, several 1PI analogs were synthesized and used for studying the protein-ligand interaction. The synthesis of 1PI analogs is shown in Scheme 3. The compounds **13**^{200,201} and **14**^{200,201} were activated with HATU and coupled with spin labeled **15** yielding target molecules **1PIP-para** and **1PIM-para**. In order to have diamagnetic controls, the nitroxide radical was blocked with a methyl group by using $\text{FeSO}_4 \cdot 7\text{H}_2\text{O}$, H_2O_2 and DMSO.^{202,203}



Scheme 3. Synthesis of spin labeled 1-phenylimidazole analogs. (a) imidazole, CuI, K_3PO_4 , DMF, 40 °C 40 h; (b) HATU, TEA, DMF, RT, 12 h; (c) $\text{FeSO}_4 \cdot 7\text{H}_2\text{O}$, H_2O_2 , DMSO.

P450cam crystallization

For protein-substrate/inhibitor recognition, conformational changes play an important role. Generally, X-ray crystallography provides a straightforward manner to visualize the recognition. Recently, Prof. Goodin and co-workers reported that the substrate recognition of P450cam occurs by a stepwise mechanism, in which the closed, intermediate, and open conformations are involved.²⁰⁴ Here, the 1PI analogs were also co-crystallized with P450cam by Mr. Yoshitaka Hiruma (Leiden University, Inst. Chemistry) and P450cam was kindly provided by Dr. Monika Timmer (Leiden University, Inst. Chemistry). The co-crystal structures of 1PI analogs with P450cam were solved by Mr. Erik van Orlé and Dr. Navraj Pannu

(Leiden University, Inst. Chemistry). They exhibit an open conformation. Interestingly, the para-substituted 1PIP-dia presents a reversed conformation in comparison with 1PI (Figure 4B). The nitroxide points to the haem iron and the imidazole ring sits in the channel. In contrast, the imidazole ring of meta-substituted 1PIM sits above the haem and the nitroxide is oriented forward the channel. These results could be explained by the structure of active site. The meta-position of 1PI points to the active channel and, conversely, the para-position faces to P450cam side-chains. Thus, linkage of groups to the para-position results in a steric clash with the protein, which explains the observed reverse orientation of the ligand (Figure 4E). The EPR spectra showed that **1PIM-para** is immobilized by P450cam (data not shown). Further studies of the protein-ligand interaction are being carried out by Mr. Martin von Son and Dr. Martina Huber (Leiden University, Inst. Physics).

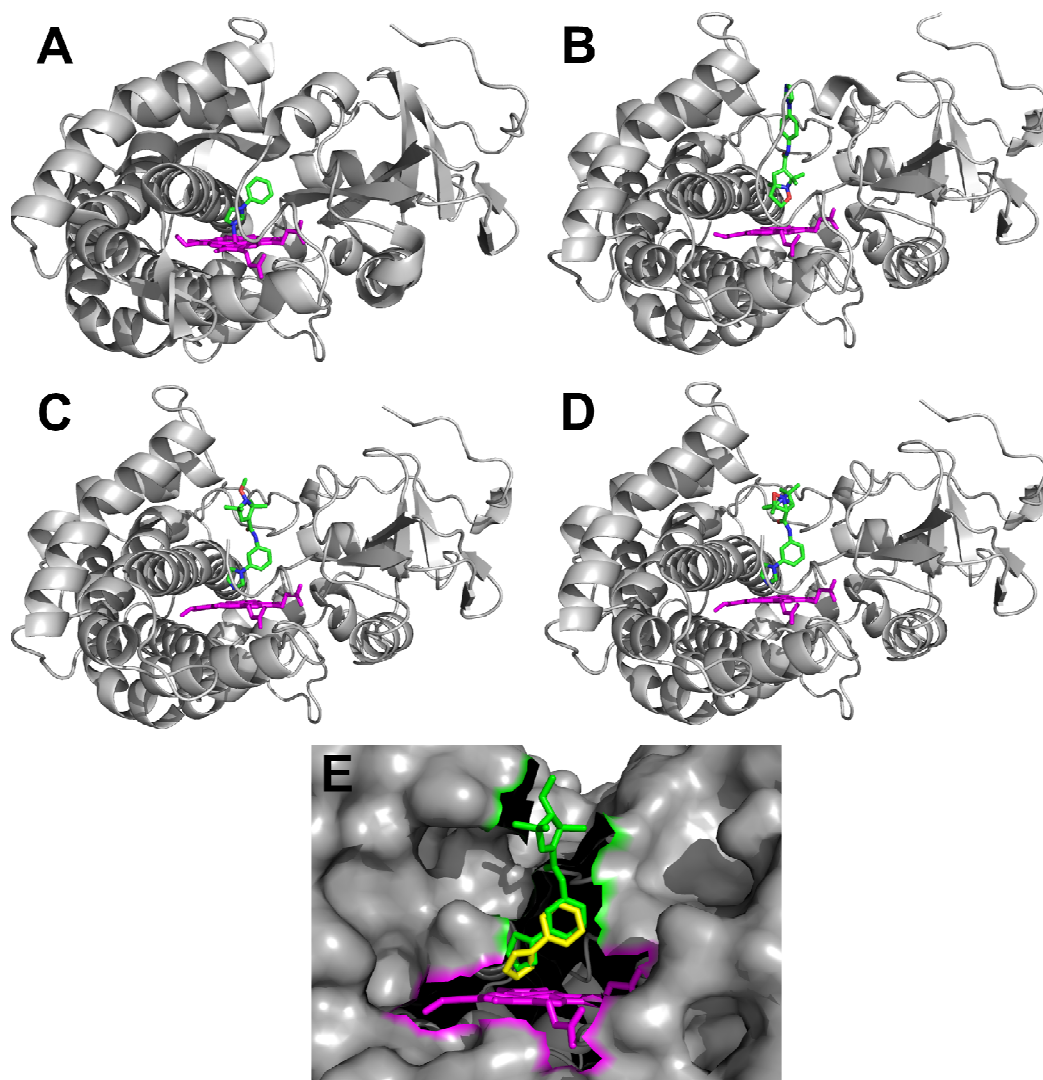


Figure 4. Crystal structures of 1PI and 1PI analogs. (A) The crystal structure of 1PI with P450cam (closed state) (PDB code 1PHD).¹⁹⁹ (B-D) The crystal structures of 1PIP-dia (B), 1PIM-dia (C), and 1PIM-para (D) with P450cam C334A present in the open state. The proteins are shown in grey, the haem in purple, the carbons of 1PI and its analogs in green, nitrogens in blue and oxygens in red. (E) Detail of the crystal structure of 1PIM-dia. The P450cam is shown in grey surface, haem in magenta, 1PIM-dia in green, and 1PI in yellow. Note that the para-position of 1PI faces the protein, whereas the meta-position faces the substrate channel in the open state.

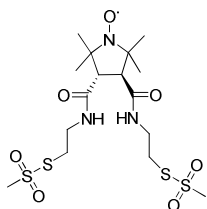
Conclusion

Rigid spin label probes were successfully synthesized and tagged on a test protein. The EPR spectra clearly showed that the mobility of probe was reduced due to two-point attachment. However, the nitroxide of DASL is unstable after attaching to this model protein. A possible explanation is the combination of strain caused by the attachment site and the mobility of the saturated five-membered ring. Hence, another test protein with closer cysteines should be tried to establish the power of DASL.

Substrate/inhibitor analogues can be considered the next generation of probes, which can interact with a designated target protein. In this context, 1-phenylimidazole derivatives, inhibitors of P450cam, were synthesized and the ligands were co-crystallized with P450cam. The imidazole ring of 1PIM-dia and 1PIM-para sits above the haem iron and the nitroxide sits in the channel. By contrast, the nitroxide group faces the haem iron in the case of 1PIP-dia. Both 1PI analogs are locked in the substrate channel, forcing the protein to be in an open state. These initial results suggest this approach is promising for the study of protein-ligand complexes. The spin labels in the P450cam analog may help to study the dynamics of the opening and closing in solution using PRE NMR spectroscopy.

Methods and Materials

Compound **1**^{205,206}, **2**²⁰⁷, **3**²⁰⁷, **8**¹⁹⁵, **9**¹⁹⁵, **10**¹⁹⁵, **HO-3606**¹⁹⁵, **13**^{200,201} and **14**^{200,201} were prepared according to the literature methods. All other chemicals were used as purchased without further purification. TLC-analysis was conducted on DC-alufolien (Merck, Kieselgel60, F254) with detection by UV-absorption (254 nm). Flash chromatography was performed on Screening Devices silica gel 60 (0.04-0.06 mm). A Biocad Vision HPLC (PerSeptive Biosystems, inc.) and an Akta Basic FPLC (GE Healthcare Inc.) were used for purifications. Analytical, semipreparative, and preparative reversed phase C18 columns were obtained from Phenomenex (Torrance, CA). Superdex 75 column was obtained from GE Healthcare. NMR spectra were recorded on a Bruker AV-400 (400/100 MHz) and Bruker Avance-III 600 (600/150 MHz) spectrometer. A LCQ LCMS system and a Finnigan LTQ Orbitrap system were used for HRMS and protein conjugation analysis. FTIR was performed on a Perkin-Elmer (Shelton, CT) Paragon 1000 FTIR spectrometer. Melting points were obtained using a SMP3 scientific melting apparatus (Stuart, Bibby Sterlin Ltd.)

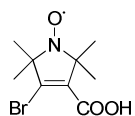


DASL

To a solution of **3** (300 mg, 1.3 mmol) in DMF (11 mL) was added NHS (320 mg, 2.7 mmol), DMAP (340 mg, 2.7 mmol), and aminoethyl-MTS (654 mg, 2.7 mmol) and the solution mixture was cooled to 0 °C. DCC (557 mg, 2.7 mmol) dissolved in 1 mL DMF was then added to the solution mixture and the reaction was allowed to move to RT and stirred continuously for 16 h. The DMF was removed under vacuo and the residue was diluted with chloroform (20 mL). The organic solution was washed with NaHCO_{3(aq.)}, dried by MgSO₄, concentrated under vacuo and purified by silica chromatography. The title compound was obtained in 60% yield. R_f = 0.25 (5% MeOH in CH₂Cl₂). HR-MS m/z : 505.1038 [M+H]⁺, calcd [C₉H₁₅N₂O]⁺: 505.1039.

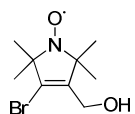
Protein labeling experiment and NMR spectroscopy

To attach DASL to the Paz, protein sample (1 mL, 150 ~ 300 μM) was treated with DTT (final concentration 5 mM) at 0 °C for 1 h to remove possible dimers. The reaction mixture was loaded on a PD-10 column (GE Healthcare) pre-equilibrated with labeling buffer (20 mM sodium phosphate, 150 mM NaCl, pH 7.0) to remove DTT. Instead of regular 3.5 mL eluent collection, 3 mL eluent was collected. Although the protein sample might partly lost, the excess DTT can be removed efficiently. To avoid any reoxidation by air, the buffer was degassed and the PD-10 column kept under an argon atmosphere. To the eluted protein 10 equivalents of DASL or MTSL and their control were added. Those compounds were dissolved in DMSO and prepared freshly. The solution was stirred 1 h at 4 °C. The probe attached Paz sample was concentrated to 500 μL and purified over a Superdex 75 gel filtration column. The purified DASL tagged protein was separated to two portions, one was for paramagnetic sample and the other for diamagnetic control. For diamagnetic control, five equiv. sodium ascorbate were added to reduce the radical. The NMR and EPR spectra were immediately recorded after sample preparation. For EPR and NMR sample, Paz spin-label (100 ~ 150 μM) were prepared in 20 mM sodium phosphate, 150 mM NaCl buffer and 6% (v/v) D₂O at pH = 7. All [¹⁵N, ¹H]-HSQC were recorded at 298 K on a Bruker Avance III 600 MHz spectrometer. Data were processed with NMRPipe and analyzed with CCPNMR Analysis version 2.1. Assignments of the resonances were based on previous work.



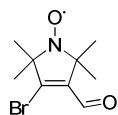
4-bromo-3-(carboxylic acid)-2,2,5,5-tetramethyl-2,5-dihydro-1H-pyrrol-1-yloxy radical (4c)

A solution mixture of H₂O (100 mL) and 1,4-dioxane (25 mL) containing 4-Oxo-TEMPO (5 g, 29.4 mmol) and NaOH (5 g, 125 mmol) was added over 10 min into a 150 mL NaOBr solution which was prepared by Br₂ (5.2 mL) and NaOH (20 g) at -2 to -5 °C. The reaction mixture was stirred at the same temperature for another 20 min, followed by adding Na₂S₂O₃ (2 g) in 6 mL H₂O and the reaction was heated until 35 °C for 30 min. After cooling to 0 ~ 5 °C, the precipitate was filtered off and the filtrate was acidified by using concentrated HCl to yielding pure compound **6** (40 %). Spectroscopic data were in agreement with those reported in the literature.²⁰⁸ HR-MS m/z: 264.0230 [M+H]⁺, calcd [C₉H₁₄BrNO₃]⁺: 264.0229.



4-bromo-3-(hydroxymethyl)-2,2,5,5-tetramethyl-2,5-dihydro-1H-pyrrol-1-yloxy radical (6b)

To a dry solution of **4c** (1 g, 3.8 mmol) and TEA (0.56 mL, 4.6 mmol) in Et₂O (40 mL) was added ethyl chloridocarbonate (500 mg, 4.6 mmol) under 0 °C, and then the reaction mixture was stirred and allowed to warm up to RT over 3 h. The reaction was extracted with water, dried by MgSO₄ and concentrated without further purification. The concentrated residue was dissolved in 4 mL EtOH under -30 ~ -40 °C and NaBH₄ (56 mg) was added into the solution mixture, stirring was continued for an additional 2 h at 0 °C. When the reaction was finished, the solvent was removed by vacuo and the residue was diluted with CH₂Cl₂, washed with brine, and recrystallized by using toluene. The title compound was obtained in 50% yield. Spectroscopic data were in agreement with those reports in the literature.²⁰⁸ R_f = 0.26 (PET/ETOAc, 3/1). HR-MS m/z: 249.0359 [M+H]⁺, calcd [C₉H₁₆BrNO₂]⁺: 249.0359.

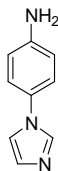


4-bromo-3-formyl-2,2,5,5-tetramethyl-2,5-dihydro-1H-pyrrol-1-yloxy radical (7)

A solution mixture of CrO₃ (1.33 g) and pyridine (2.16 mL) in 6.7 mL dry CH₂Cl₂ was stirred for 15 mins in an ice bath, after which **6b** (562 mg, 2.3 mmol) dissolved in 3.3 mL dry CH₂Cl₂ was added. After an additional 20min stirring, Et₂O was added into the mixture and the precipitate was washed with Et₂O. The Et₂O was collected, washed with 5% HCl_(aq), water, sat. NaHCO₃, brine, dried by MgSO₄ and

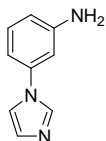
purified by silica column chromatography. Spectroscopic data were in agreement with those reports in the literature.²⁰⁸ $R_f = 0.77$ (PET/EtOAc, 3/1).

4-(1H-imidazol-1-yl)benzenamine (**13**)



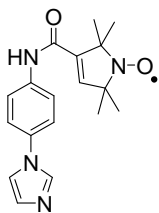
The title compound was prepared according to literature procedures.^{200,201} ^1H NMR (400 MHz, d^4 -MeOD): $\delta = 7.91$ (t, 1H, $J = 1.2$ Hz), 7.37 (t, 1H, $J = 1.2$ Hz), 7.22 (dt, 2H, $J = 8.8$ Hz, $J = 3.2$ Hz), 7.08 (t, 1H, $J = 1.2$ Hz), 6.79 (td, 2H, $J = 8.8$ Hz, $J = 3.2$ Hz). ^{13}C NMR (100 MHz, d^4 -MeOD): $\delta = 149.3$, 136.9, 129.4, 129.0, 123.9, 120.3, 116.7. FTIR: 3340.7, 3184.5, 3113.1, 1608.6, 1517.9, 1253.7, 827.5 cm^{-1} . HR-MS m/z : 160.1076 $[\text{M}+\text{H}]^+$, calcd $[\text{C}_9\text{H}_{10}\text{N}_3]^+$: 160.0869.

3-(1H-imidazol-1-yl)benzenamine (**14**)

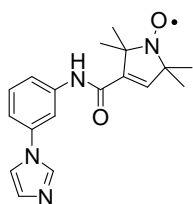


The title compound was prepared according to literature procedures.^{200,201} ^1H NMR (400 MHz, CDCl_3): $\delta = 7.81$ (s, 1H), 7.22-7.15 (m, 2H), 6.75-6.72 (m, 1H), 6.66-6.64 (m, 2H). ^{13}C NMR (100 MHz, CDCl_3): $\delta = 147.9$, 138.2, 135.4, 130.5, 129.9, 118.1, 113.7, 110.9, 107.5. FTIR: 3415.9, 3340.7, 3199.9, 3111.2, 1606.7, 1458.2, 1234.4, 1055.0, 740.7 cm^{-1} . HR-MS m/z : 160.1076 $[\text{M}+\text{H}]^+$, calcd $[\text{C}_9\text{H}_{10}\text{N}_3]^+$: 160.0869.

1PIP-para

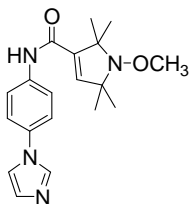


To a solution of **13** (283 mg, 1.8 mmol) in 20 mL DMF was added HATU (640 mg, 2 mmol). After stirring for 30 second, spin labeled **5** (334 mg, 1.8 mmol) was added into the mixture. The reaction was allowed to stir at RT for 16 h. The residue was diluted in water and extracted with CH_2Cl_2 . The organic layer was dried by MgSO_4 , filtered and concentrated. The concentrated crude compound was purified by HPLC (0.1% NH_4OAc and a 10-50% acetonitrile gradient on C18 preparative column). FTIR: 3493.1, 3304.1, 3228.8, 3134.3, 2978.1, 2935.6, 1668.4, 1521.8, 1319.3, 1068.6 cm^{-1} . HR-MS m/z : 326.1737 $[\text{M}+\text{H}]^+$, calcd $[\text{C}_{18}\text{H}_{22}\text{N}_4\text{O}_4]^+$: 326.1737.



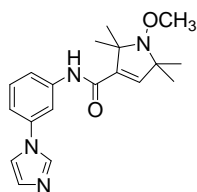
1PIP-para

Following the same protocol with **1PIP-para**, **1PIM-para** was synthesized and purified by HPLC (0.1% NH_4OAc and a 10-50% acetonitrile gradient on C18 preparative column). FTIR: 3448.7, 3253.9, 3205.7, 3082.3, 2978.1, 2931.8, 1664.6, 1600.9, 1550.8, 1440.8, 1217.1, 796.6 cm^{-1} . HR-MS m/z : 326.1738 $[\text{M}+\text{H}]^+$, calcd $[\text{C}_{18}\text{H}_{22}\text{N}_4\text{O}_2]$: 326.1737.



1PIP-dia

A mixture of **1PIP-para** (160 mg, 0.49 mmol) and $\text{FeSO}_4 \cdot 7\text{H}_2\text{O}$ (178 mg, 0.98 mmol) was dissolved in 10 mL DMSO, and then H_2O_2 (140 μL , 1.43 mmol) was added into the reaction mixture. After stirring for 1 h at RT, the residue was diluted with water and extracted with CH_2Cl_2 . The organic layer was dried over MgSO_4 , filtered, concentrated under reduce pressure and purified by HPLC (0.2% TFA and a 25-45% acetonitrile gradient on C18 preparative column) yielding colorless oil **1PIP-dia** (30 mg, 18%). R_f = 0.75 (10% MeOH in CH_2Cl_2). ^1H NMR (600 MHz, d^4 -MeOD): δ = 9.42 (s, 1H), 8.04 (t, 1H, J = 3 Hz), 7.91 (t, 2H, J = 13.2 Hz), 7.75 (t, 1H, J = 2.4 Hz), 7.67 (t, 2H, J = 13.2 Hz), 6.44 (s, 1H), 3.75 (s, 3H), 1.48-1.38 (br, 12H). ^{13}C NMR (150 MHz, d^4 -MeOD): δ = 165.6, 141.9, 141.3, 141.0, 135.6, 131.9, 124.1, 122.9, 122.8, 121.9, 72.7, 69.8, 65.7, 27.5, 21.4. FTIR: 3111.2, 2974.2, 2935.6, 1666.5, 1521.8, 1197.8, 1128.4, 829.4, 719.5 cm^{-1} . HR-MS m/z : 341.1974 $[\text{M}+\text{H}]^+$, calcd $[\text{C}_{19}\text{H}_{25}\text{N}_4\text{O}_2]^+$: 341.1972.



1PIM-dia

Following the same protocol with **1PIP-dia**, **1PIM-dia** was synthesized and purified by HPLC (0.2% TFA and a 25-45% acetonitrile gradient on C18 preparative column). ^1H NMR (600 MHz, d^4 -MeOD): δ = 9.46 (s, 1H), 8.24 (s, 1H), 8.06 (s, 1H), 7.77 (s, 1H), 7.65 (d, 1H, J = 8.4 Hz), 7.58 (t, 1H, J = 8.4 Hz), 7.44 (d, 1H, J = 7.8 Hz), 6.45 (s, 1H), 3.78 (s, 3H), 1.47-1.37 (br, 12H). ^{13}C NMR (150 MHz, d^4 -MeOD): δ = 165.7, 142.0, 141.5, 140.9, 136.8, 135.9, 131.9, 122.9, 122.8, 122.1, 118.9, 115.6, 72.8, 69.9, 65.7, 29.4, 23.2. FTIR: 3410.1, 3128.5, 2991.6, 1666.5, 1606.7, 1170.8,

1130.3, 796.6, 719.5 cm^{-1} . HR-MS m/z : 341.2152 $[\text{M}+\text{H}]^+$, calcd $[\text{C}_{19}\text{H}_{25}\text{N}_4\text{O}_2]^+$: 341.1972.

Chapter VI

General discussion, conclusions and prospects

The majority of the work presented in this thesis involves the design and synthesis of paramagnetic NMR probes, including lanthanoids caged probes and spin labels. An overview of the development of different types of lanthanoids caged probes is given in Chapter 1. In order to design a proper paramagnetic probe, several issues have to be considered: *i*) The ligand must rigidly bind to the lanthanoids with high-affinity. *ii*) The symmetry of the probe is important. *iii*) Site-specific labeling is necessary for generating unambiguous paramagnetic restraints. DOTA, an octadentate ligand, is an outstanding lanthanoids cage compared with others, such as DTPA. It rigidly coordinates to the lanthanoids due to the macrocyclic ring and presents high thermal stability. Among all of the reported lanthanoid probes, the caged lanthanoid NMR probe version 5 (CLaNP-5) shows the largest paramagnetic effects due to the fact that it is tagged to proteins *via* two-point attachment and its free complex presents a single conformation. The attachment site also plays an important role in getting optimal paramagnetic effects. Generalized observations for a CLaNP binding site have been reported by Keizers *et al.*¹¹ It was reported that the distance between the C α atoms of the two cysteines should be roughly 8 Å. Moreover, the incorporated cysteines should be solvent-exposed, with sufficient room for the CLaNP, so not in a cleft. For rigid attachment, an α -helix (at positions *i* & *i*+3 or *i* & *i*+4) or a β -sheet (at positions *i* & *i*+2) are ideal locations. Cross-strand attachments have not been reported for CLaNPs. Such cross-links could interfere with the natural dynamics of the protein. In the case of CLaNP-5, two pyridine-*N*-oxides were introduced to the opposite sites of DOTA ring for reasons of symmetry and disulfide bridges were employed in site-specific labeling. Although CLaNP-5 is successfully applied to study proteins and protein complexes, the net charge of Ln CLaNP-5 complex and the weak disulfide linker are the drawbacks.

Development of next generation lanthanoid-chelating probes

In Chapter 2, the replacement of pyridine-*N*-oxide with *p*-nitrophenol produced a next generation probe, CLaNP-7. The phenolic groups are deprotonated upon coordinating to lanthanoids, giving a lanthanoid complex with one positive charge. In the case of CLaNP-9 (Chapter 3), the linkers were rearranged to the *meta*-position of pyridine-*N*-oxides, keeping the carboxylic acids as the ligands to reduce the net charge of lanthanoid complexes. The introduction of carboxylic acid or negative functional groups such as phosphonic and sulfonic groups on the cyclen ring or the

ethylene of chelating arms may be an alternative approach to reduce the net charge. Another advantage for adding hydrophilic groups is that the undesired hydrophobicity, which arises from the exposed cyclen ring after attachment, can be balanced.

Cysteine is the most commonly modified residue for paramagnetic probe attachment. The thiol group can undergo disulfide exchange to form disulfide bridges as well as Michael addition with α,β -unsaturated carbonyl compounds or electron-poor enes to form a thio-ether. In order to enhance the stability of probe tagged protein, thio-ether linkage using α -ketobromide was utilized in CLaNP-9 (Chapter 3). Two vinyl functionalized dipicolinic acid based probes were also reported to form stable products.^{47,54} Besides electron-poor vinyl group, acrylates/acrylamides and methacrylates/methacrylamides can also be considered.⁴⁶

Bioorthogonal reactions are a new approach to rigidly tag a probe on protein surface at specific site. So far, only one example was reported based on this approach by using copper catalyst click chemistry.⁵⁰ It is clear that this method remains unexploited and different types of bioorthogonal reactions such as photoclick chemistry, norbornene cycloaddition, and [4+1] cycloaddition have to be considered in the future.⁴⁸ The advantage of the use of bioorthogonal reaction is that the probe could be attached to specific site without any side-products. Also dual probe attachment, using both a disulphide linkage and a bioorthogonal reaction are then possible. Disadvantages are that most of the unnatural amino acids are not commercially available and that the linkers are generally longer than disulfide bridges and thioether bonds. Rigid probe attachment requires two-armed attachment, but we found that incorporation of two unnatural amino acids close together in an amino acid sequence affects the yield of the engineered protein quite negatively.

The rigidity and chirality of next generation probes

CLaNP-7 and CLaNP-5-OMe (Chapter 2 and 4) tagged to a protein showed pH-dependent and temperature-dependent magnetic susceptibility tensors, respectively, due to the influence of neighboring amino acids. As a consequence two sets of paramagnetic restraints were observed. These results point out that not only the attachment site but also the conformation of the probe is important to obtain unambiguous paramagnetic NMR restraints. Generally, DOTA-based probe undergoes enantiomerization and the exchange rate is on the NMR time scale. In

solution the lanthanoid caged probes present a single enantiomeric pair but the symmetry of probe is broken upon tagging on a protein surface and a pair of diastereoisomers is obtained. As long as these diastereoisomers are similar to each other, they may still present a single set of paramagnetic effects. If the change in the ligand orientation between the two diastereoisomers is somehow correlated to the orientations of the arms and the protein, the two forms can exhibit different $\Delta\chi$ -tensors and a second set of paramagnetic effects will be present. In order to avoid the enantiomerization, the decoration of amide arms with chiral centers in CLaNP-5-like paramagnetic probes may be one solution (Figure 1). The chirality will force the probe in a single conformation and the complementary conformation can be easily provided by using opposite chirality. In this way, two different orientated magnetic susceptibility tensors can be obtained.

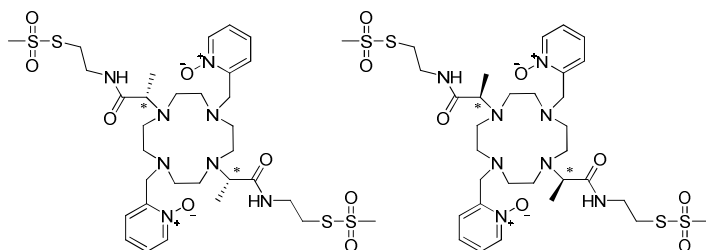


Figure 1. Structures of methyl functionalized CLaNP-5 like chiral probes.

Development of substrate- and inhibitor- based paramagnetic probes

In Chapter 5, the co-crystal structures of protein with inhibitor-based spin label probes were presented. These results show promise for an approach in which protein-ligand interactions are studied by using substrate- and inhibitor- based paramagnetic probes. Also, the dynamics of small compounds have recently been studied by paramagnetic restraints.²⁰⁹⁻²¹¹ Instead of functionalized protein, the lanthanoids were linked to the oligosaccharides. Dedicated paramagnetic ligand derivatives represent a new alternative way for paramagnetic NMR to study protein-ligand interactions. In order to obtain large and unambiguous effects the paramagnetic center should be linked rigidly. CLaNP-11 and CLaNP-12 can be employed in this approach *via* copper-click chemistry due to the rigid and stereoselective cyclic products. However, the aqueous solubility and other properties of substrates and inhibitors may be influenced by the paramagnetic center, especially

for lanthanoid ligands which are relatively large. Nevertheless, it can be foreseen that the future will bring the development of paramagnetic ligands for specific proteins.

Reference List

- (1) Bünzli, J.-C. G. *Chem. Rev.* **2010**, *110*, 2729-2755.
- (2) Edelmann, F. T. *Coord. Chem. Rev.* **2013**, *257*, 1122-1231.
- (3) Butler, S. J.; Parker, D. *Chem. Soc. Rev.* **2013**, *42*, 1652-1666.
- (4) Viswanathan, S.; Kovacs, Z.; Green, K. N.; Ratnakar, S. J.; Sherry, A. D. *Chem. Rev.* **2010**, *110*, 2960-3018.
- (5) Keizers, P. H. J.; Ubbink, M. *Prog. Nucl. Magn. Reson. Spectrosc.* **2011**, *58*, 88-96.
- (6) Reuben, J.; Leigh, J. S. *J. Am. Chem. Soc.* **1972**, *94*, 2789-2793.
- (7) Dwek, R. A.; Richards, R. E.; Morallee, K. G.; Nieboer, E.; Williams, R. J. P.; Xavier, A. V. *Eur. J. Biochem.* **1971**, *21*, 204-209.
- (8) Bünzli, J.-C. G. *Acc. Chem. Res.* **2006**, *39*, 53-61.
- (9) Otting, G. *Annu. Rev. Biophys.* **2010**, *39*, 387-405.
- (10) Allen, K. N.; Imperiali, B. *Curr. Opin. Chem. Biol.* **2010**, *14*, 247-254.
- (11) Keizers, P. H. J.; Saragliadis, A.; Hiruma, Y.; Overhand, M.; Ubbink, M. *J. Am. Chem. Soc.* **2008**, *130*, 14802-14812.
- (12) Madl, T.; Güttler, T.; Görlich, D.; Sattler, M. *Angew. Chem. Int. Ed.* **2011**, *50*, 3993-3997.
- (13) Koehler, J.; Meiler, J. *Prog. Nucl. Magn. Reson. Spectrosc.* **2011**, *59*, 360-389.
- (14) Clore, G. M. *Mol. Biosyst.* **2008**, *4*, 1058-1069.
- (15) Arnesano, F.; Banci, L.; Piccioli, M. *Q. Rev. Biophys.* **2005**, *38*, 167-219.
- (16) Banci, L.; Bertini, I.; Marconi, S.; Pierattelli, R. *Eur. J. Biochem.* **1993**, *215*, 431-437.
- (17) Tolman, J. R.; Ruan, K. *Chem. Rev.* **2006**, *106*, 1720-1736.
- (18) Cotton, S. *Lanthanoid and Actinide Chemistry*; Wiley, 2007.
- (19) Gaponenko, V.; Altieri, A.; Li, J.; Byrd, R. A. *J. Biomol. NMR* **2002**, *24*, 143-148.
- (20) Dvoretzky, A.; Gaponenko, V.; Rosevear, P. R. *FEBS Lett* **2002**, *528*, 189-192.
- (21) Kamen, D. E.; Cahill, S. M.; Girvin, M. E. *J. Am. Chem. Soc.* **2007**, *129*, 1846-1847.
- (22) Ikegami, T.; Verdier, L.; Sakhaei, P.; Grimme, S.; Barbara, P.; Krishna, S.; Fiebig, K. M.; Griesinger, C. *J. Biomol. NMR* **2004**, *29*, 339-349.

- (23) Pintacuda, G.; Moshref, A.; Leonchiks, A.; Sharipo, A.; Otting, G. *J. Biomol. NMR* **2004**, *29*, 351-361.
- (24) Rodriguez-Castañeda, F.; Haberz, P.; Leonov, A.; Griesinger, C. *Magn. Reson. Chem.* **2006**, *44*, S10-S16.
- (25) Leonov, A.; Voigt, B.; Rodriguez-Castañeda, F.; Sakhaei, P.; Griesinger, C. *Chem. Eur. J.* **2005**, *11*, 3342-3348.
- (26) Haberz, P.; Rodriguez-Castañeda, F.; Junker, J.; Becker, S.; Leonov, A.; Griesinger, C. *Org. Lett.* **2006**, *8*, 1275-1278.
- (27) Peters, F.; Maestre-Martinez, M.; Leonov, A.; Kovačič, L.; Becker, S.; Boelens, R.; Griesinger, C. *J. Biomol. NMR* **2011**, *51*, 329-337.
- (28) Viguier, R.; Serratrice, G.; Dupraz, A.; Dupuy, C. *Eur. J. Inorg. Chem.* **2001**, *2001*, 1789-1795.
- (29) Franklin, S. J.; Raymond, K. N. *Inorg. Chem.* **1994**, *33*, 5794-5804.
- (30) Parker, D.; Dickins, R. S.; Puschmann, H.; Crossland, C.; Howard, J. A. K. *Chem. Rev.* **2002**, *102*, 1977-2010.
- (31) Prudêncio, M.; Rohovec, J.; Peters, J. A.; Tocheva, E.; Boulanger, M. J.; Murphy, M. E. P.; Hupkes, H.-J.; Kusters, W.; Impagliazzo, A.; Ubbink, M. *Chem. Eur. J.* **2004**, *10*, 3252-3260.
- (32) Vlasie, M. D.; Fernández-Busnadiego, R.; Prudêncio, M.; Ubbink, M. *J. Mol. Biol.* **2008**, *375*, 1405-1415.
- (33) De León-Rodríguez, L. M.; Kovacs, Z. *Bioconjugate Chem.* **2008**, *19*, 391-402.
- (34) Woods, M.; Kovacs, Z.; Kiraly, R.; Brücher, E.; Zhang, S.; Sherry, A. D. *Inorg. Chem.* **2004**, *43*, 2845-2851.
- (35) Sarka, L.; Burai, L.; Brücher, E. *Chem. Eur. J.* **2000**, *6*, 719-724.
- (36) Vlasie, M. D.; Comuzzi, C.; van den Nieuwendijk, A. M. C. H.; Prudêncio, M.; Overhand, M.; Ubbink, M. *Chem. Eur. J.* **2007**, *13*, 1715-1723.
- (37) Mayer, F.; Platas-Iglesias, C.; Helm, L.; Peters, J. A.; Djanashvili, K. *Inorg. Chem.* **2012**, *51*, 170-178.
- (38) Polášek, M.; Rudovský, J.; Hermann, P.; Lukes, I.; Elst, L. V.; Muller, R. N. *Chem. Commun.* **2004**, *0*, 2602-2603.
- (39) Polášek, M.; Kotek, J.; Hermann, P.; Císařová, I.; Binnemans, K.; Lukeš, I. *Inorg. Chem.* **2009**, *48*, 466-475.
- (40) Keizers, P. H. J.; Desreux, J. F.; Overhand, M.; Ubbink, M. *J. Am. Chem. Soc.* **2007**, *129*, 9292-9293.

- (41) De León-Rodríguez, L. M.; Kovacs, Z.; Esqueda-Oliva, A. C.; Miranda-Olvera, A. D. *Tetrahedron Lett.* **2006**, *47*, 6937-6940.
- (42) Liu, W.-M.; Keizers, P. H. J.; Hass, M. A. S.; Blok, A.; Timmer, M.; Sarris, A. J. C.; Overhand, M.; Ubbink, M. *J. Am. Chem. Soc.* **2012**, *134*, 17306-17313.
- (43) Woods, M.; Kiefer, G. E.; Bott, S.; Castillo-Muzquiz, A.; Eshelbrenner, C.; Michaudet, L.; McMillan, K.; Mudigunda, S. D. K.; Ogrin, D.; Tircsó, G.; Zhang, S.; Zhao, P.; Sherry, A. D. *J. Am. Chem. Soc.* **2004**, *126*, 9248-9256.
- (44) Häussinger, D.; Huang, J.-r.; Grzesiek, S. *J. Am. Chem. Soc.* **2009**, *131*, 14761-14767.
- (45) Graham, B.; Loh, C. T.; Swarbrick, J. D.; Ung, P.; Shin, J.; Yagi, H.; Jia, X.; Chhabra, S.; Barlow, N.; Pintacuda, G.; Huber, T.; Otting, G. *Bioconjugate Chem.* **2011**, *22*, 2118-2125.
- (46) Hoyle, C. E.; Lowe, A. B.; Bowman, C. N. *Chem. Soc. Rev.* **2010**, *39*, 1355-1387.
- (47) Yang, Y.; Li, Q.-F.; Cao, C.; Huang, F.; Su, X.-C. *Chem. Eur. J.* **2013**, *19*, 1097-1103.
- (48) Sletten, E. M.; Bertozzi, C. R. *Angew. Chem. Int. Ed.* **2009**, *48*, 6974-6998.
- (49) Spiteri, C.; Moses, J. E. *Angew. Chem. Int. Ed.* **2010**, *49*, 31-33.
- (50) Loh, C. T.; Ozawa, K.; Tuck, K. L.; Barlow, N.; Huber, T.; Otting, G.; Graham, B. *Bioconjugate Chem.* **2013**, *24*, 260-268.
- (51) Yagi, H.; Maleckis, A.; Otting, G. *J. Biomol. NMR* **2013**, *55*, 157-166.
- (52) Man, B.; Su, X.-C.; Liang, H.; Simonsen, S.; Huber, T.; Messerle, B. A.; Otting, G. *Chem. Eur. J.* **2010**, *16*, 3827-3832.
- (53) Su, X.-C.; Man, B.; Beeren, S.; Liang, H.; Simonsen, S.; Schmitz, C.; Huber, T.; Messerle, B. A.; Otting, G. *J. Am. Chem. Soc.* **2008**, *130*, 10486-10487.
- (54) Li, Q.-F.; Yang, Y.; Maleckis, A.; Otting, G.; Su, X.-C. *Chem. Commun.* **2012**, *48*, 2704-2706.
- (55) Swarbrick, J. D.; Ung, P.; Chhabra, S.; Graham, B. *Angew. Chem. Int. Ed.* **2011**, *50*, 4403-4406.
- (56) Swarbrick, J. D.; Ung, P.; Su, X.-C.; Maleckis, A.; Chhabra, S.; Huber, T.; Otting, G.; Graham, B. *Chem. Commun.* **2011**, *47*, 7368-7370.
- (57) Su, X.-C.; Liang, H.; Loscha, K. V.; Otting, G. *J. Am. Chem. Soc.* **2009**, *131*, 10352-10353.

- (58) Harrowfield, J.; Kim, Y.; Skelton, B.; White, A. *Aust. J. Chem.* **1995**, *48*, 807-823.
- (59) Jia, X.; Yagi, H.; Su, X.-C.; Stanton-Cook, M.; Huber, T.; Otting, G. *J. Biomol. NMR* **2011**, *50*, 411-420.
- (60) Wei, Z.; Yang, Y.; Li, Q.-F.; Huang, F.; Zuo, H.-H.; Su, X.-C. *Chem. Eur. J.* **2013**, *19*, 5758-5764.
- (61) Almeida, R. M.; Geraldies, C. F. G. C.; Pauleta, S. R.; Moura, J. J. G. *Inorg. Chem.* **2011**, *50*, 10600-10607.
- (62) Snyder, E. E.; Buoscio, B. W.; Falke, J. J. *Biochemistry* **1990**, *29*, 3937-3943.
- (63) Lee, L.; Sykes, B. D. *Biochemistry* **1981**, *20*, 1156-1162.
- (64) Lee, L.; Sykes, B. D. *Biochemistry* **1983**, *22*, 4366-4373.
- (65) Allegrozzi, M.; Bertini, I.; Janik, M. B. L.; Lee, Y.-M.; Liu, G.; Luchinat, C. *J. Am. Chem. Soc.* **2000**, *122*, 4154-4161.
- (66) Bertini, I.; Gupta, Y. K.; Luchinat, C.; Parigi, G.; Peana, M.; Sgheri, L.; Yuan, J. *J. Am. Chem. Soc.* **2007**, *129*, 12786-12794.
- (67) Bertini, I.; Gelis, I.; Katsaros, N.; Luchinat, C.; Provenzani, A. *Biochemistry* **2003**, *42*, 8011-8021.
- (68) Bertini, I.; Janik, M. B. L.; Lee, Y.-M.; Luchinat, C.; Rosato, A. *J. Am. Chem. Soc.* **2001**, *123*, 4181-4188.
- (69) Brautigam, C. A.; Aschheim, K.; Steitz, T. A. *Chem. Biol.* **1999**, *6*, 901-908.
- (70) Capozzi, F.; Casadei, F.; Luchinat, C. *J. Biol. Inorg. Chem.* **2006**, *11*, 949-962.
- (71) Ma, C.; Opella, S. J. *J. Magn. Reson.* **2000**, *146*, 381-384.
- (72) Nitz, M.; Franz, K. J.; Maglathlin, R. L.; Imperiali, B. *ChemBioChem* **2003**, *4*, 272-276.
- (73) Franz, K. J.; Nitz, M.; Imperiali, B. *ChemBioChem* **2003**, *4*, 265-271.
- (74) Barthelmes, K.; Reynolds, A. M.; Peisach, E.; Jonker, H. R. A.; DeNunzio, N. J.; Allen, K. N.; Imperiali, B.; Schwalbe, H. *J. Am. Chem. Soc.* **2011**, *133*, 808-819.
- (75) Barb, A. W.; Ho, T. G.; Flanagan-Steet, H.; Prestegard, J. H. *Protein Sci.* **2012**, *21*, 1456-1466.
- (76) Su, X.-C.; Huber, T.; Dixon, N. E.; Otting, G. *ChemBioChem* **2006**, *7*, 1599-1604.
- (77) Su, X.-C.; McAndrew, K.; Huber, T.; Otting, G. *J. Am. Chem. Soc.* **2008**, *130*, 1681-1687.

- (78) Saio, T.; Ogura, K.; Yokochi, M.; Kobashigawa, Y.; Inagaki, F. *J. Biomol. NMR* **2009**, *44*, 157-166.
- (79) Sattler, M.; Schleucher, J.; Griesinger, C. *Prog. Nucl. Magn. Reson. Spectrosc.* **1999**, *34*, 93-158.
- (80) Keizers, P. H. J.; Mersinli, B.; Reinle, W.; Donauer, J.; Hiruma, Y.; Hannemann, F.; Overhand, M.; Bernhardt, R.; Ubbink, M. *Biochemistry* **2010**, *49*, 6846-6855.
- (81) Schmitz, C.; John, M.; Park, A. Y.; Dixon, N.; Otting, G.; Pintacuda, G.; Huber, T. *J. Biomol. NMR* **2006**, *35*, 79-87.
- (82) Pintacuda, G.; Keniry, M. A.; Huber, T.; Park, A. Y.; Dixon, N. E.; Otting, G. *J. Am. Chem. Soc.* **2004**, *126*, 2963-2970.
- (83) John, M.; Schmitz, C.; Park, A. Y.; Dixon, N. E.; Huber, T.; Otting, G. *J. Am. Chem. Soc.* **2007**, *129*, 13749-13757.
- (84) Skinner, S.; Moshev, M.; Hass, M. S.; Ubbink, M. *J. Biomol. NMR* **2013**, *55*, 379-389.
- (85) Bertini, I.; Kursula, P.; Luchinat, C.; Parigi, G.; Vahokoski, J.; Wilmanns, M.; Yuan, J. *J. Am. Chem. Soc.* **2009**, *131*, 5134-5144.
- (86) Dasgupta, S.; Hu, X.; Keizers, P. J.; Liu, W.-M.; Luchinat, C.; Nagulapalli, M.; Overhand, M.; Parigi, G.; Sgheri, L.; Ubbink, M. *J. Biomol. NMR* **2011**, *51*, 253-263.
- (87) Raitsimring, A. M.; Gunanathan, C.; Potapov, A.; Efremenko, I.; Martin, J. M. L.; Milstein, D.; Goldfarb, D. *J. Am. Chem. Soc.* **2007**, *129*, 14138-14139.
- (88) Stoll, S.; Lee, Y.-T.; Zhang, M.; Wilson, R. F.; Britt, R. D.; Goodin, D. B. *Proc. Natl. Acad. Sci. U.S.A.* **2012**, *109*, 12888-12893.
- (89) Liepinsh, E.; Baryshev, M.; Sharipo, A.; Ingelman-Sundberg, M.; Otting, G.; Mkrtchian, S. *Structure* **2001**, *9*, 457-471.
- (90) Barak, N. N.; Neumann, P.; Sevvana, M.; Schutkowski, M.; Naumann, K.; Malešević, M.; Reichardt, H.; Fischer, G.; Stubbs, M. T.; Ferrari, D. M. *J. Mol. Biol.* **2009**, *385*, 1630-1642.
- (91) Yagi, H.; Banerjee, D.; Graham, B.; Huber, T.; Goldfarb, D.; Otting, G. *J. Am. Chem. Soc.* **2011**, *133*, 10418-10421.
- (92) de la Cruz, L.; Nguyen, T. H. D.; Ozawa, K.; Shin, J.; Graham, B.; Huber, T.; Otting, G. *J. Am. Chem. Soc.* **2011**, *133*, 19205-19215.

- (93) Pervushin, K.; Riek, R.; Wider, G.; Wüthrich, K. *Proc. Natl. Acad. Sci. U.S.A.* **1997**, *94*, 12366-12371.
- (94) Saio, T.; Yokochi, M.; Kumeta, H.; Inagaki, F. *J. Biomol. NMR* **2010**, *46*, 271-280.
- (95) Kobashigawa, Y.; Saio, T.; Ushio, M.; Sekiguchi, M.; Yokochi, M.; Ogura, K.; Inagaki, F. *J. Biomol. NMR* **2012**, *53*, 53-63.
- (96) Tripathi, S.; Li, H.; Poulos, T. L. *Science* **2013**, *340*, 1227-1230.
- (97) Hiruma, Y.; Hass, M. A. S.; Kikui, Y.; Liu, W.-M.; Ölmez, B.; Skinner, S. P.; Blok, A.; Kloosterman, A.; Koteishi, H.; Löhr, F.; Schwalbe, H.; Nojiri, M.; Ubbink, M. *J. Mol. Biol.* **2013**. DOI: 10.1016/j.jmb.2013.07.006
- (98) Xu, X.; Keizers, P. J.; Reinle, W.; Hannemann, F.; Bernhardt, R.; Ubbink, M. *J. Biomol. NMR* **2009**, *43*, 247-254.
- (99) Xu, X.; Reinle, W.; Hannemann, F.; Konarev, P. V.; Svergun, D. I.; Bernhardt, R.; Ubbink, M. *J. Am. Chem. Soc.* **2008**, *130*, 6395-6403.
- (100) Hajduk, P. J.; Greer, J. *Nat. Rev. Drug Discovery* **2007**, *6*, 211-219.
- (101) Saio, T.; Ogura, K.; Shimizu, K.; Yokochi, M.; Burke, T., Jr.; Inagaki, F. *J. Biomol. NMR* **2011**, *51*, 395-408.
- (102) Guan, J.-Y.; Keizers, P. H. J.; Liu, W.-M.; Löhr, F.; Skinner, S. P.; Heeneman, E. A.; Schwalbe, H.; Ubbink, M.; Siegal, G. *J. Am. Chem. Soc.* **2013**, *135*, 5859-5868.
- (103) Zhuang, T.; Lee, H.-S.; Imperiali, B.; Prestegard, J. H. *Protein Sci.* **2008**, *17*, 1220-1231.
- (104) Assfalg, M.; Gianolio, E.; Zanzoni, S.; Tomaselli, S.; Lo Russo, V.; Cabella, C.; Ragona, L.; Aime, S.; Molinari, H. *J. Med. Chem.* **2007**, *50*, 5257-5268.
- (105) Eisenmesser, E. Z.; Millet, O.; Labeikovsky, W.; Korzhnev, D. M.; Wolf-Watz, M.; Bosco, D. A.; Skalicky, J. J.; Kay, L. E.; Kern, D. *Nature* **2005**, *438*, 117-121.
- (106) Boehr, D. D.; McElheny, D.; Dyson, H. J.; Wright, P. E. *Science* **2006**, *313*, 1638-1642.
- (107) Mittermaier, A.; Kay, L. E. *Science* **2006**, *312*, 224-228.
- (108) Vallurupalli, P.; Hansen, D. F.; Stollar, E.; Meirovitch, E.; Kay, L. E. *Proc. Natl. Acad. Sci. U.S.A.* **2007**, *104*, 18473-18477.
- (109) Vallurupalli, P.; Hansen, D. F.; Kay, L. E. *Proc. Natl. Acad. Sci. U.S.A.* **2008**, *105*, 11766-11771.

- (110) Eichmüller, C.; Skrynnikov, N. *J. Biomol. NMR* **2007**, *37*, 79-95.
- (111) Hass, M. A. S.; Keizers, P. H. J.; Blok, A.; Hiruma, Y.; Ubbink, M. *J. Am. Chem. Soc.* **2010**, *132*, 9952-9953.
- (112) Hormel, S.; Adman, E.; Walsh, K. A.; Beppu, T.; Titani, K. *FEBS Lett.* **1986**, *197*, 301-304.
- (113) Kakutani, T.; Watanabe, H.; Arima, K.; Beppu, T. *J. Biochem.* **1981**, *89*, 463-472.
- (114) Brown, I. D. *Acta Crystallogr.* **1988**, *B44*, 545-553.
- (115) Vakoufari, E.; Wilson, K. S.; Petratos, K. *FEBS Lett.* **1994**, *347*, 203-206.
- (116) Kato, H.; Feng, H.; Bai, Y. *J. Mol. Biol.* **2007**, *365*, 870-880.
- (117) Sagermann, M.; Baase, W. A.; Mooers, B. H. M.; Gay, L.; Matthews, B. W. *Biochemistry* **2004**, *43*, 1296-1301.
- (118) Louie, G. V.; Brayer, G. D. *J. Mol. Biol.* **1990**, *214*, 527-555.
- (119) Baistrocchi, P.; Banci, L.; Bertini, I.; Turano, P.; Bren, K. L.; Gray, H. B. *Biochemistry* **1996**, *35*, 13788-13796.
- (120) Louie, G. V.; Hutcheon, W. L. B.; Brayer, G. D. *J. Mol. Biol.* **1988**, *199*, 295-314.
- (121) Berghuis, A. M.; Brayer, G. D. *J. Mol. Biol.* **1992**, *223*, 959-976.
- (122) Banci, L.; Bertini, I.; Bren, K. L.; Gray, H. B.; Sompornpisut, P.; Turano, P. *Biochemistry* **1997**, *36*, 8992-9001.
- (123) Nelson, D. *Hum. Genomics* **2009**, *4*, 59 - 65.
- (124) Lee, Y.-T.; Wilson, R. F.; Rupniewski, I.; Goodin, D. B. *Biochemistry* **2010**, *49*, 3412-3419.
- (125) Poulos, T. L.; Finzel, B. C.; Gunsalus, I. C.; Wagner, G. C.; Kraut, J. *J. Biol. Chem.* **1985**, *260*, 16122-30.
- (126) Poulos, T. L.; Finzel, B. C.; Howard, A. J. *J. Mol. Biol.* **1987**, *195*, 687-700.
- (127) Libeu, C. A. P.; Kukimoto, M.; Nishiyama, M.; Horinouchi, S.; Adman, E. T. *Biochemistry* **1997**, *36*, 13160-13179.
- (128) Weaver, L. H.; Matthews, B. W. *J. Mol. Biol.* **1987**, *193*, 189-199.
- (129) Bertini, I.; Luchinat, C.; Parigi, G.; Pierattelli, R. *ChemBioChem* **2005**, *6*, 1536-1549.
- (130) Clore, G. M. *Protein Sci.* **2011**, *20*, 229-246.
- (131) Pintacuda, G.; John, M.; Su, X.-C.; Otting, G. *Acc. Chem. Res.* **2007**, *40*, 206-212.

- (132) Su, Y.; Hu, F.; Hong, M. *J. Am. Chem. Soc.* **2012**, *134*, 8693-8702.
- (133) Bernini, A.; Spiga, O.; Venditti, V.; Prischi, F.; Botta, M.; Croce, G.; Tong, A. P.-L.; Wong, W.-T.; Niccolai, N. *J. Inorg. Biochem.* **2012**, *112*, 25-31.
- (134) Otting, G. *J. Biomol. NMR* **2008**, *42*, 1-9.
- (135) Biekofsky, R. R.; Muskett, F. W.; Schmidt, J. M.; Martin, S. R.; Browne, J. P.; Bayley, P. M.; Feeney, J. *FEBS Lett.* **1999**, *460*, 519-526.
- (136) Gay, G. L.; Lindhout, D. A.; Sykes, B. D. *Protein Sci.* **2004**, *13*, 640-651.
- (137) Gaponenko, V.; Dvoretzky, A.; Walsby, C.; Hoffman, B. M.; Rosevear, P. R. *Biochemistry* **2000**, *39*, 15217-15224.
- (138) Aime, S.; Botta, M.; Ermondi, G. *Inorg. Chem.* **1992**, *31*, 4291-4299.
- (139) Aime, S.; Botta, M.; Fasano, M.; Marques, M. P. M.; Geraldès, C. F. G. C.; Pubanz, D.; Merbach, A. E. *Inorg. Chem.* **1997**, *36*, 2059-2068.
- (140) Cosentino, U.; Villa, A.; Pitea, D.; Moro, G.; Barone, V.; Maiocchi, A. *J. Am. Chem. Soc.* **2002**, *124*, 4901-4909.
- (141) Ranganathan, R. S.; Raju, N.; Fan, H.; Zhang, X.; Tweedle, M. F.; Desreux, J. F.; Jacques, V. *Inorg. Chem.* **2002**, *41*, 6856-6866.
- (142) Dapporto, P.; Fusi, V.; Micheloni, M.; Palma, P.; Paoli, P.; Pontellini, R. *Inorganica Chimica Acta* **1998**, 275-276, 168-174.
- (143) Li, C.; Winnard Jr, P.; Bhujwalla, Z. M. *Tetrahedron Lett.* **2009**, *50*, 2929-2931.
- (144) Ni, W.; Fang, H.; Springsteen, G.; Wang, B. *J. Org. Chem.* **2004**, *69*, 1999-2007.
- (145) Polášek, M.; Šedinová, M.; Kotek, J.; Vander Elst, L.; Muller, R. N.; Hermann, P.; Lukeš, I. *Inorg. Chem.* **2009**, *48*, 455-465.
- (146) Green, K. N.; Viswanathan, S.; Rojas-Quijano, F. A.; Kovacs, Z.; Sherry, A. D. *Inorg. Chem.* **2011**, *50*, 1648-1655.
- (147) Parker, D.; Puschmann, H.; Batsanov, A. S.; Senanayake, K. *Inorg. Chem.* **2003**, *42*, 8646-8651.
- (148) Zhang, S.; Jiang, X.; Sherry, A. D. *Helvetica Chimica Acta* **2005**, *88*, 923-935.
- (149) Aime, S.; Barge, A.; Botta, M.; Fasano, M.; Danilo Ayala, J.; Bombieri, G. *Inorganica Chimica Acta* **1996**, *246*, 423-429.
- (150) Jacques, V.; Desreux, J. F. *Inorg. Chem.* **1994**, *33*, 4048-4053.
- (151) Ho, S. N.; Hunt, H. D.; Horton, R. M.; Pullen, J. K.; Pease, L. R. *Gene* **1989**, *77*, 51-59.

- (152) Tjandra, N.; Omichinski, J. G.; Gronenborn, A. M.; Clore, G. M.; Bax, A. *Nat. Struct. Mol. Biol.* **1997**, *4*, 732-738.
- (153) Delaglio, F.; Grzesiek, S.; Vuister, G. W.; Zhu, G.; Pfeifer, J.; Bax, A. *J. Biomol. NMR* **1995**, *6*, 277-293.
- (154) Vranken, W. F.; Boucher, W.; Stevens, T. J.; Fogh, R. H.; Pajon, A.; Llinas, M.; Ulrich, E. L.; Markley, J. L.; Ionides, J.; Laue, E. D. *Proteins* **2005**, *59*, 687-696.
- (155) Worrall, J. A. R.; Kolczak, U.; Canters, G. W.; Ubbink, M. *Biochemistry* **2001**, *40*, 7069-7076.
- (156) Schwieters, C. D.; Kuszewski, J. J.; Tjandra, N.; Marius Clore, G. *J. Mag. Reson.* **2003**, *160*, 65-73.
- (157) Banci, L.; Bertini, I.; Cavallaro, G.; Giachetti, A.; Luchinat, C.; Parigi, G. *J. Biomol. NMR* **2004**, *28*, 249-261.
- (158) Bashir, Q.; Volkov, A. N.; Ullmann, G. M.; Ubbink, M. *J. Am. Chem. Soc.* **2009**, *132*, 241-247.
- (159) Allen, K. N.; Imperiali, B. *Curr. Opin. Chem. Biol.* **2010**, *14*, 247-254.
- (160) Qi, D.; Tann, C.-M.; Haring, D.; Distefano, M. D. *Chem. Rev.* **2001**, *101*, 3081-3112.
- (161) Liu, C. C.; Schultz, P. G. *Annu. Rev. Biochem.* **2010**, *79*, 413-444.
- (162) Yang, Z.; Attygalle, A. B. *J. Mass Spectrom.* **2007**, *42*, 233-243.
- (163) Lang, S.; Spratt, D. E.; Guillemette, J. G.; Palmer, M. *Anal. Biochem.* **2005**, *342*, 271-279.
- (164) Behr, J.-B.; Gurlain, T.; Helimi, A.; Guillerme, G. *Bioorg. Med. Chem. Lett.* **2003**, *13*, 1713-1716.
- (165) Lee, J.; Kang, S.-U.; Kil, M.-J.; Shin, M.; Lim, J.-O.; Choi, H.-K.; Jin, M.-K.; Kim, S. Y.; Kim, S.-E.; Lee, Y.-S.; Min, K.-H.; Kim, Y.-H.; Ha, H.-J.; Tran, R.; Welter, J. D.; Wang, Y.; Szabo, T.; Pearce, L. V.; Lundberg, D. J.; Toth, A.; Pavlyukovets, V. A.; Morgan, M. A.; Blumberg, P. M. *Bioorg. Med. Chem. Lett.* **2005**, *15*, 4136-4142.
- (166) Mitsuya, M.; Kobayashi, K.; Kawakami, K.; Satoh, A.; Ogino, Y.; Kakikawa, T.; Ohtake, N.; Kimura, T.; Hirose, H.; Sato, A.; Numazawa, T.; Hasegawa, T.; Noguchi, K.; Mase, T. *J. Med. Chem.* **2000**, *43*, 5017-5029.
- (167) Norberg, O.; Deng, L.; Aastrup, T.; Yan, M.; Ramström, O. *Anal. Chem.* **2011**, *83*, 1000-1007.

- (168) Schmitz, C.; Stanton-Cook, M.; Su, X.-C.; Otting, G.; Huber, T. *J. Biomol. NMR* **2008**, *41*, 179-189.
- (169) Do-Thanh, C.-L.; Rowland, M. M.; Best, M. D. *Tetrahedron* **2011**, *67*, 3803-3808.
- (170) Kornmayer, S. C.; Rominger, F.; Gleiter, R. *Synthesis* **2009**, *2009*, 2547-2552.
- (171) van Delft, P.; Meeuwenoord, N. J.; Hoogendoorn, S.; Dinkelaar, J.; Overkleef, H. S.; van der Marel, G. A.; Filippov, D. V. *Org. Lett.* **2010**, *12*, 5486-5489.
- (172) Shelbourne, M.; Chen, X.; Brown, T.; El-Sagheer, A. H. *Chem. Commun.* **2011**, *47*, 6257-6259.
- (173) Shetty, D.; Jeong, J. M.; Ju, C. H.; Kim, Y. J.; Lee, J.-Y.; Lee, Y.-S.; Lee, D. S.; Chung, J.-K.; Lee, M. C. *Bioorg. Med. Chem.* **2010**, *18*, 7338-7347.
- (174) Wang, L.; Schultz, P. G. *Angew. Chem. Int. Ed.* **2005**, *44*, 34-66.
- (175) Beck-Sickinger, A. G.; Budisa, N. *Angew. Chem. Int. Ed.* **2012**, *51*, 310-312.
- (176) Hong, V.; Presolski, S. I.; Ma, C.; Finn, M. G. *Angew. Chem. Int. Ed.* **2009**, *48*, 9879-9883.
- (177) Besanceney-Webler, C.; Jiang, H.; Zheng, T.; Feng, L.; Soriano del Amo, D.; Wang, W.; Klivansky, L. M.; Marlow, F. L.; Liu, Y.; Wu, P. *Angew. Chem. Int. Ed.* **2011**, *50*, 8051-8056.
- (178) Hlavaty, J. J.; Nowak, T. *Biochemistry* **1997**, *36*, 15514-15525.
- (179) Milles, S.; Tyagi, S.; Banterle, N.; Koehler, C.; VanDelinder, V.; Plass, T.; Neal, A. P.; Lemke, E. A. *J. Am. Chem. Soc.* **2012**, *134*, 5187-5195.
- (180) Norholm, M. *BMC Biotechnology* **2010**, *10*, 21.
- (181) McIntosh, L. P.; Wand, A. J.; Lowry, D. F.; Redfield, A. G.; Dahlquist, F. W. *Biochemistry* **1990**, *29*, 6341-6362.
- (182) Polasek, M.; Rudovsky, J.; Hermann, P.; Lukes, I.; Elst, L. V.; Muller, R. N. *Chem. Commun.* **2004**, *0*, 2602-2603.
- (183) Ishida, Y.; Inoue, M.-a.; Inoue, T.; Ojida, A.; Hamachi, I. *Chem. Commun.* **2009**, *45*, 2848-2850.
- (184) Gerald, C. F. G. C. In *Encyclopedia of Inorganic and Bioinorganic Chemistry*; John Wiley & Sons, Ltd: 2012.
- (185) Grey, M. J.; Wang, C.; Palmer, A. G. *J. Am. Chem. Soc.* **2003**, *125*, 14324-14335.
- (186) Cornilescu, G.; Marquardt, J. L.; Ottiger, M.; Bax, A. *J. Am. Chem. Soc.* **1998**, *120*, 6836-6837.

- (187) Kuehler, T. C.; Fryklund, J.; Bergman, N.-k.; Weilitz, J.; Lee, A.; Larsson, H. *J. Med. Chem.* **1995**, *38*, 4906-4916.
- (188) Kühler, T. C.; Swanson, M.; Shcherbuchin, V.; Larsson, H.; Mellgård, B.; Sjöström, J.-E. *J. Med. Chem.* **1998**, *41*, 1777-1788.
- (189) Stoll, S.; Lee, Y.-T.; Zhang, M.; Wilson, R. F.; Britt, R. D.; Goodin, D. B. *Proc. Nat. Acad. Sci. U. S. A.* **2012**, *109*, 12888-12893.
- (190) Bashir, Q.; Scanu, S.; Ubbink, M. *FEBS J.* **2011**, *278*, 1391-1400.
- (191) Chatani, S.; Nakamura, M.; Akahane, H.; Kohyama, N.; Taki, M.; Arata, T.; Yamamoto, Y. *Chem. Commun.* **2005**, *0*, 1880-1882.
- (192) Fleissner, M. R.; Bridges, M. D.; Brooks, E. K.; Cascio, D.; Kálai, T.; Hideg, K.; Hubbell, W. L. *Proc. Nat. Acad. Sci. U. S. A.* **2011**, *108*, 16241-16246.
- (193) Hirayama, T.; Taki, M.; Nakamura, M.; Arata, T.; Yamamoto, Y. *Chem. Lett.* **2006**, *35*, 834-835.
- (194) Columbus, L.; Kálai, T.; Jekö, J.; Hideg, K.; Hubbell, W. L. *Biochemistry* **2001**, *40*, 3828-3846.
- (195) Fawzi, N.; Fleissner, M.; Anthis, N.; Kálai, T.; Hideg, K.; Hubbell, W.; Clore, G. M. *J. Biomol. NMR* **2011**, *51*, 105-114.
- (196) Berliner, L. J.; Grunwald, J.; Hankovszky, H. O.; Hideg, K. *Anal. Biochem.* **1982**, *119*, 450-455.
- (197) McHaourab, H. S.; Kálai, T.; Hideg, K.; Hubbell, W. L. *Biochemistry* **1999**, *38*, 2947-2955.
- (198) Fleissner, M. R.; Cascio, D.; Hubbell, W. L. *Protein Sci.* **2009**, *18*, 893-908.
- (199) Poulos, T. L.; Howard, A. J. *Biochemistry* **1987**, *26*, 8165-8174.
- (200) Xie, Y.-X.; Pi, S.-F.; Wang, J.; Yin, D.-L.; Li, J.-H. *J. Org. Chem.* **2006**, *71*, 8324-8327.
- (201) Zhu, L.; Li, G.; Luo, L.; Guo, P.; Lan, J.; You, J. *J. Org. Chem.* **2009**, *74*, 2200-2202.
- (202) Morris, J. C.; McMurtrie, J. C.; Bottle, S. E.; Fairfull-Smith, K. E. *J. Org. Chem.* **2011**, *76*, 4964-4972.
- (203) Blinco, J. P.; McMurtrie, J. C.; Bottle, S. E. *Eur. J. Org. Chem.* **2007**, *2007*, 4638-4641.
- (204) Lee, Y.-T.; Glazer, E. C.; Wilson, R. F.; Stout, C. D.; Goodin, D. B. *Biochemistry* **2011**, *50*, 693-703.

- (205) Wright, K.; Dutot, L.; Wakselman, M.; Mazaleyrat, J.-P.; Crisma, M.; Formaggio, F.; Toniolo, C. *Tetrahedron* **2008**, *64*, 4416-4426.
- (206) Wright, K.; Formaggio, F.; Toniolo, C.; Török, R.; Péter, A.; Wakselman, M.; Mazaleyrat, J.-P. *Tetrahedron Lett.* **2003**, *44*, 4183-4186.
- (207) Miyake, M.; Shen, J.; Liu, S.; Shi, H.; Liu, W.; Yuan, Z.; Pritchard, A.; Kao, J. P. Y.; Liu, K. J.; Rosen, G. M. *JEPT* **2006**, *318*, 1187-1193.
- (208) Chudinov, A. V.; Rozantsev, É. G.; Rozynov, B. V. *Izv. Akad. Nauk SSSR, Ser. Khim* **1983**, *32*, 409-413.
- (209) Erdélyi, M.; d'Auvergne, E.; Navarro-Vázquez, A.; Leonov, A.; Griesinger, C. *Chem. Eur. J.* **2011**, *17*, 9368-9376.
- (210) Yamamoto, S.; Yamaguchi, T.; Erdélyi, M.; Griesinger, C.; Kato, K. *Chem. Eur. J.* **2011**, *17*, 9280-9282.
- (211) Mallagaray, A.; Canales, A.; Dominguez, G.; Jimenez-Barbero, J.; Perez-Castells, J. *Chem. Commun.* **2011**, *47*, 7179-7181.

Nederlandse Samenvatting

Paramagnetische kernspinresonantiespectroscopie is krachtig gereedschap om eiwitstructuren mee te bepalen, om onzichtbare toestanden van eiwitten zichtbaar te maken, om de dynamica van eiwitten te observeren en om eiwit-eiwit en eiwit-ligand interacties te bestuderen. Synthetische sondes worden regelmatig gebruikt om een paramagnetisch centrum op een eiwit aan te brengen. Het doel van het onderzoek in dit proefschrift was om nieuwe paramagnetische sondes te ontwikkelen gebaseerd op nitroxide radicalen of lanthanide ionen, om daar vervolgens biomoleculen mee te bestuderen. Een overzicht van de huidige op lanthanide ionen gebaseerde sondes is gegeven in Hoofdstuk 1.

In Hoofdstuk 2 is een nieuwe paramagnetische sonde, CLaNP-7, beschreven. De netto lading van deze sonde is +1 in plaats van +3 zoals in de succesvolle CLaNP-5, door *p*-nitrophenol te introduceren als liganden voor de metaal. De $\Delta\chi$ -tensor van Yb-CLaNP-7 heeft een meer rhombisch karakter dan die van CLaNP-5. Dit zou kunnen komen door aanwezigheid van een negende ligand; een watermolecuul of een hydroxylion. Als er een histidine residue dicht in de buurt is van de verankeringsplaats van de sonde, lijkt het alsof de imidazol zijketen van de histidine een waterstofbrug vormt met het negende ligand, resulterend in een pH-afhankelijke $\Delta\chi$ -tensor.

Zwavelbruggen worden veelvuldig gebruikt voor plaats-specifieke verankering van paramagnetische sondes aan doeleiwitten. Maar deze zwakke covalente binding is instabiel onder reducerende omstandigheden. Om de stabiliteit van de verankering van de sonde te verhogen zijn er twee verschillende aanpakken onderzocht in Hoofdstuk 3. Benzylbromide, α -ketobromide en primair bromide werden geplaatst op paramagnetische sondes om zo een thio-ether te kunnen vormen. Van deze sondes bleek het Ln-CLaNP-9 complex, gebaseerd op een α -ketobromide, stabiel te zijn in waterige oplossing en kon succesvol op een eiwit worden geplaatst. Bovendien was de verbinding stabiel onder reducerende omstandigheden. De $\Delta\chi$ -tensoren van Yb³⁺ en Tm³⁺ in CLaNP-9 zijn bepaald met twee model-eiwitten. Daarom is het een aantrekkelijke sonde voor paramagnetische kernspinresonantiespectroscopie.

Voor de bio-orthogonale aanpak is er een artificieel aminozuur, *p*-azido feny alanine (AzF), succesvol geïncorporeerd in T4 lysozym. Helaas was de reactiviteit van het eiwit twijfelachtig, gezien de resultaten gevonden met massaspectrometrie. Verscheidene azide bevattende reactieve groepen, zoals

terminale alkyn en cyclooctyn, werden geïntroduceerd op de sondes en in reactie gebracht met AzF-gefunctionaliseerde eiwitten. Uiteindelijk bleek uit de experimenten dat het bijzonder lastig en onpraktisch is om voldoende opbrengst te verkrijgen voor kernspinresonantiespectroscopie.

In Hoofdstuk 4 zijn er derivaten van CLaNP-5 en een modelsysteem gesynthetiseerd om zo een alternatieve methode te ontwikkelen om meervoudige gegevens te verkrijgen van een enkele mutatieplaats. De ^1H kernspinresonantiespectra van het modelsysteem laten zien dat de paramagnetische verschuiving aangetast wordt door de substituties op de sonde en dat alle sondes in oplossing een enkelvoudig enantiomeerpaar vormen. Echter, de $\Delta\chi$ -tensoren bepaald met eiwitdata laten zien dat CLaNP-5-OMe en CLaNP-5 vergelijkbare magnetische susceptibiliteit tensoren hebben. Daaruit volgt dat veranderingen in de periferie van het coördinatiesysteem resulteren in te vergelijkbare $\Delta\chi$ -tensoren om praktische nut te hebben. Daarentegen, heeft de toegevoegde functionele groep (methoxyl) wel een effect op het fysische gedrag van de sonde na verankering. Twee sets van paramagnetische effecten waren aanwezig in het geval van CLaNP-5-OMe, waar er slechts een enkele set is voor CLaNP-5. Dit is waarschijnlijk te verklaren door interacties van de sonde met de aminozuren in de omgeving, door de toegenomen omvang van CLaNP-5-OMe. Deze bevinding, tezamen met die in Hoofdstuk 2, laten zien dat zijketens van aminozuren directe interacties met de sonde aan kunnen gaan en op die manier het paramagnetisch gedrag kunnen beïnvloeden.

Sondes op basis van nitroxide radicalen zijn beschreven in Hoofdstuk 5. Een twee-armige nitroxide sonde is gesynthetiseerd. Maar deze bleek instabiel na verankering aan een model eiwit. Een mogelijke verklaring hiervoor is de combinatie van spanning veroorzaakt door de verankeringplaats en de beweeglijkheid van de verzadigde vijfring. Analoga van substraten en remmers kunnen worden gezien als de volgende generatie van sondes, die een gerichte interactie kunnen aan gaan met een doeleiwit. In dit hoofdstuk zijn derivaten van 1-fenylimidazol, remmers van P450cam, gesynthetiseerd en gekristalliseerd in aanwezigheid van P450cam. De imidazolring van de meta-gesubstitueerde fenylring van 1-fenylimidazol is gelokaliseerd boven het ijzeratoom van de heemgroep en de nitroxide in het substraattoegangskanaal, waarbij het eiwit in een open toestand wordt gedwongen. Dit initiële resultaat suggereert dat deze aanpak veelbelovend is voor studies naar eiwit-ligand complexen.

In Hoofdstuk 6 zijn de toekomstperspectieven van paramagnetische sondes geschetst en bediscussieerd.

English Summary

Paramagnetic NMR is a powerful tool to determine protein structure, to investigate invisible states of proteins, to observe protein dynamics and study protein-protein and protein-ligand interactions. Synthetic probes are commonly used to introduce a paramagnetic center on target protein. The aim of the research in this thesis was to develop new paramagnetic probes containing nitroxide radicals or lanthanoids for the study of biomolecules. An overview of the current lanthanoid containing probes is given in Chapter 1.

In Chapter 2, a new paramagnetic probe, CLaNP-7, is described. Its net charge is +1, instead of +3 as in the successful CLaNP-5, which is achieved by introducing *p*-nitrophenol as metal ligands. The $\Delta\chi$ -tensor of Yb-CLaNP-7 is much more rhombic than for CLaNP-5. This might be due to the presence of a ninth ligand, a water molecule or hydroxyl ion. When a histidine residue is located close to the attachment site, the imidazole side-chain of histidine appears to form a hydrogen bond with the ninth ligand resulting in a pH-dependent $\Delta\chi$ -tensor.

Disulfide bridges are widely used for site-specific attachment of paramagnetic probes to target proteins. However, this weak covalent bond is not stable under reducing conditions. In order to enhance the stability of the tag linkers, two approaches, thioether and bioorthogonal reactions, were investigated in Chapter 3. Benzylic bromide, α -ketobromide and primary bromide were decorated on paramagnetic probes in the case of the thioether approach. Among these probes, the Ln-CLaNP-9 complex based on an α -ketobromide was stable in aqueous solution and successfully attached to proteins. Moreover, the linkage was stable under reductive conditions. The $\Delta\chi$ -tensors for Yb³⁺ and Tm³⁺ of CLaNP-9 were defined using two model proteins. It is therefore an attractive probe for paramagnetic NMR. For the bioorthogonal approach, an artificial amino acid, *p*-azido phenylalanine (AzF), was successfully incorporated in T4 lysozyme. However, the reactivity of protein is questionable in the light of the results of mass spectrometry. Several azide reactive groups, such as terminal alkyne and cyclooctyne, were introduced to the probes and reacted with AzF functionalized protein. However, the experiments show that it is very difficult and impractical to obtain yields sufficient for NMR spectroscopy.

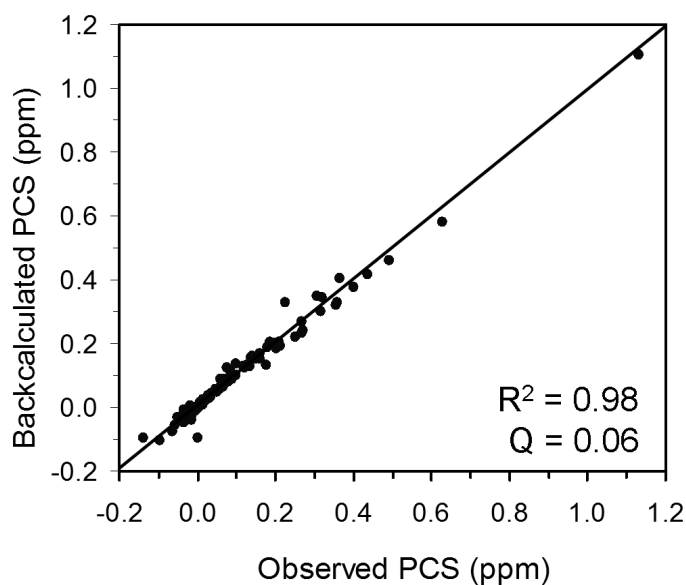
In Chapter 4, CLaNP-5 derivatives as well as a model system were synthesized to develop an alternative method for getting multiple data restraints from a single

mutant site. The ^1H NMR spectra of the model system show that the paramagnetic shift is affected due to the substitutions and all present a single enantiomeric pair in solution. However, the $\Delta\chi$ -tensor based on protein data shows that CLaNP-5-OMe and CLaNP-5 have similar magnetic susceptibility tensors. Consequently, remote changes in the coordination system result in $\Delta\chi$ -tensors that are too similar to be of practical use. In contrast, the additional functional group (methoxyl) does affect the physical behavior of the probe after attachment. Two sets of paramagnetic effects were present in the case of CLaNP-5-OMe, whereas a single set is seen for CLaNP-5. This could be explained by interactions of the probe with the surrounding amino acids, because of the increased bulkiness of the CLaNP-5-OMe. This finding, together with that in Chapter 2, demonstrates that amino acid side-chains can readily interact with the probe and influence its behavior.

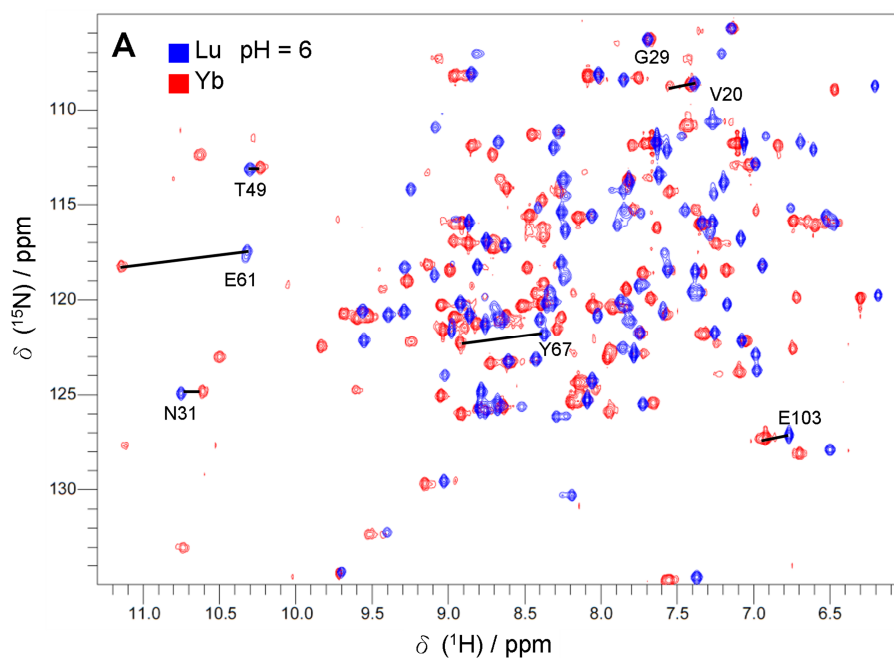
Nitroxide radical probes are described in Chapter 5. A double-armed nitroxide probe was synthesized. It was, however, unstable after attaching to a model protein. A possible explanation is the combination of strain caused by the attachment site and the mobility of the saturated five-membered ring. Substrate/inhibitor analogues can be considered the next generation of probes, which can interact with a designated target protein. In this chapter, 1-phenylimidazole derivatives, inhibitors of P450cam, were synthesized and these spin label probes were co-crystalized with P450cam. The imidazole ring of the meta-position substituted phenyl ring of 1-phenylimidazole sits above the haem iron and the nitroxide sits in the channel, forcing the protein to be in an open state. These initial results suggest this approach is promising for the study of protein-ligand complexes.

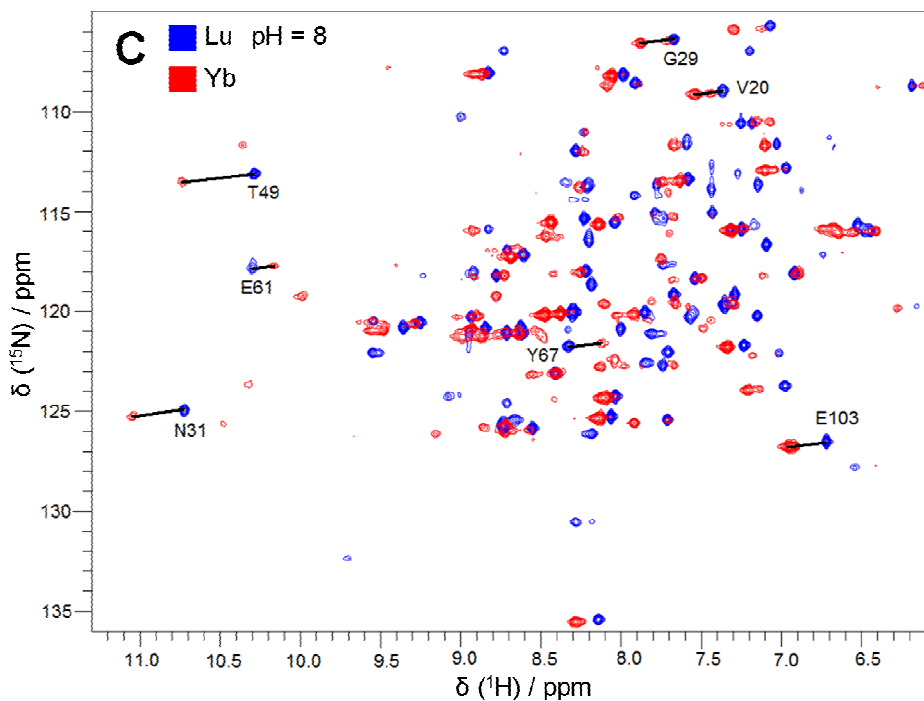
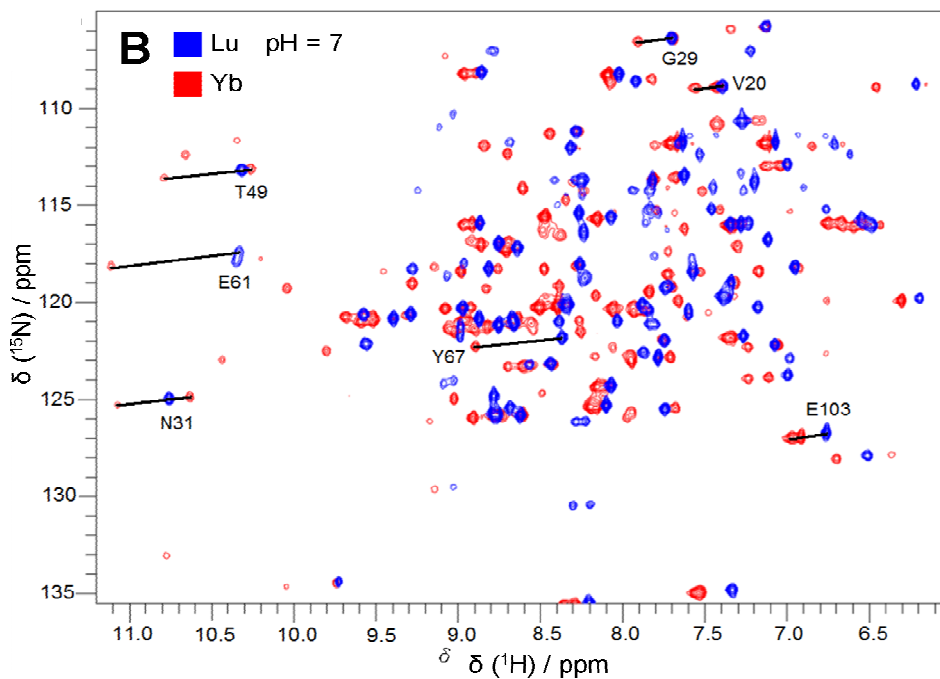
In Chapter 6, the future perspective of paramagnetic probes has been discussed and suggested.

Appendices

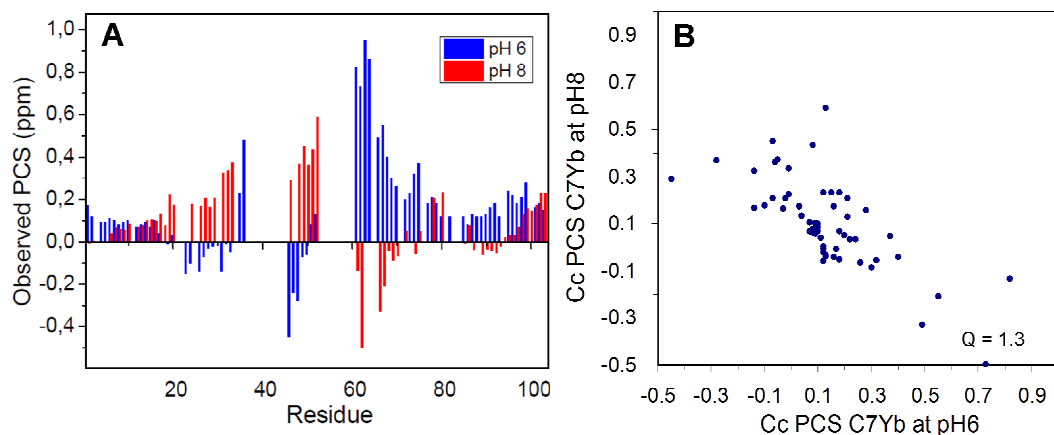


Appendix 1. Experimentally observed PCSs of Paz E51C/E54C Yb-CLaNP-7 plotted against the back-calculated PCSs ($Q = 0.06$). The solid line represents a perfect correlation.

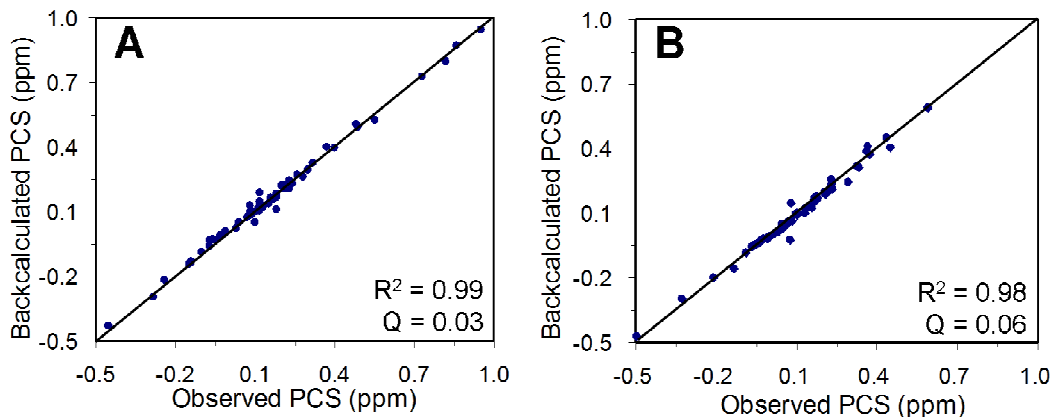




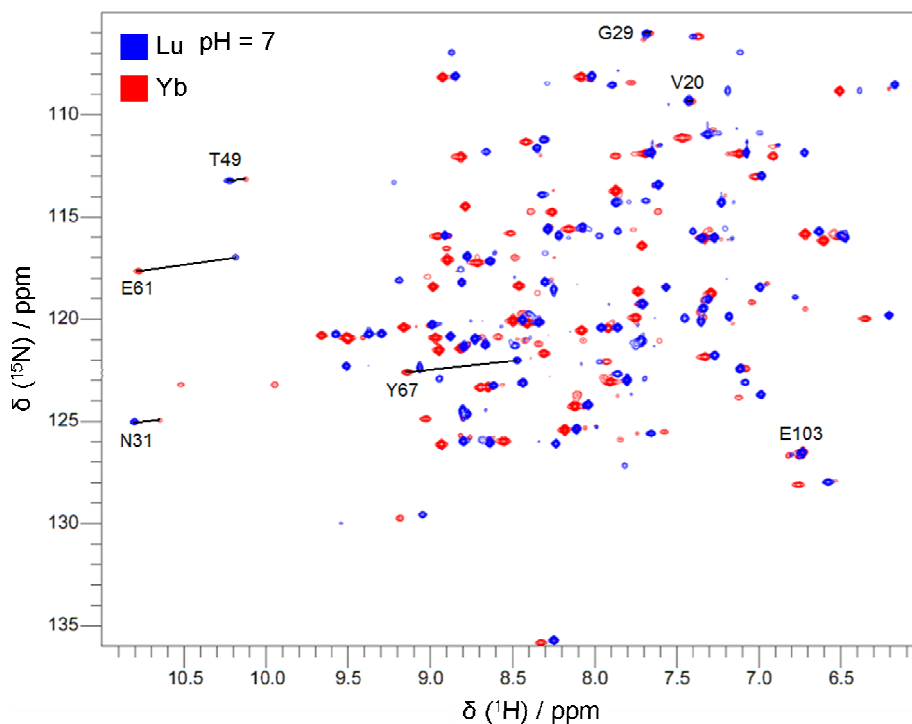
Appendix 2. pH dependence of CLaNP-7. [^{15}N , ^1H]-HSQC spectra of Cyt *c* N56C/L58C attached to Lu-CLaNP-7 (blue) and Yb-CLaNP-7 (red) at pH = 6.0 (A), pH = 7.0 (B) and pH = 8.0 (C). Several PCSs are indicated with solid lines.



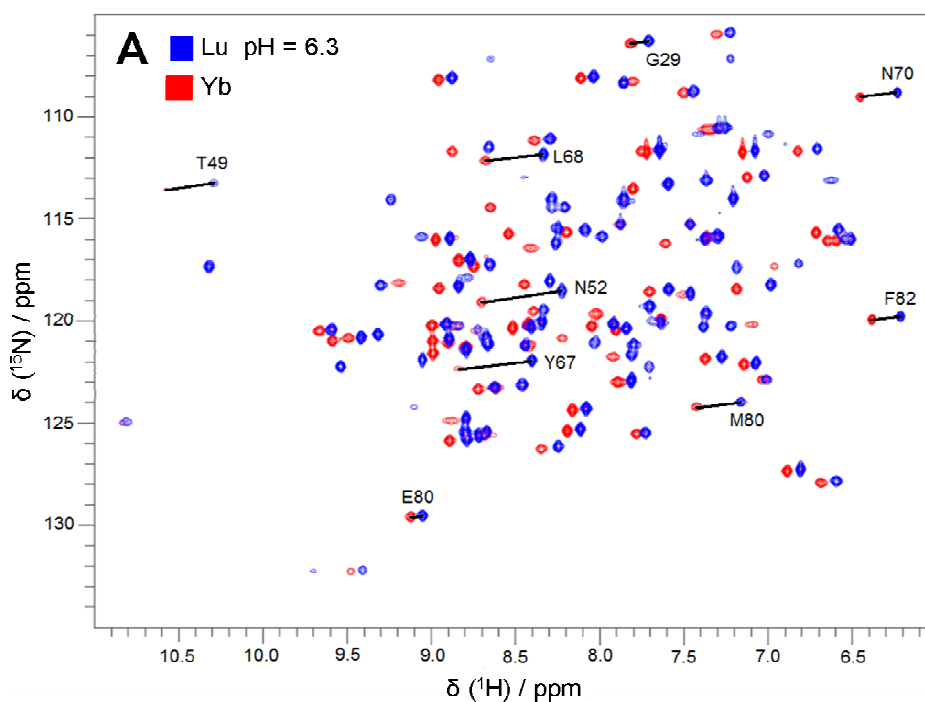
Appendix 3. Comparison of the PCSs at different pH. (A) The experimentally observed PCSs at pH 6 (blue) and 8 (Red); (B) Experimentally observed PCSs of Cyt *c* N56C/L58C Yb-CLaNP-7 at pH 6 plotted against the observed PCSs at pH 8 ($Q = 1.3$).

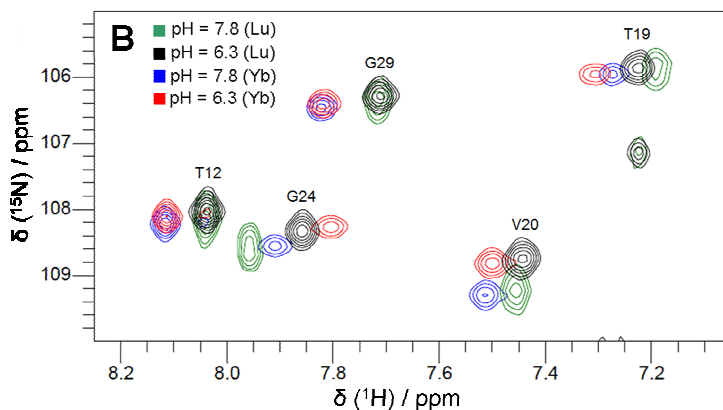


Appendix 4. Experimentally observed PCSs of Cyt *c* N56C/L58C Yb-CLaNP-7 plotted against the back-calculated PCSs at pH = 6 (A, $Q = 0.03$) and pH = 8 (B, $Q = 0.06$). The solid line represents a perfect correlation

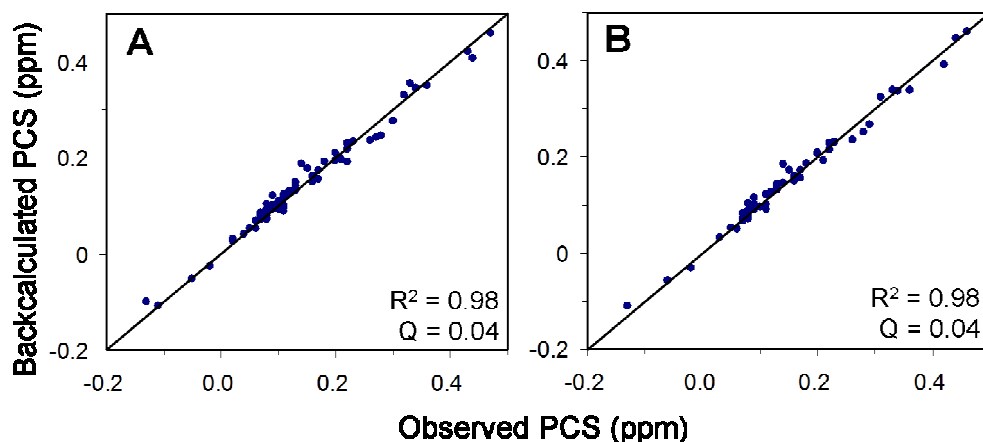


Appendix 5. CLaNP-5 linked to Cyt *c*. [^{15}N , ^1H]-HSQC spectra of Cyt *c* N56C/L58C attached to Lu-CLaNP-5 (blue) and Yb-CLaNP-5 (red) at pH = 7.0. Several PCSs are indicated with solid lines.

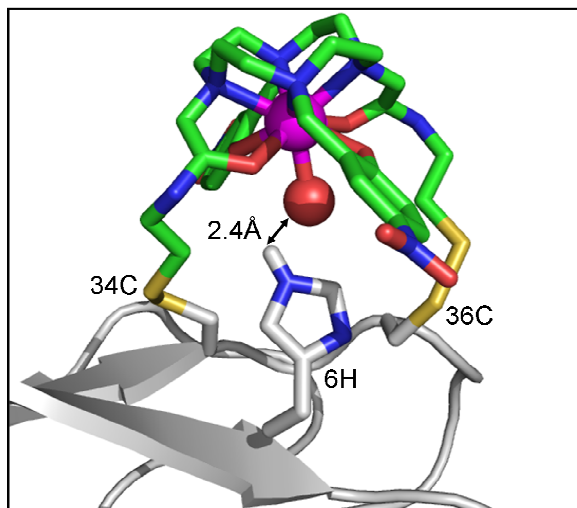




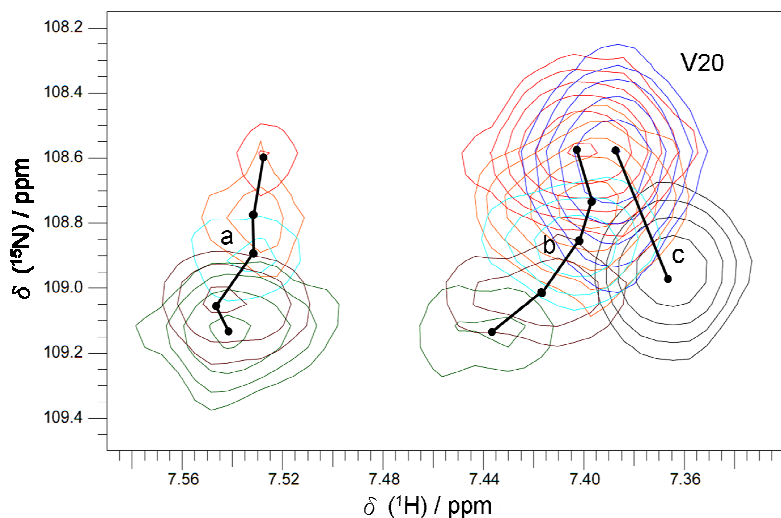
Appendix 6. Overlay of [^{15}N , ^1H]-HSQC spectra of Cyt *c* N56C/L58C/H39A attached to Lu-CLaNP-7 (blue) and Yb-CLaNP-7 (red) at pH = 6.3 (A); (B) Detail of [^{15}N , ^1H]-HSQC spectra of Ln-CLaNP-7 tagged ^{15}N -labeled Cyt *c* N56C/L58C/H39A. The spectra were recorded at pH = 6.3 (black, Lu; red, Yb) and 7.8 (green, Lu; blue, Yb).



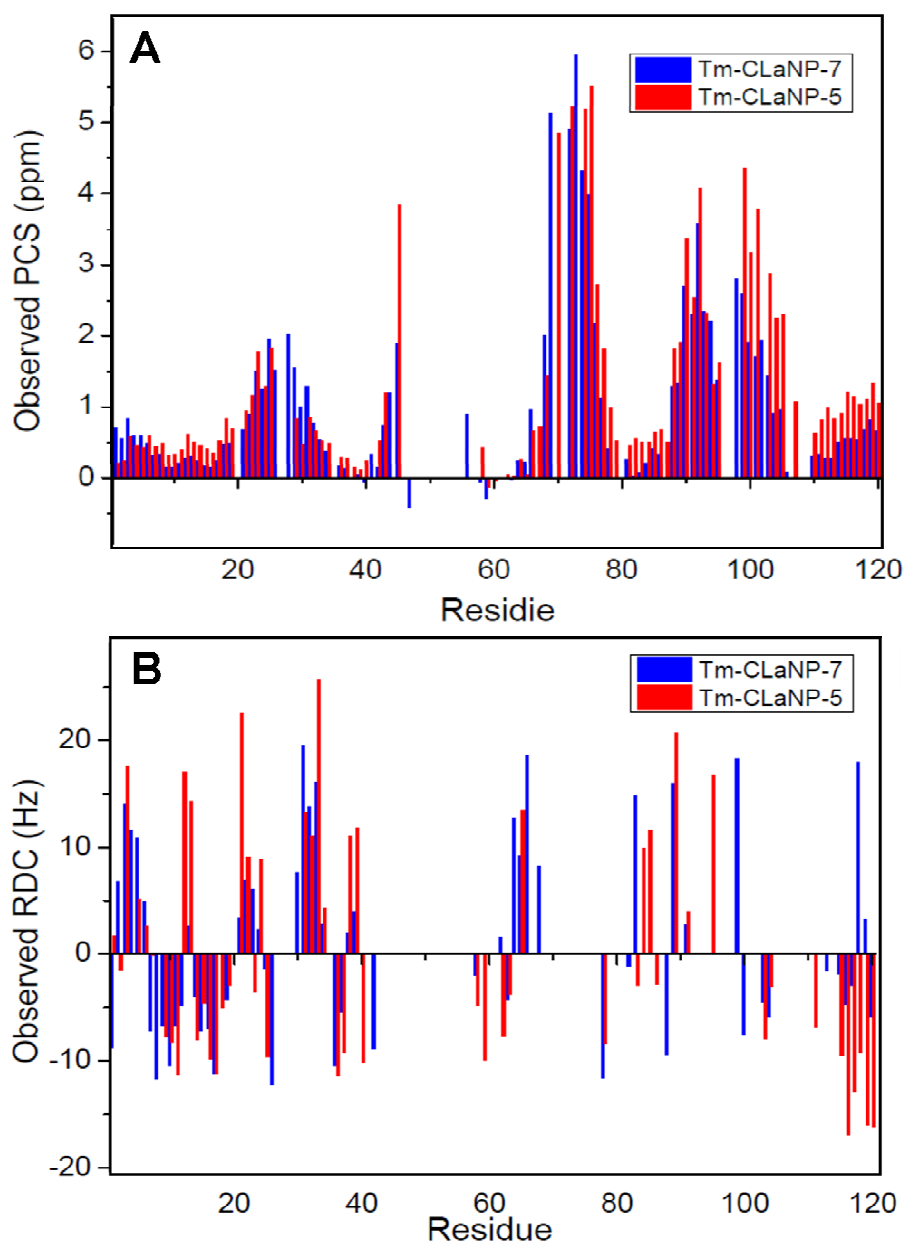
Appendix 7. Experimentally observed PCSs plotted against the back-calculated PCSs for Cyt *c* N56C/L58C/H39A Yb-CLaNP-7 at pH = 6.3 (A, $Q = 0.04$) and pH = 7.8 (B, $Q = 0.04$). The solid line represents a perfect correlation.



Appendix 8. Model of CLaNP-7 linked to C34, C36 and H6 of the I34C/V36C mutant of Paz. The position of Yb^{3+} is shown in magenta. The protein main chain is shown in grey. The Cys (I34C/V36C) and the His 6 side-chains are shown in CPK colors. The carbon atoms from CLaNP-7 are shown in green, nitrogen atoms in blue, oxygen atoms in red and sulfur atoms in yellow. The distance between the $\text{H}^{\epsilon 2}$ of His 6 and the ligating oxygen atom is 2.4 Å.



Appendix 9. Detail of $[\text{}^{15}\text{N}, \text{}^1\text{H}]$ -HSQC spectra of Ln-CLaNP-7 tagged ^{15}N -labeled Cyt *c* N56C/L58C. The spectra of Lu^{3+} tagged protein were recorded at pH = 6 (blue) and 8 (black). The spectra of Yb^{3+} tagged protein were recorded at pH = 6.0 (red), 6.6 (orange), 7.0 (cyan), 7.4 (brown) and 7.9 (green). Shifting resonances are connected by lines (a = basic PCS, b = acidic PCS, c = diamagnetic basic shift).



Appendix 10. Comparison of CLaNP-5 and CLaNP-7. The experimentally observed PCSs (A) and RDCs (B) of Paz E51C/E54C Tm-CLaNP-7 (blue) and Tm-CLaNP-5 (red) are shown for each Paz residue.

List of Publications

1. Dasgupta, S.; Hu, X.; Keizers, P. H. J.; **Liu, W. -M.**; Luchinat, C.; Nagulapalli, M.; Overhand, M.; Parigi, G.; Sgheri, L.; Ubbink, M. "Narrowing the conformational space sampled by two domain proteins with paramagnetic probes in both domains" *J. Biomol. NMR* **2011**, *51*, 253-263.
2. **Liu, W. -M.**; Keizers, P. H. J.; Hass, M. A. S.; Blok, A.; Timmer, M.; Sarris, A. J. C.; Overhand, M.; Ubbink, M. "A pH-sensitive, colorful, lanthanide-chelating paramagnetic NMR probe" *J. Am. Chem. Soc.* **2012**, *134*, 17306-17313.
3. Guan, J.-Y.; Keizers, P. H. J.; **Liu, W. -M.**; Loehr, F.; Skinner, S. P.; Heeneman, E. A.; Schwalbe, H.; Ubbink, M.; Siegal, G. D. "Small molecule binding sites on proteins established by paramagnetic NMR spectroscopy" *J. Am. Chem. Soc.* **2013**, *135*, 5859-5868.
4. Hiruma, Y.; Hass, M. A. S.; Kikui, Y.; **Liu, W. -M.**; Olmez, B.; Skinner, P. S.; Blok, A.; Kloosterman, A.; Koteishi, H.; Loehr, F.; Schwalbe, H.; Nojiri, M.; Ubbink, M. 'The structure of the Cytochrome P450cam-Putidaredoxin complex determined by paramagnetic NMR spectroscopy and crystallography' (*J. Mol. Biol.* **2013**, DOI: 10.1016/j.jmb.2013.07.006)
5. **Liu, W. -M.**; Overhand, M.; Ubbink, M. 'The application of paramagnetic lanthanoid ions in NMR spectroscopy on proteins' (*Coord. Chem. Rev.* **2013**, under revision)
6. **Liu, W. -M.**; Skinner, S. P.; Timmer, M.; Blok, A.; Filippov, D.; Overhand, M.; Ubbink, M. 'A two-armed lanthanoid-chelating paramagnetic NMR probe linked to proteins via thioether linkages' manuscript to be submitted (**2013**)

Curriculum vitae

Wei-Min Liu, who has always been interested in science, was born on 26th of August 1983 in Kaohsiung, Taiwan. When he was a high school student, he joined a “National and Private High School Science Fair” and got an award of excellent work. After high school, he was recommended to National Taiwan Normal University and obtained his bachelor degree in 2005. After his graduation, he began his master degree in the field of organic chemistry at National Taiwan University and started his first research project, which was correlative with drug discovery, under the supervision of Prof. Chao-Tsen Chen. He obtained his master degree in July 2007. After his master, he left the academic field and was a high school chemistry teacher to have a break from study and to find his own way for his future career. During this period, he supervised his students in their preparation and attendance of the high school science fair and realized his commitment to research. Therefore, he decided to come back the academic field. He started in September 2009 as a Ph.D student in the group of Protein Chemistry, Leiden Institute of Chemistry, under supervision of Prof. Dr. Marcellus Ubbink. During his Ph.D, he designed and synthesized several paramagnetic probes for the study of protein-protein and protein-ligand interactions in close collaboration with Dr. Mark Overhand in the Bio-organic synthesis group. The results of this research are described in this thesis.